

AD-A166 391

DESIGN AND DEVELOPMENT OF A SECOND GENERATION CLOSED
CENTER VALVE PNEUMAT. (U) ARMY MISSILE COMMAND REDSTONE
ARSENAL AL GUIDANCE AND CONTROL... R P BERRY APR 85

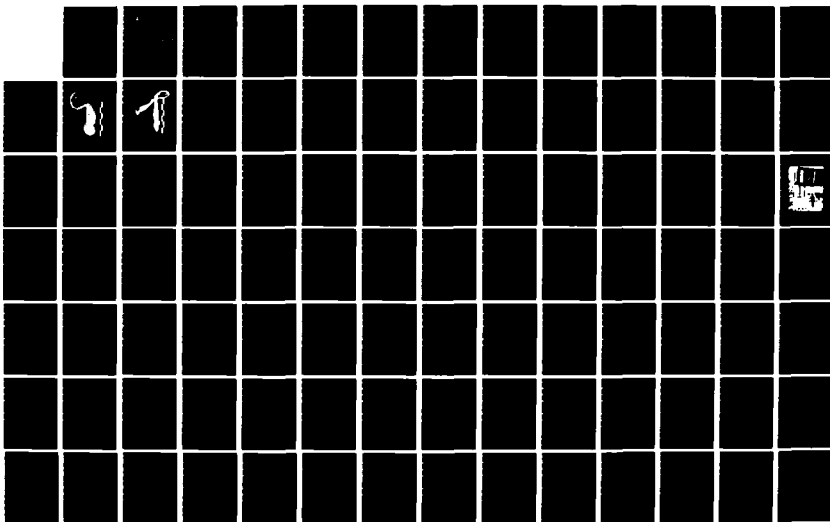
1/2

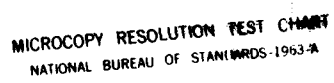
UNCLASSIFIED

AMSNI/RG-85-14-TR SBT-AD-E958 823

F/G 13/7

NL





MICROCOPY RESOLUTION TEST CHART
NATIONAL BUREAU OF STANDARDS-1963-A

AD-A166 391



TECHNICAL REPORT RG-85-14

DESIGN AND DEVELOPMENT OF A SECOND GENERATION
CLOSED CENTER VALVE PNEUMATIC ACTUATOR FOR THE
FIBER OPTIC GUIDED MISSILE (FOG-M)

Roger P. Berry
Guidance and Control Directorate
Research, Development and
Engineering Center

DTIC
ELECTE
MAR 28 1986
S B

APRIL 1985



U.S. ARMY MISSILE COMMAND

Redstone Arsenal, Alabama 35898-5000

Approved for public release; distribution is unlimited.

MMF FIVE COPY

DISPOSITION INSTRUCTIONS

**DESTROY THIS REPORT WHEN IT IS NO LONGER NEEDED. DO NOT
RETURN IT TO THE ORIGINATOR.**

DISCLAIMER

**THE FINDINGS IN THIS REPORT ARE NOT TO BE CONSTRUED AS AN
OFFICIAL DEPARTMENT OF THE ARMY POSITION UNLESS SO DESIGNATED
BY OTHER AUTHORIZED DOCUMENTS.**

TRADE NAMES

**USE OF TRADE NAMES OR MANUFACTURERS IN THIS REPORT DOES
NOT CONSTITUTE AN OFFICIAL INDORSEMENT OR APPROVAL OF
THE USE OF SUCH COMMERCIAL HARDWARE OR SOFTWARE.**

UNCLASSIFIED

SECURITY CLASSIFICATION OF THIS PAGE (When Data Entered)

REPORT DOCUMENTATION PAGE		READ INSTRUCTIONS BEFORE COMPLETING FORM
1. REPORT NUMBER TR-RG-85-14	2. GOVT ACCESSION NO. AD-A166391	3. RECIPIENT'S CATALOG NUMBER
4. TITLE (and Subtitle) Design and Development of a Second Generation Closed Center Valve Pneumatic Actuator for the Fiber Optic Guided Missile (FOG-M)		5. TYPE OF REPORT & PERIOD COVERED Technical Report
7. AUTHOR(s) Roger P. Berry		6. PERFORMING ORG. REPORT NUMBER
9. PERFORMING ORGANIZATION NAME AND ADDRESS Commander, US Army Missile Command ATTN: AMSMI-RD-GC Redstone Arsenal, AL 35898-5254		8. CONTRACT OR GRANT NUMBER(s)
11. CONTROLLING OFFICE NAME AND ADDRESS Commander, US Army Missile Command ATTN: AMSMI-RD-GC Redstone Arsenal, AL 35898-5254		10. PROGRAM ELEMENT, PROJECT, TASK AREA & WORK UNIT NUMBERS
14. MONITORING AGENCY NAME & ADDRESS (if different from Controlling Office)		12. REPORT DATE APRIL 1985
		13. NUMBER OF PAGES 115
		15. SECURITY CLASS. (of this report) UNCLASSIFIED
		15a. DECLASSIFICATION/DOWNGRADING SCHEDULE
16. DISTRIBUTION STATEMENT (of this Report) Approved for public release; distribution is unlimited.		
17. DISTRIBUTION STATEMENT (of the abstract entered in Block 20, if different from Report)		
18. SUPPLEMENTARY NOTES		
19. KEY WORDS (Continue on reverse side if necessary and identify by block number) Control System Pneumatic Actuator Actuator Design Closed Center Valve Actuator		
20. ABSTRACT (Continue on reverse side if necessary and identify by block number) This report describes the design and development of a second generation closed center valve pneumatic actuator for the Fiber Optic Guided Missile (FOG-M). A second generation design was desirable because of a reduction in the control force requirements. This allowed the size and weight of the first generation actuator design to be reduced significantly. This report discusses the detailed hardware design, presents test results (CONTINUED ON BACK)		

DD FORM 1 JAN 73 1473

EDITION OF 1 NOV 65 IS OBSOLETE

UNCLASSIFIED

SECURITY CLASSIFICATION OF THIS PAGE (When Data Entered)

UNCLASSIFIED

SECURITY CLASSIFICATION OF THIS PAGE(When Data Entered)

20. ABSTRACT (Continued from reverse).

and estimates the actuators production cost. The advantages, disadvantages and unique problems associated with the smaller actuator design are also discussed.

Accession For	
NTIS GRA&I	<input checked="checked" type="checkbox"/>
DTIC TAB	<input type="checkbox"/>
Unannounced	<input type="checkbox"/>
Justification	
By	
Distribution/	
Availability Codes	
Dist	Avail and/or Special
A-1	

UNCLASSIFIED

TABLE OF CONTENTS

	<u>Page</u>
I. INTRODUCTION.....	1
II. ACTUATOR DESCRIPTION.....	2
A. Preliminary Design Specifications.....	2
B. Actuator Description.....	2
C. Closed Center Valve/Upstream Orifice Description.....	6
III. ACTUATOR DESIGN.....	7
A. Shaft/Bearing Design.....	7
B. Shaft/Bearing Revisions.....	13
C. Piston Design.....	16
D. Crank Design.....	18
E. Ball Poppet Valve/Upstream Orifice Design.....	19
F. Ball Poppet Valve/Upstream Orifice Revisions.....	22
G. Housing Design.....	25
IV. TEST RESULTS.....	27
V. COST ANALYSIS.....	76
VI. RECOMMENDATIONS AND CONCLUSIONS.....	77
REFERENCES.....	79
NOMENCLATURE.....	80-81
APPENDIX A. ACTUATOR EQUATIONS.....	A-1
APPENDIX B. ACTUATOR DETAILED DRAWINGS.....	B-1

LIST OF ILLUSTRATIONS

<u>Figure</u>	<u>Page</u>
1. Second generation FOG-M schematic.....	3
2. Second generation FOG-M actuator (View A).....	4
Second generation FOG-M actuator (View B).....	5
3. Ball poppet valve/upstream orifice.....	6
4. Ball poppet valve/upstream orifice flow characteristics.....	7
5. Bearing dimensions.....	8
6. Crank loading diagram.....	8
7. Actuator/control surface freebody diagram.....	9
8. Shaft bending moment diagram.....	12
9. FOG-M small pneumatic actuator.....	13
10. FOG-M small pneumatic actuator (revised design).....	14
11. Actuator/control surface diagram (revised design).....	14
12. Shaft bending moment diagram (revised design).....	15
13. Effect of wear on bearing surface.....	16
14. Piston freebody diagram.....	17
15. Crank freebody diagram.....	18
16. Ball valve height.....	22
17. Solenoid force versus stroke.....	23
18. Ball valve stuck in open position.....	24
19. Ball freebody diagram.....	25
20. Actuator structural loads.....	26
21. Actuator test set-up.....	29
22. Actuator test set-up.....	30
23. Small closed actuator electronics.....	31

LIST OF ILLUSTRATIONS (Continued)

<u>Figure</u>	<u>Page</u>
24. Charge slew rate actuator SN-018 - 0.62 in ² -lb inertia load.....	32
25. Discharge slew rate actuator SN-018 - 0.62 in ² -lb inertia load.....	33
26. Hysteresis actuator SN-018 - 0.62 in ² -lb inertia load, 0.30 in-lb/deg hinge load.....	34
27. 1° P-P frequency response actuator SN-018 - 0.62 in ² -lb inertia load, 0.30 in-lb/deg hinge load.....	35
28. 3° P-P frequency response actuator SN-018 - 0.62 in ² -lb inertia load, 0.30 in-lb/deg hinge load.....	36
29. 6° P-P frequency response actuator SN-018 - 0.62 in ² -lb inertia load, 0.30 in-lb/deg hinge load.....	37
30. 1° P-P sine wave output at 1 Hz actuator SN-018 - 0.62 in ² -lb inertia load, 0.30 in-lb/deg hinge load.....	38
31. 1° P-P sine wave output at 6 Hz actuator SN-018 - 0.62 in ² -lb inertia load, 0.30 in-lb/deg hinge load.....	39
32. 1° P-P sine wave output at 8 Hz actuator SN-018 - 0.62 in ² -lb inertia load, 0.30 in-lb/deg hinge load.....	40
33. 3° P-P sine wave output at 1 Hz actuator SN-018 - 0.62 in ² -lb inertia load, 0.30 in-lb/deg hinge load.....	41
34. 3° P-P sine wave output at 8 Hz actuator SN-018 - 0.62 in ² -lb inertia load, 0.30 in-lb/deg hinge load.....	42
35. 3° P-P sine wave output at 12 Hz actuator SN-018 - 0.62 in ² -lb inertia load, 0.30 in-lb/deg hinge load.....	43
36. 6° P-P sine wave output at 1 Hz actuator SN-018 - 0.62 in ² -lb inertia load, 0.30 in-lb/deg hinge load.....	44
37. 6° P-P sine wave output at 8 Hz actuator SN-018 - 0.62 in ² -lb inertia load, 0.30 in-lb/deg hinge load.....	45
38. 6° P-P sine wave output at 12 Hz actuator SN-018 - 0.62 in ² -lb inertia load, 0.30 in-lb/deg hinge load.....	46
39. 3° P-P square wave output at 1 Hz actuator SN-018 - 0.62 in ² -lb inertia load.....	47

LIST OF ILLUSTRATIONS (Continued)

<u>Figure</u>	<u>Page</u>
40. 6° P-P square wave output at 1 Hz actuator SN-018 - 0.62 in ² -1b inertia load.....	48
41. 15° P-P square wave output at 1 Hz actuator SN-018 - 0.62 in ² -1b inertia load.....	49
42. 30° P-P square wave output at 1 Hz actuator SN-018 - 0.62 in ² -1b inertia load.....	50
43. Charge slew rate, 140 °F actuator SN-002 - 0.62 in ² -1b inertia load, no hinge load.....	52
44. Charge slew rate, -25 °F actuator SN-002 - 0.62 in ² -1b inertia load, no hinge load.....	53
45. Discharge slew rate, 140 °F actuator SN-002 - 0.62 in ² -1b inertia load, no hinge load.....	54
46. Discharge slew rate, -25 °F actuator SN-002 - 0.62 in ² -1b inertia load, no hinge load.....	55
47. 1° P-P frequency response, 140 °F actuator SN-002 - 0.62 in ² -1b inertia load, 0.30 in-lb/deg hinge load.....	56
48. 1° P-P frequency response, 68 °F actuator SN-002 - 0.62 in ² -1b inertia load, 0.30 in-lb/deg hinge load.....	57
49. 1° P-P frequency response, -25 °F actuator SN-002 - 0.62 in ² -1b inertia load, 0.30 in-lb/deg hinge load.....	58
50. 6° P-P frequency response, 140 °F actuator SN-002 - 0.62 in ² -1b inertia load, 0.30 in-lb/deg hinge load.....	59
51. 6° P-P frequency response, 68 °F actuator SN-002 - 0.62 in ² -1b inertia load, 0.30 in-lb/deg hinge load.....	60
52. 6° P-P frequency response, -25 °F actuator SN-002 - 0.62 in ² -1b inertia load, 0.30 in-lb/deg hinge load.....	61
53. 1° P-P frequency response, 140 °F actuator SN-002-T - 0.62 in ² -1b inertia load, 0.30 in-lb/deg hinge load.....	63
54. 1° P-P frequency response, 68 °F actuator SN-002-T - 0.62 in ² -1b inertia load, 0.30 in-lb/deg hinge load.....	64
55. 1° P-P frequency response, -25 °F actuator SN-002-T - 0.62 in ² -1b inertia load, 0.30 in-lb/deg hinge load.....	65

LIST OF ILLUSTRATIONS (Concluded)

<u>Figure</u>	<u>Page</u>
56. 6° P-P frequency response, 140 °F actuator SN-002-T - 0.62 in ² -lb inertia load, 0.30 in-lb/deg hinge load.....	66
57. 6° P-P frequency response, 68 °F actuator SN-002-T - 0.62 in ² -lb inertia load, 0.30 in-lb/deg hinge load.....	67
58. 6° P-P frequency response, -25 °F actuator SN-002-T - 0.62 in ² -lb inertia load, 0.30 in-lb/deg hinge load.....	68
59. Applied torque versus vane deflection - 300 psig supply pressure, 0.50 degree deadzone.....	71
60. Applied torque versus vane deflection - 350 psig supply pressure, 0.50 degree deadzone.....	72
61. Applied torque versus vane deflection - 400 psig supply pressure, 0.50 degree deadzone.....	73

LIST OF TABLES

<u>Table</u>	<u>Page</u>
1. Rolling Element Bearings.....	10
2. Typical Bearing Materials.....	11
3. Plain Bearings.....	11
4. Actuator SN-018 Performance Summary.....	28
5. Environmental Test Results Actuator SN-002 (Anodized Housing).....	51
6. Environmental Test Results Actuator SN-002-T (Ti-dized Housing).....	62
7. Gas Consumption Test Results Actuator SN-002.....	69
8. Gas Consumption Test Results Actuator SN-002.....	70
9. Actuator Performance Summary.....	74
10. Actuator Leakage Test Summary.....	75
11. Second Generation Closed Center Pneumatic Actuator Major Cost Items.....	76
12. Actuator Comparison.....	78

I. INTRODUCTION

This report describes the design and development of a second generation closed center valve pneumatic actuator for the Fiber Optic Guided Missile (FOG-M). The need for a second generation actuator design arose because of a reduction in the control surface force requirements. This allowed the size and weight of the original actuator design, which is described in Reference [3], to be reduced significantly. The primary objective was to design an actuator which could be packaged within the minimum possible cross section required to provide adequate bearing support for the control surface.

A description of the detailed hardware design is presented along with the design calculations required to assure that the preliminary performance specifications are satisfied. Development of the initial design, in order to eliminate problems, is also discussed.

A cost analysis of the actuator is presented, based on a production quantity of 200,000 actuators. This analysis recommends a specific manufacturing process for each fabricated part which is selected based on design, economics, functional requirements and strength requirements.

Detailed test procedures and data for a single axis unit are presented along with a summary of the results.

II. ACTUATOR DESCRIPTION

A. Preliminary Design Specifications

The design of a second generation closed center valve pneumatic actuator for the FOG missile is based on the following preliminary specifications.

Structural - Minimum 15 lbs Shear, 60 in-lbs bending capability.

Stall Torque - Minimum 6 in-lbs capability.

No Load Slew Rate - 1,300 - 1,500 deg/sec.

Travel - Minimum ± 20 deg.

Environmental - 25 °F to 150 °F.

Pneumatic Power Supply - Air or Nitrogen at 68 °F,
375 psig to 425 psig.

Frequency Response - 1°P-P inputs, 6.0 Hz
6°P-P inputs, 10.0 Hz.

Aerodynamic Loading - 0.30 in-lb/deg.

Control Surface Inertia - 0.62 in²-lb.

B. Actuator Description

The second generation FOG-M actuator is a basic differential area design which uses a single double-acting piston and two pulse width modulated ball poppet valves. A schematic of the conceptual design is shown in Figure 1 along with a photograph of the actual hardware in Figure 2. For rotation in the counter-clockwise direction, the charge valve opens and allows gas to flow into the control chamber causing the control pressure to increase. The increased pressure causes an unbalanced force on the piston resulting in movement in the extend direction which causes a counterclockwise rotation of the output shaft. To maintain a stationary position, the charge and discharge valves are both closed. The control chamber volume changes until the control chamber pressure is such that a force balance on the piston is achieved. For rotation in the clockwise direction, the discharge valve opens and allows gas to flow out of the control chamber causing the control pressure to decrease. The decreased pressure causes an unbalanced force on the piston resulting in movement in the retract direction which causes a clockwise rotation of the output shaft.

A segment potentiometer converts the output shafts angular position into a proportional voltage signal. The signal is fed back to sum with the input command for closed loop operation.

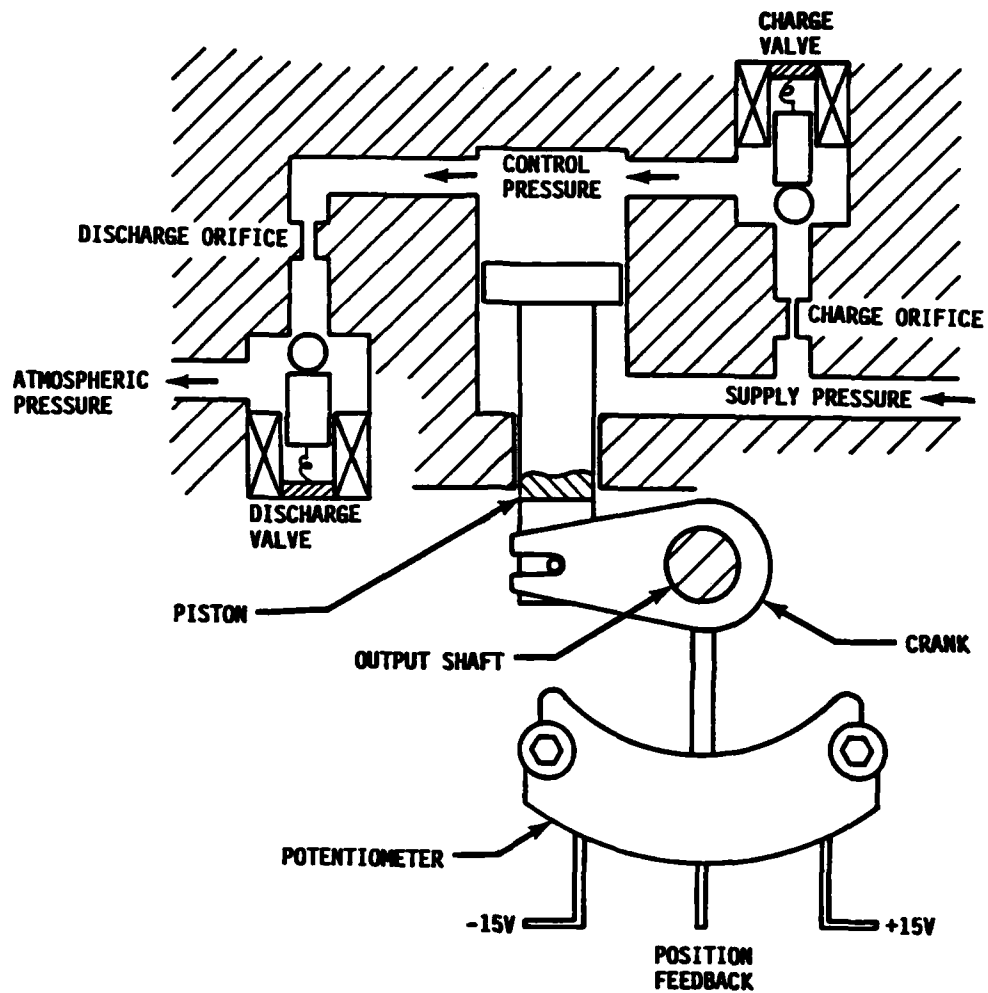


Figure 1. Second generation FOG-M actuator schematic.

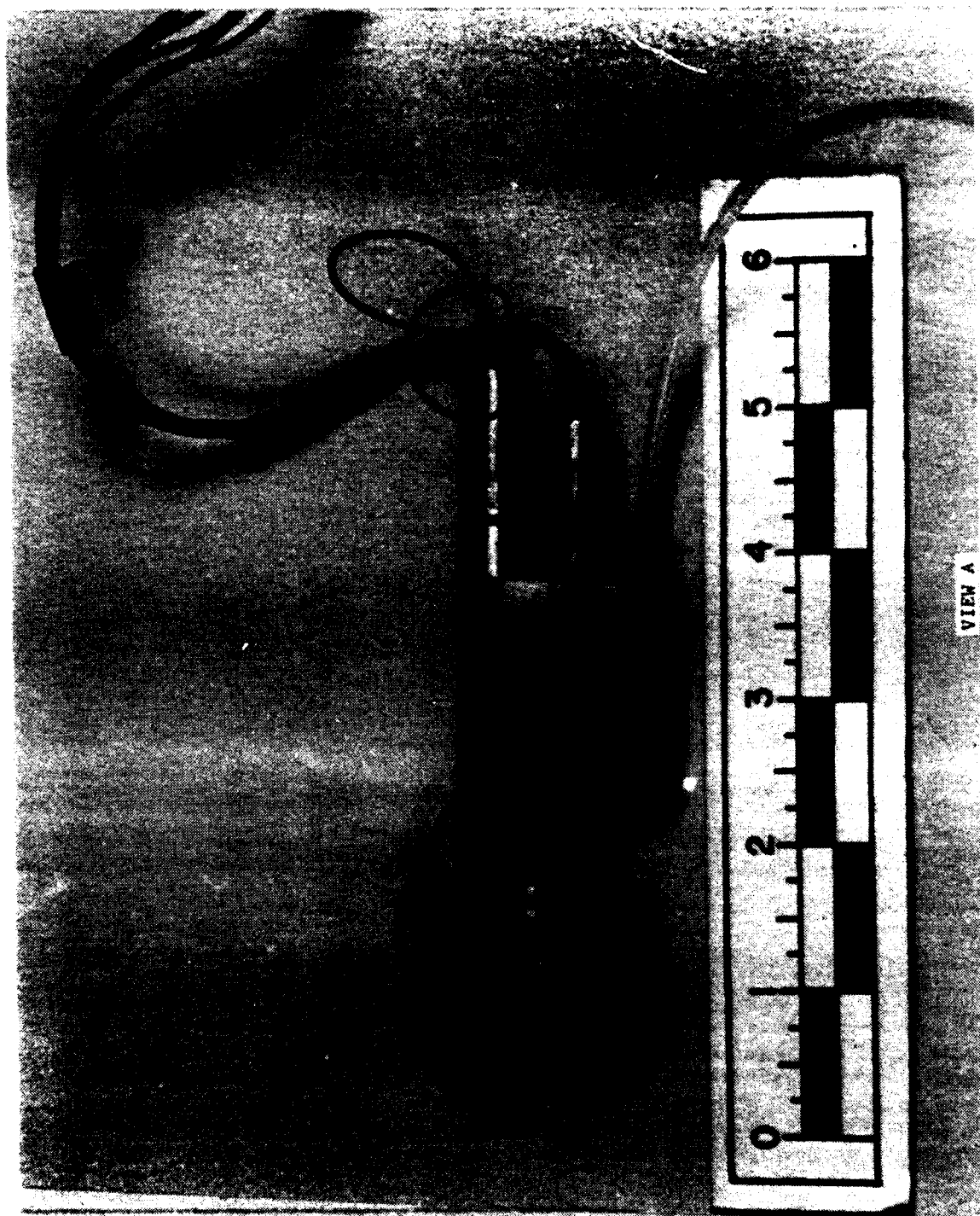


Figure 2. Second generation FOG-M actuator.

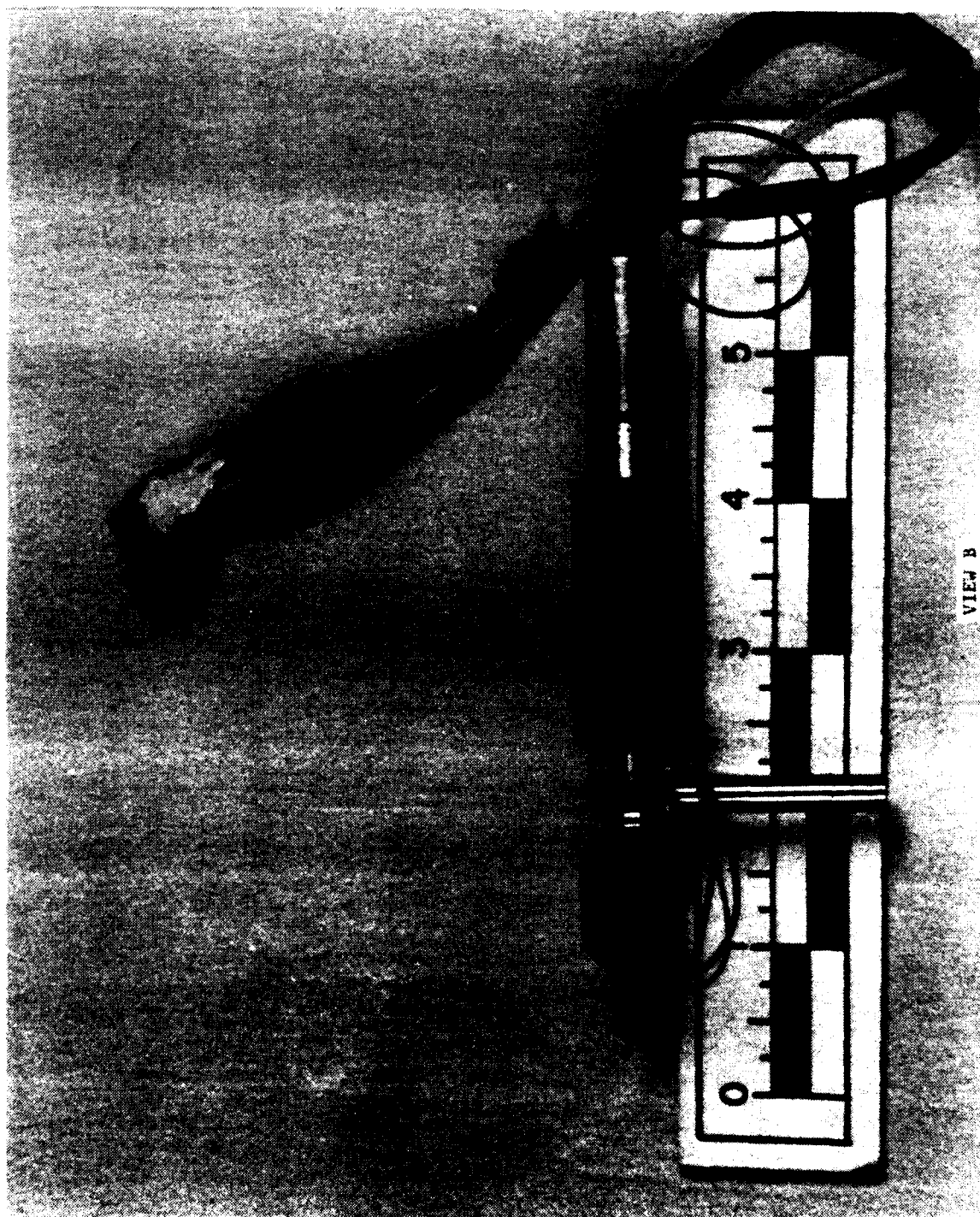


Figure 2. Second generation FOG-M actuator. (continued)

C. Closed Center Valve/Upstream Orifice Description

The second generation FOG-M actuator uses two ball poppet valves with a flow control orifice located upstream of each valve as shown in Figure 3. When the solenoid coil is not energized, the force exerted on the push rod by the compressed spring holds the ball against the valve seat preventing the flow of gas. When the solenoid coil is energized, the magnetic force exceeds the spring force and the push rod moves off the ball until the plunger rests against the solenoid pole face. The inlet pressure pushes the ball against the push rod permitting gas to flow through the upstream orifice, around the ball, through the spacer holes, and through the outlet passage. The distance the ball moves off the seat is determined by the distance between the pole face and plunger which is adjustable by the addition or subtraction of shims. If the valve flow area is sufficiently larger than the upstream orifice flow area, then the flow rate is controlled by the upstream orifice flow area, as shown in Figure 4.

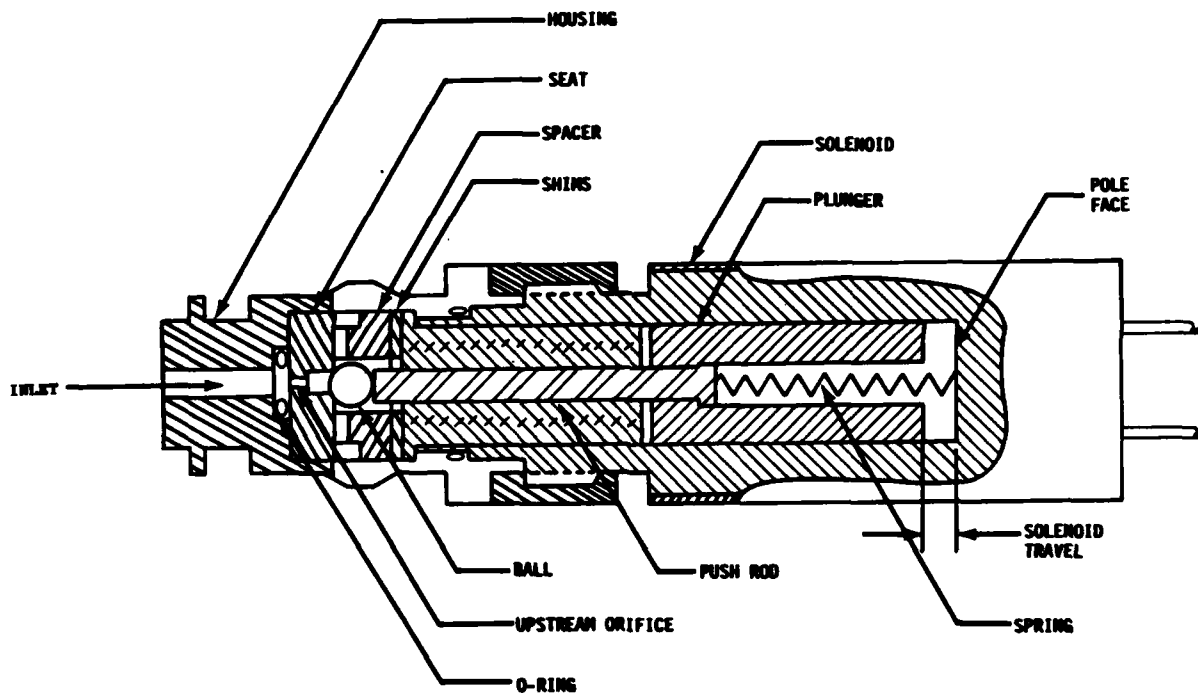


Figure 3. Ball poppet valve/upstream orifice.

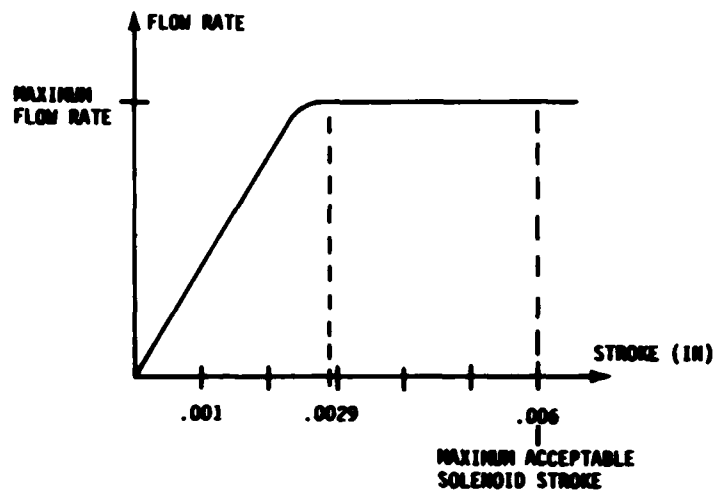


Figure 4. Ball poppet valve/upstream orifice flow characteristics.

III. ACTUATOR DESIGN

A. Shaft/Bearing Design

The final detailed shaft design which satisfies the actuator's functional requirements is fabricated according to drawing FOG-RGC-13-1075. The nominal shaft diameter selected is $\frac{1}{4}$ inch. The shaft is supported by two Garlock 04DU04 self-lubricating bearings, which are pressed into the actuator housing. A $\frac{1}{16}$ inch diameter roll pin is used to connect the crank to the shaft.

The primary design objective in the selection of a shaft and bearings is to provide adequate support for the control surface within the minimum possible cross section, where adequate support is defined as supporting the maximum specified load without effecting the actuator's performance. The following approach is selected to accomplish the stated objective.

- (1) Assume a nominal shaft diameter of $\frac{1}{4}$ inch.
- (2) Estimate the minimum acceptable crank width, dimension F in Figure 5, required to transfer the maximum expected hinge moment.
- (3) Determine the minimum acceptable bearing width, dimension W in Figure 5, required to support the maximum expected control surface forces and bending moments.
- (4) Check shaft diameter assumption to verify that it is acceptable for the maximum expected loading conditions.

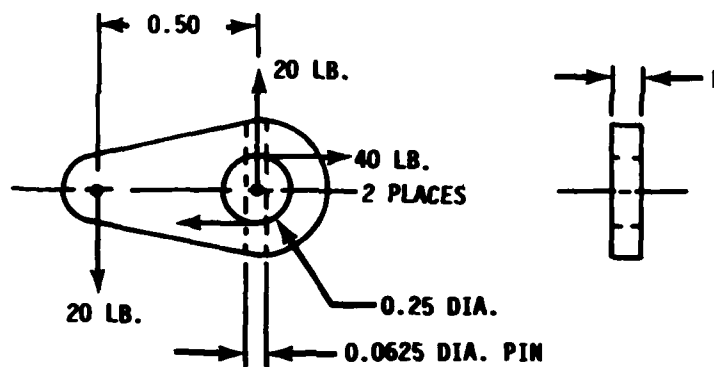


Figure 5. Bearing dimensions.

The minimum acceptable crank width is determined based on an estimated maximum hinge moment of 10 in-lb. This results in a roll pin shear force of 40 lbs as shown in Figure 6. A 1/16 inch diameter spiral roll pin, which has a shear strength of 190 lbs, is selected resulting in a safety factor of 4.75. In order to provide adequate edge margin for the 1/16 diameter roll pin, a crank width of $F = 1/8$ inch is required.

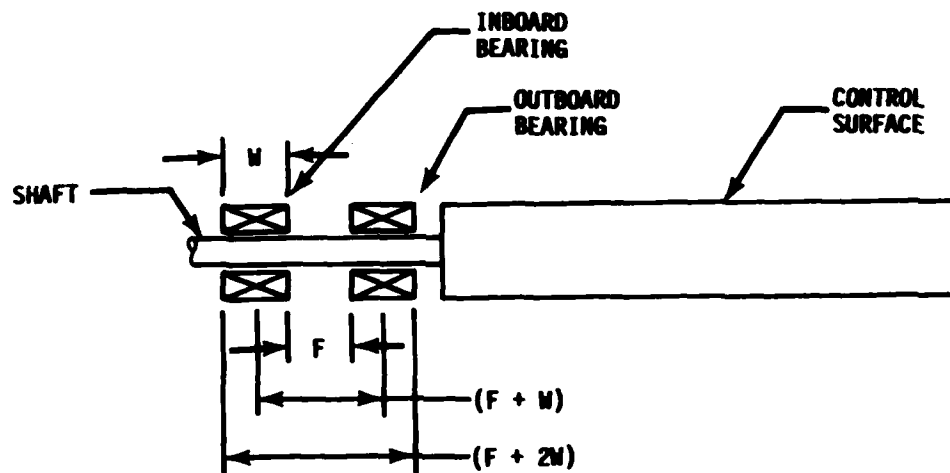


Figure 6. Crank loading diagram.

The static bearing loads R_1 and R_2 are determined from the freebody diagram shown in Figure 7 which depicts the specified structural loading conditions. The bearing load R_1 is determined by a summation of the vertical forces,

$$R_1 = R_2 - 15 \quad (1)$$

which implies that R_2 should be used to select a bearing since it is the maximum bearing load. The bearing load R_2 is determined by a summation of moments about R_1 ,

$$R_2 (F+W) = 15 \left\{ (F+W) + \frac{W}{2} + 4.1 \right\} \quad (2)$$

$$R_2 = 15 + \frac{61.5}{(F+W)} + 7.5 \frac{W}{(F+W)} \quad (3)$$

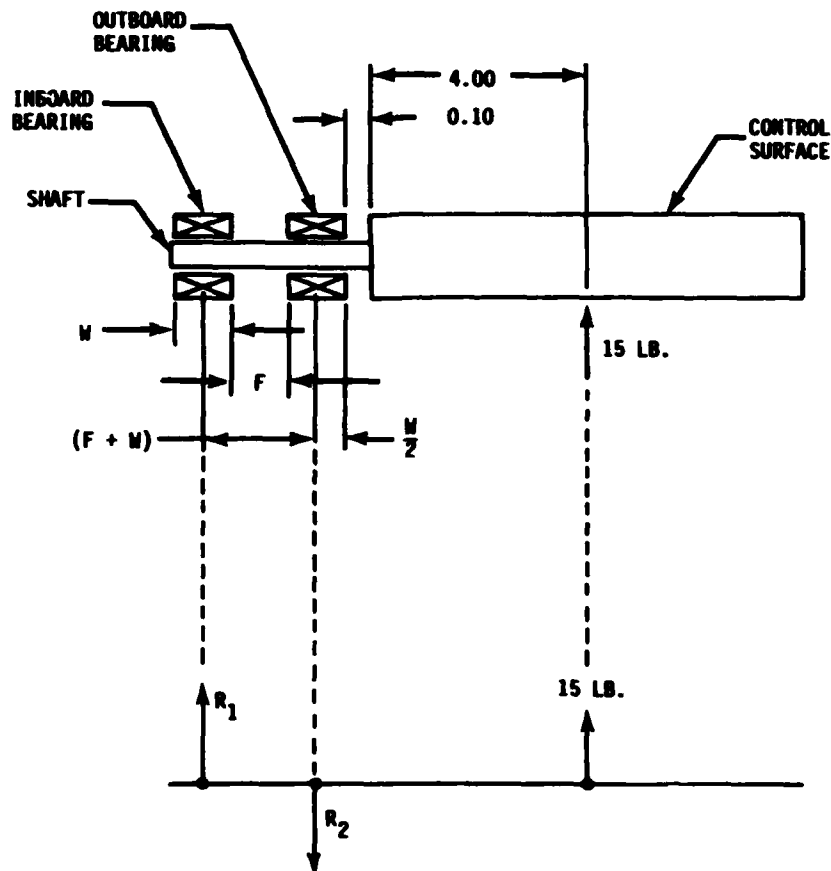


Figure 7. Actuator/control surface freebody diagram.

Two basic bearing groups will be considered in the selection of a bearing, namely, Rolling Element Bearings and Plain Bearings. The minimum possible bearing width (W), which determines the minimum actuator width (F+2W), is determined using equation (3). In the case of rolling, element bearing R₂ is allowed to equal the bearings Static Load Rating. Based on this, the minimum actuator width, assuming F = 1/8 inch using a standard size, rolling element type bearing is determined from Table 1 to be 0.437 inches using grease retained rollers. In the case of Plain Bearings, selection is based on the maximum journal pressure (P) and the product of journal pressure with sliding velocity (PV). The journal pressure is determined by,

$$P = \frac{R_2 \text{ (psi)}}{(0.25) W} \quad (4)$$

and the sliding velocity is determined from the specified maximum 1500°/sec Slew Rate to be 16.4 FPM which results in,

$$PV = P (16.4) \text{ (psi - FPM)} \quad (5)$$

A portion of the bearing materials considered are listed in Table 2. The PTFE-lead overlay which has a porous bronze interstructure with a steel backing was found to have the highest P and PV rating of the bearing materials considered. Based on these ratings, the minimum actuator width using a plain bearing is determined in Table 3.

TABLE 1. Rolling Element Bearings.

	Bore (in)	OD (in)	W (in)	Static Load Rating (lbs)	Applied Radial Load R ₂ (lbs)
Deep Groove Ball Bearings	0.250	0.375	0.125	21	265
	0.250	0.500	0.125	40	265
	0.250	0.625	0.196	70	211
	*0.250	0.750	0.219	193	199
	TOTAL ACTUATOR WIDTH = 0.563				
Full Complement Needle Roller Bearings	*0.250	0.438	0.250	325	184
	TOTAL ACTUATOR WIDTH = 0.625				
Grease Retained Rollers	*0.250	0.313	0.156	300	238
	TOTAL ACTUATOR WIDTH = 0.437				

* Selected Bearing Size.

TABLE 2. Typical Bearing Materials.

<u>Bearing Materials</u>	<u>Max. P (PSI)</u>	<u>Max. PV (PSI-FPM)</u>
1. PTFE Lead Overlay, DU	20,000	100,000
2. Slip-Liner Rulon	10,000	100,000
3. Super Oilite - 16 PM	8,000	75,000
4. Cast Molded Nylon	2,000	30,000
5. TFE Rulon	1,000	20,000

TABLE 3. Plain Bearings.

<u>Bore (in)</u>	<u>W (in)</u>	<u>Applied Radial Load R₂ (lb)</u>	<u>P (PSI)</u>	<u>PV (PSI-FPM)</u>
0.250	0.094	299	12,720	208,610
0.250	0.125	265	8,480	139,070
0.250	0.156	238	6,100	100,040
*0.250	0.187	217	4,640	76,100

TOTAL ACTUATOR WIDTH = 0.499

*Selected Bearing Size

Since the use of grease retained rollers would increase the complexity of the actuator design and be difficult to assemble, the PTFE-lead overlay bearings are selected. The nominal dimensions of the final actuator design are $F = 1/8$ inch and $W = 3/16$ inch. Substituting these values into equation (3) results in a maximum bearing load of $R_2 = 217$ lbs. This causes a journal pressure of $P = 4,640$ psi and a product of journal pressure with sliding velocity of $PV = 76,100$ psi - PFM, which are well below the maximum load ratings for the selected bearing material.

A stress analysis of the shaft is performed to determine if the assumed $1/4$ inch diameter is adequate to support the expected loads. The most severe loading condition expected during operation, which is derived from Figure 7 for $F = 1/8$ inch and $W = 3/16$ inch, along with the corresponding Bending Moment Diagram, is shown in Figure 8. Since the shafts section modulus is constant, the maximum bending stress occurs where the bending moment is 63 in-lbs.

$$\sigma = \frac{(63 \text{ in-lbs})}{\left(\frac{\pi(0.25 \text{ in})^3}{32}\right)} = 41,070 \text{ psi}$$

Based on this, the selected shaft material is 17-4 PH stainless steel which has a yield strength of 110,000 psi in the annealed condition resulting in a safety factor of 2.7.

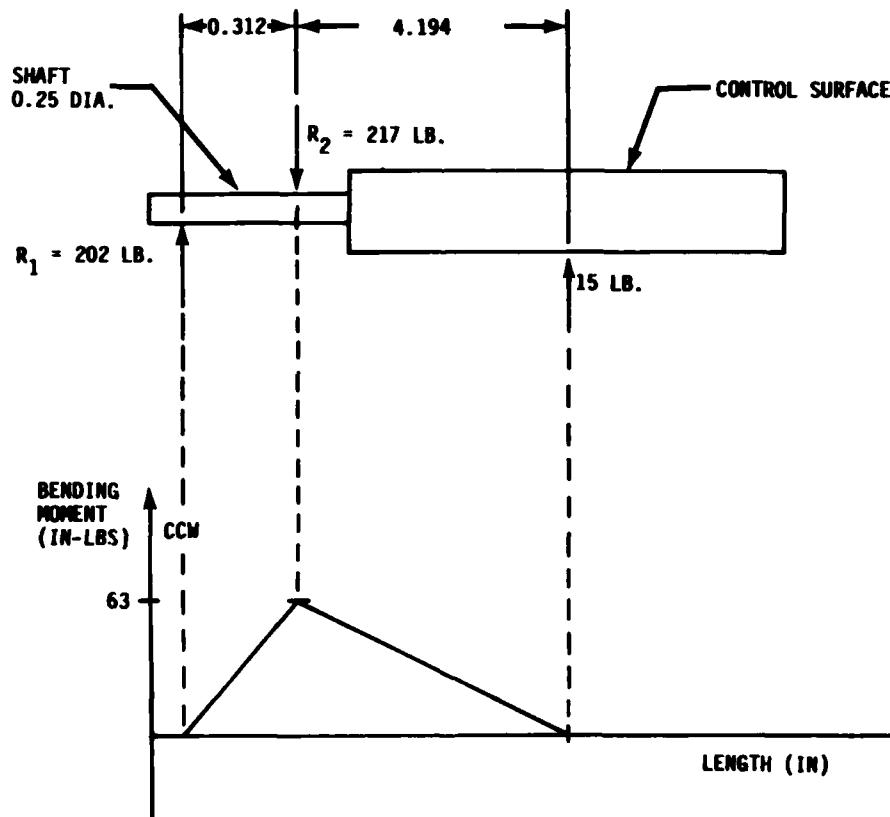


Figure 8. Shaft bending moment diagram.

B. Shaft/Bearing Revisions

Prior to the first actuator flight test, a change was made in the actuator fairing which impacted the Shaft/Bearing design. The original second generation actuator fairing, shown in Figure 9, caused an increase in missile drag force over that caused by the first generation actuator fairing. Since an increase in drag force would require an increase in thrust, a decision was made to use the first generation actuator fairing as shown in Figure 10. This change requires an increase in the shafts cantilever which causes increased bearing loads and shaft stresses. The extent of the increased bearing loads are determined from Figure 11 resulting in $P = 5,280$ psi and $PV = 86,590$ psi-Fpm. Since this is below the maximum rated bearing loads of the PTFE lead, a new bearing design was not required. The extent of the increased shaft stresses are determined from Figure 12,

$$\sigma = \frac{(72 \text{ in-lbs})}{\left(\frac{\pi(0.25 \text{ in})^3}{32}\right)} = 46,940 \text{ psi}$$

which reduces the shaft safety factor to 2.3.

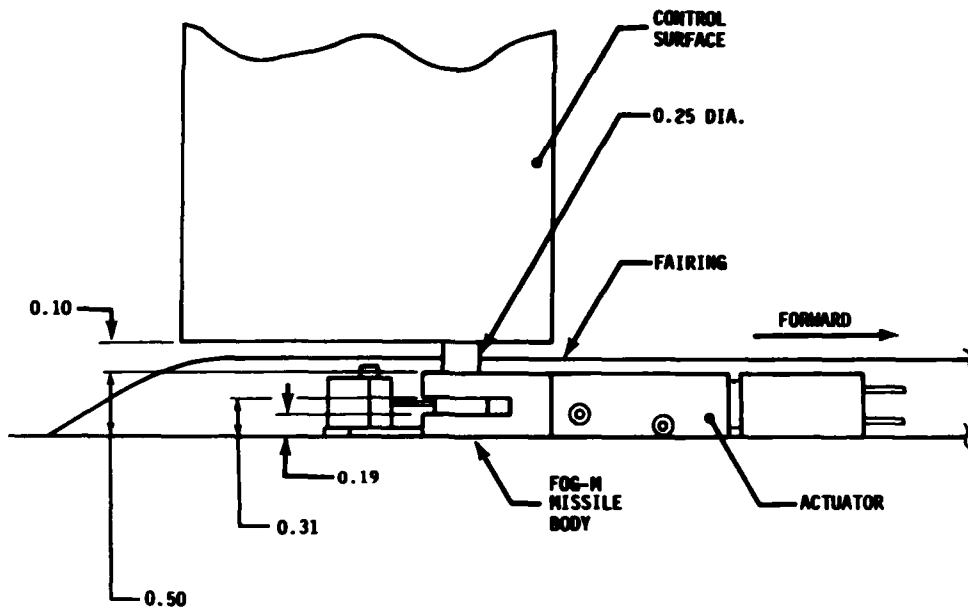


Figure 9. FOG-M small pneumatic actuator.

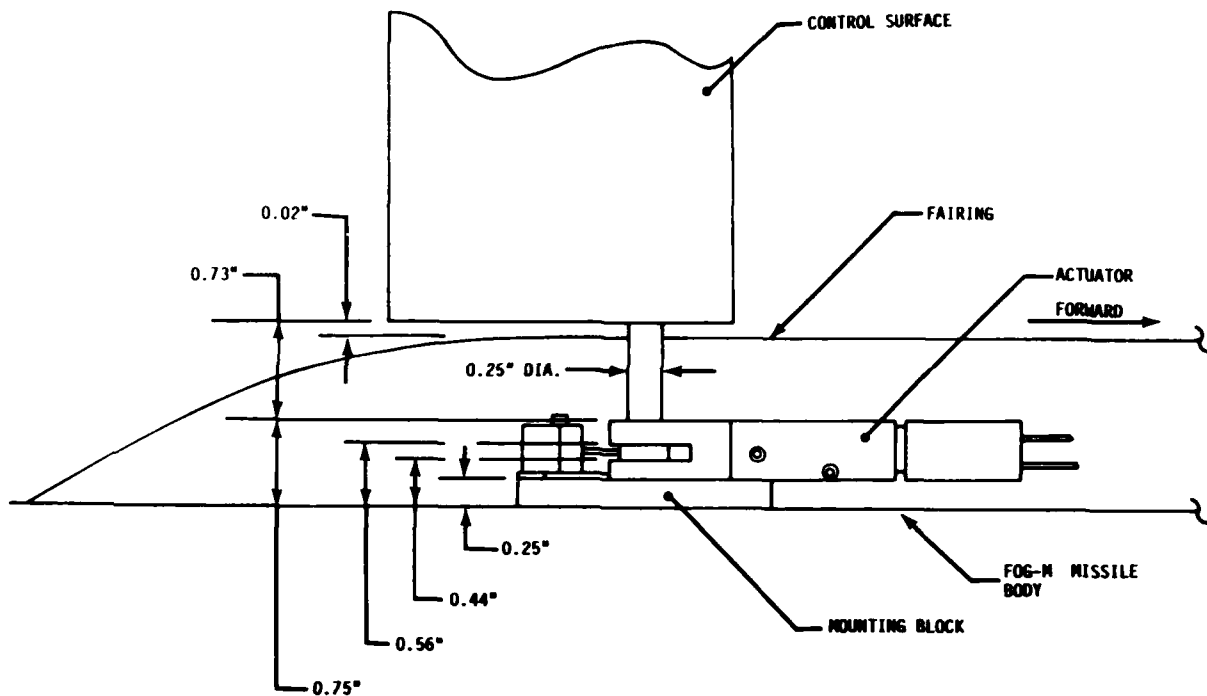


Figure 10. FOG-M small pneumatic actuator (revised design).

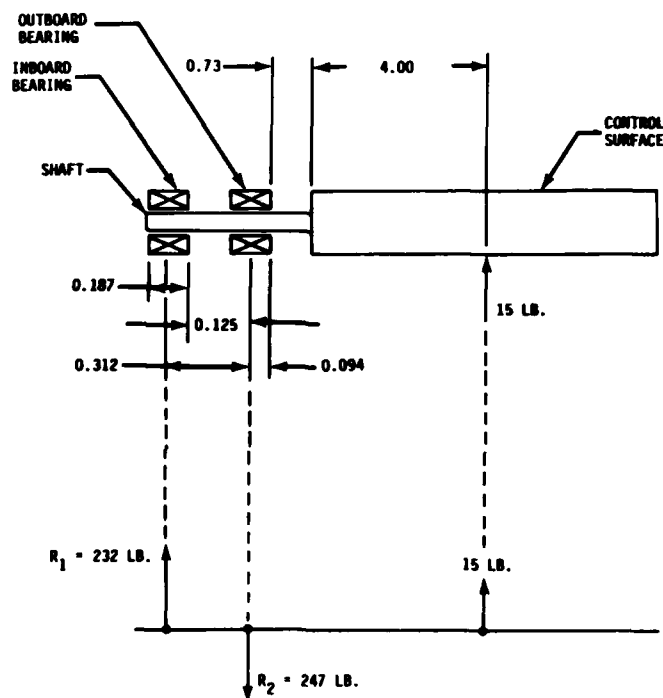


Figure 11. Actuator/control surface freebody diagram (revised design).

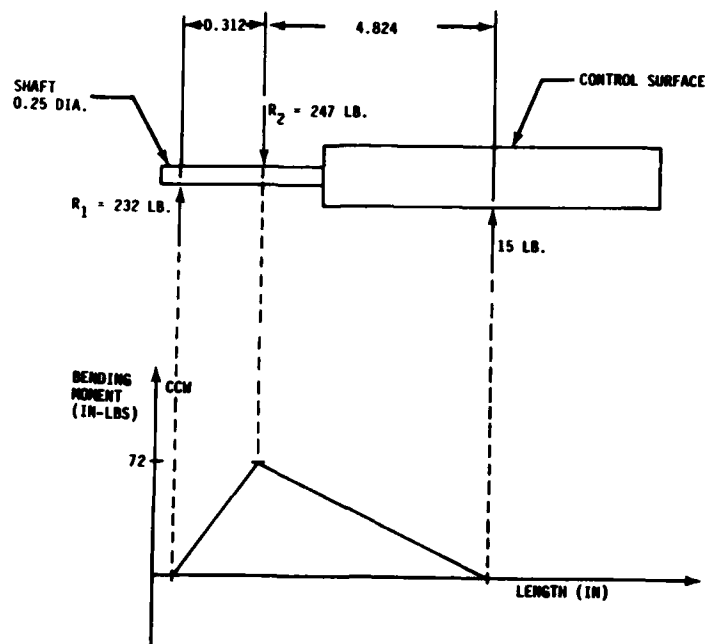


Figure 12. Shaft bending moment diagram (revised design).

The preliminary shaft/bearing design, which used the bearing manufacturers recommended shaft diameter of 0.2481 - 0.2490 inches, resulted in an extremely loose shaft/bearing fit allowing approximately 0.78° of shaft movement. In some actuators, this problem was present upon assembly, and in others, it occurred after a brief period of run time. Actuator serial numbers 006, 007, 008, and 010 which were used in FOG-M flight MIL-5 used the recommended shaft diameter allowing a loose shaft/bearing fit. This flight resulted in a control surface flutter which occurred on each of the four axes shortly after launch. Among the suspected causes of this problem was the loose shaft/bearing fit. A limited amount of wind tunnel testing, described in Reference [4], which was done following flight MIL-5, supported this to some extent. It was determined that the loose shaft/bearing fit was a contributing element in the flutter problem among other things such as Aerodynamically unstable control surfaces, unbalanced control surfaces, control surface stiffness, actuator hinge stiffness and actuator shaft bending stiffness.

Following this, a revision which increased the actuator shaft diameter to 0.2500 - 0.2505 inch was incorporated. This caused a slight interference fit of the shaft into the bearing. The shaft was forced through the bearings causing a small amount of bearing material to be removed. This resulted in a tight shaft/bearing fit with only 0.20° of shaft movement. Removal of the shaft and examination of the bearings revealed that a portion of the PTFE-lead overlay had been removed which exposed the bronze interstructure. This indicates the bearing is in the low wear rate portion of the curve shown in Figure 13.

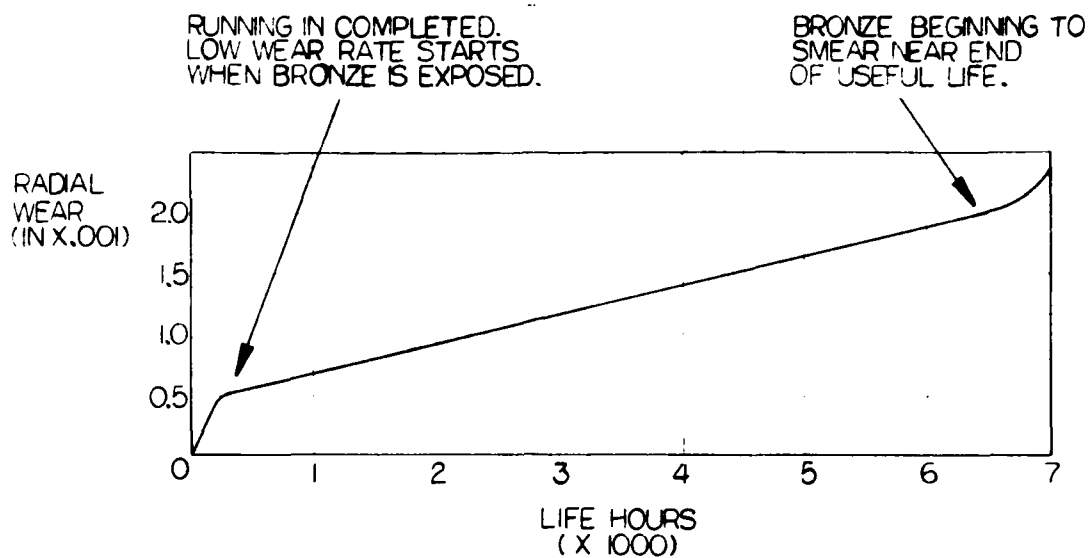


Figure 13. Effect of wear on bearing surface.

Actuators which were prepared for FOG-M Flight MIL-6 used the revised 0.2500 - 0.2505 inch shaft diameter. The bearing wear which occurred during acceptance testing and hardware-in-the-loop simulations was not significant to cause a measurable change in the shaft/bearing fit.

C. Piston Design

The final detailed piston design, which satisfies the actuators functional requirements, is fabricated according to drawing FOG-RGC-13-1074. This is a double acting piston design which must maintain control pressure on the piston side and supply pressure on the rod side. A nominal 3/8 inch piston diameter and 9/32 inch rod diameter are selected. The piston and rod are sealed with standard size -010 and -007 Buna-N O-Ring seals. A 1/16 inch diameter roll pin, which is pressed into an interference fit hole in the piston, is used to connect to the crank. As shown on sheet 2 of drawing FOG-RGC-13-1074, the piston's internal portion has been drilled out. This was done to increase the actuator's control volume which was necessary to improve closed loop stability.

The nominal piston and rod diameter selection is influenced by the required actuator cross section and the desire to have an equal stall force in the extend and retract directions. In Paragraph III.A., it was determined that the actuator would be packaged within a 1/2 inch wide cross section. In order to reduce the crank lever arm, the largest possible piston diameter should be selected. The largest standard size piston seal which will package within the 1/2 cross section is 7/16 inch. The use of a 7/16 inch piston diameter results in a 0.031 inch cylinder wall thickness which eliminates the possibility of using a threaded insert to seal the cylinder. This requires that a smaller 3/8 inch piston diameter be selected. The rod diameter is selected to achieve an equal stall force in the extend and retract directions. The following equation is determined from the freebody diagram of the piston shown in Figure 14.

The critical stress for these loading conditions is a bending stress which occurs at section A-A and is given by,

$$\sigma = \frac{(0.075 \text{ in})(24.8 \text{ lb})\cos 20^\circ}{\left\{ \frac{(0.125 \text{ in})(0.062 \text{ in})^2}{6} \right\}}$$

$$\sigma = 21,800 \text{ psi}$$

Based on this, a 7075-T6 Aluminum Alloy would be an acceptable material. However, the sliding action of the piston pin against the crank may result in excessive wear of a soft material such as aluminum. Based on this consideration, 17-4 PH stainless steel, heat-treated to a hardness of Rockwell-C 43, is the selected crank material.

E. Ball Poppet Valve/Upstream Orifice Design

The ball poppet valve/upstream orifice, which was described in section 2c, is designed based on the specified no load slew rate of 1400°/sec. The required flow rate through either the charge or discharge valve to achieve this slew rate is determined from equation (11).

$$W_n = \frac{\pi^2 \omega P_c d_p^2 L}{720 R T_c \cos^2 \theta} \quad (11)$$

Substituting the following parameters into equation (11),

$$\omega = 1400^\circ/\text{sec}$$

$$P_c = 197 \text{ psia}$$

$$d_p = 0.375 \text{ in}$$

$$L = 0.50 \text{ in}$$

$$R = 640 \text{ (in-lb)/(lbm-}^\circ\text{R)}$$

$$T_c = 527^\circ\text{R}$$

$$\theta = 0^\circ$$

Results in a flow rate of $W_n = 7.88(10)^{-4} \text{ lb/sec.}$

The charge and discharge valve upstream orifice flow areas can now be determined based on the required flow rate. The equations used, (12) through (16), are derived in Appendix A of Reference [3]. The effective charge valve upstream orifice flow area is given by

$$A'_{12} = \frac{W_n \sqrt{T_1}}{C_1 P_1 N_{12}}$$

substituting the following parameters into equation (12).

$$W_n = 7.88(10)^{-4} \text{ lb/sec}$$

$$T_1 = 527^\circ \text{ R}$$

$$C_1 = 0.5318^\circ \text{R/sec}$$

$$P_1 = 415 \text{ psia}$$

$$N_{12} = 1.0 \text{ Assuming } P_2 = \text{Critical Pressure}$$

resulting in $A'_{12} = 8.20(10)^{-5} \text{ in}^2$. Assuming a discharge coefficient of 0.80 results in a charge valve upstream orifice diameter of 0.0114 in. The same procedure is used for the discharge valve except that $P_1 = 197 \text{ psia}$. This results in a discharge valve upstream orifice diameter of 0.0166 in. Based on these results, a #84 bit and a 0.42 mm bit were used to drill the charge and discharge orifices respectively.

The charge and discharge ball poppet valves are designed such that their flow area will not restrict the flow of gas through the upstream orifice. A sufficient valve flow area is achieved when the pressure between the valve and orifice is such that sonic flow occurs at the orifice. The minimum charge and discharge valve flow areas required are determined by,

$$A'_{23} = \frac{P_1 N_{12}}{P_2 N_{23}} A'_{12} \quad (13)$$

assuming the discharge coefficient of the valve and upstream orifice to be equal results in,

$$A_{23} = \frac{P_1 N_{12}}{P_2 N_{23}} A_{12} \quad (14)$$

for sonic flow to exist at the orifice $N_{12} = 1.0$ and $(P_1/P_2) \geq 1.89$ for $K = 1.4$. The parameter N_{23} is determined from,

$$N_{23} = \left\{ \frac{(P_3/P_2)^{2/K} - (P_3/P_2)^{(K+1)/K}}{(K+1)/(K-1)} \right\}^{1/2} \quad \text{For } \frac{P_3}{P_2} > \left(\frac{2}{K+1} \right)^{K/(K-1)} \quad (15a)$$

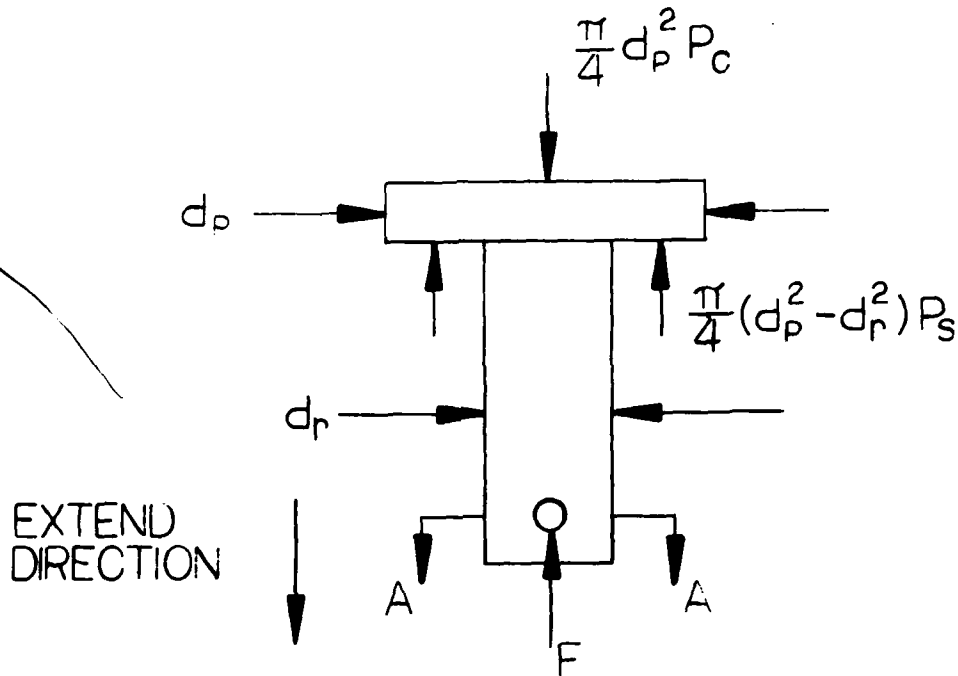


Figure 14. Piston freebody diagram.

$$F + \frac{\pi}{4} (d_p^2 - d_r^2) P_s = \frac{\pi}{4} d_p^2 P_c \quad (6)$$

For the case in which the piston is stalled in the extend direction, the control pressure (P_c) will become equal to the supply pressure (P_s) and the stall force will be,

$$F_s = \frac{\pi}{4} d_r^2 P_s \quad (7)$$

For the case in which the piston is stalled in the retract direction, the control pressure (P_c) will become equal to zero and the stall force will be,

$$F_s = - \frac{\pi}{4} (d_p^2 - d_r^2) P_s \quad (8)$$

equating the stall forces given by equations (7) and (8) results in,

$$\frac{\pi}{4} d_r^2 P_s = \frac{\pi}{4} (d_p^2 - d_r^2) P_s \quad (9)$$

$$d_r = \frac{d_p}{\sqrt{2}} \quad (10)$$

which for the 3/8 inch piston diameter requires a rod diameter $d_r = 0.265$ inches. Selection of the closest standard size rod seal results in a 9/32 inch rod diameter.

An analysis of the piston design in which the critical stresses are determined must be performed before the piston material is selected. The most severe loading occurs when the piston is stalled in the extend direction resulting in,

$$F_s = \frac{\pi}{4} (0.281 \text{ in})^2 (400 \text{ psig}) = 24.8 \text{ lb}$$

This causes a tensile stress in Section A-A of 2,250 psi. Based on this, the selected material 7075-T6 Aluminum, which has a yield strength of 70,000 psi, results in a large margin of safety.

D. Crank Design

The final detailed crank design, which satisfies the actuator's functional requirements, is fabricated according to drawing FOG-FGC-13-1082. A unique feature of the design is the crank/piston connection. A slot is machined into the crank to allow the piston pin to slide as the crank rotates. The tolerances are such that the maximum possible backlash is 0.23°. A 1/16 inch diameter roll pin secures the crank to the output shaft and a 1/16 inch diameter drill rod, which is epoxied to the crank, drives the potentiometer.

The nominal crank lever arm is selected based on the specified supply pressure and stall torque. The piston force available at stall is determined from equations 3-7 and 3-8 to be 24.8 lb extend and 19.4 lb retract. From this, a nominal crank lever arm of 1/2 inch is selected, resulting in a minimum stall torque of 9.7 in-lb which is 3.7 in-lb greater than the minimum requirement.

An analysis of the crank design in which the critical stresses are determined must be performed before the crank material can be selected. The most severe loading condition expected occurs when the actuator is stalled at 20° in the extend direction. The resulting loads are shown in Figure 15.

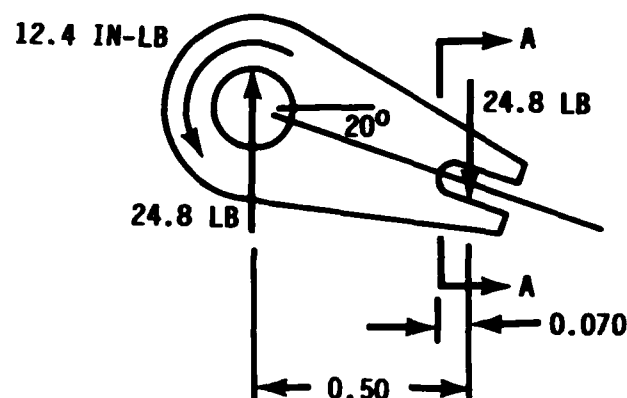


Figure 15. Crank freebody diagram.

$$N_{23} = 1.0 \text{ For } \frac{P_3}{P_2} \leq \left(\frac{2}{K+1} \right)^{K/(K-1)} \quad (15b)$$

by noting that

$$\frac{P_3}{P_2} = \left\{ \frac{P_3}{P_1} \right\} \left\{ \frac{P_1}{P_2} \right\} = \frac{P_3}{P_1} \quad (1.89) \quad (16)$$

for the charge valve $P_1 = 415$ psia and $P_3 = 197$ psia resulting in $N_{23} = 0.6256$. For the discharge valve $P_1 = 197$ psia and $P_3 = 15$ psia resulting in $N_{23} = 1.0$. Substituting these values into equation (14) results in a minimum required flow area of $3.14(10)^{-4}$ in² and $4.04(10)^{-4}$ in² for the charge and discharge valves respectively.

The preliminary design of the charge and discharge valves can now be completed based on the minimum required flow area and the expected solenoid performance. The primary solenoid parameters which effect the valve design are the internal return spring force and the magnetic pull force. The valve seat diameter is selected such that only 50% of the solenoid spring force will be required to hold the ball against the seat under worst case conditions. These conditions occur when the actuator is stalled resulting in a 400 psig pressure drop across the valve. Assuming a 2-lb solenoid spring force the seat diameter is determined by,

$$\frac{\pi}{4} d_s^2 (400 \text{ psig}) = (2 \text{ lb})(0.50) \quad (17)$$

which results in a seat diameter $d_s = 0.056$ inches. Based on this, the ball diameter of at least 3/32 inch is required to assure that the ball will not stick in the seat as was experienced with the first generation actuator valve design, which used a 0.048 inch seat diameter and a 1/16 inch ball diameter. The flow area of an ideal ball poppet valve is given by,

$$A_{23} = \frac{\pi d_s^2}{4} \left\{ \frac{(((2X/d_s) + \sqrt{(d_B^2/d_s^2) - 1})^2 + 1 - (d_B^2/d_s^2))}{(((2X/d_s) + (d_B^2/d_s^2) - 1)^2 + 1)^{1/2}} \right\} \quad (18)$$

from which the solenoid travel, necessary to achieve a valve flow area of $4.04(10)^{-4}$ in², is determined to be 0.0029 inch for the 0.056 seat diameter and 3/32 inch ball diameter. Based on this, it was specified that the solenoid magnetic force should exceed the spring force at a travel of at least 0.006 inch. This means that the valve will operate as desired at solenoid travels between 0.0029 inch and 0.0060 inch which is a much wider operating range than could be achieved without the upstream orifice.

The critical stresses which must be considered in the valve design are those caused by contact of the valve ball against the solenoid push rod and valve seating surface. The stresses experienced during operation are a

fluctuating type ranging from zero when the valve is opened to a maximum value when the valve closes. This type of loading causes fatigue and will result in permanent deformation after a finite number of cycles causing an undesirable increase in solenoid travel. To determine the stresses which occur and the number of operating cycles before permanent deformation occurred would be impractical and require many simplifying assumptions. Therefore the valve seating surface area will be determined based on the static stress caused by the 2.0 lb solenoid spring. In the first generation actuator valve design, this stress was 1250 psi. To maintain the same stress in this design, a valve ball height as shown in Figure 16 is required. The valve seat material is the same as that used for the first generation actuator valve seats. The solenoid push rod is fabricated from 440c stainless steel heat-treated to Rockwell-C 58-60 as used in the first generation actuator valve design. Since the push rod stresses in this value are lower than those in the first generation actuator design, no permanent deformation should occur.

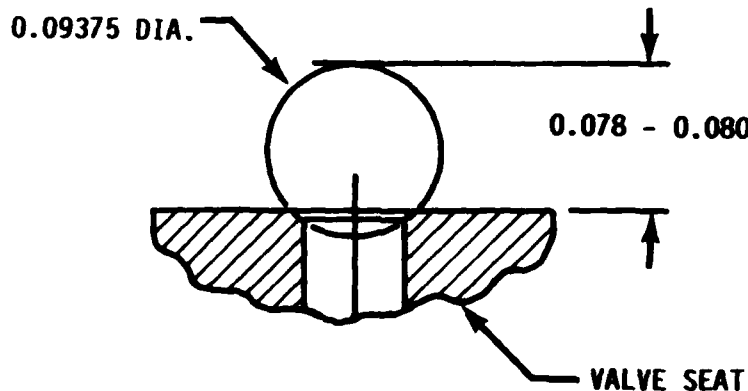


Figure 16. Ball valve height.

F. Ball Poppet Valve/Upstream Orifice Revisions

The initial Ball Poppet Valve/Upstream Orifice design which used a 0.0115 inch diameter charge valve upstream orifice results in a charge no-load slew rate of 1740°/sec. Based on this, the orifice was resized according to the ratio,

$$\frac{d_o^2}{(0.0115 \text{ in})^2} = \frac{(1400^\circ/\text{sec})}{(1740^\circ/\text{sec})}$$

which results in $d_o = 0.0103$ inch. Tests using the resized charge orifice resulted in a charge slew rate of 1520°/sec, which is still slightly greater than specified. The charge orifice was resized again to $d_o = 0.0098$ inch which resulted in a charge slew rate of 1376°/sec as specified. The discharge orifice was resized in a similar manner to a diameter of 0.0150 inches which resulted in a discharge slew rate of 1440°/sec.

The initial solenoid design, which is fabricated according to source control drawing FOG-RCG-13-1089, specified a 1/2 inch coil length. Testing of this design by the solenoid manufacturer, resulted in a magnetic pull force of 2.0 lb at a 0.006 inch travel. Since the specified spring force at 0.006 inch travel is 1.8 lb to 2.2 lb, the solenoid operation would be marginal. Therefore the revised design increased the coil length to 1.0 inch in order to increase the magnetic pull force. Results from testing of the revised design are shown in Figure 17. Notice that at a 0.0060 inch travel, the solenoids magnetic pull force is 3.3 lbs which is 1.1 lb greater than the maximum spring force.

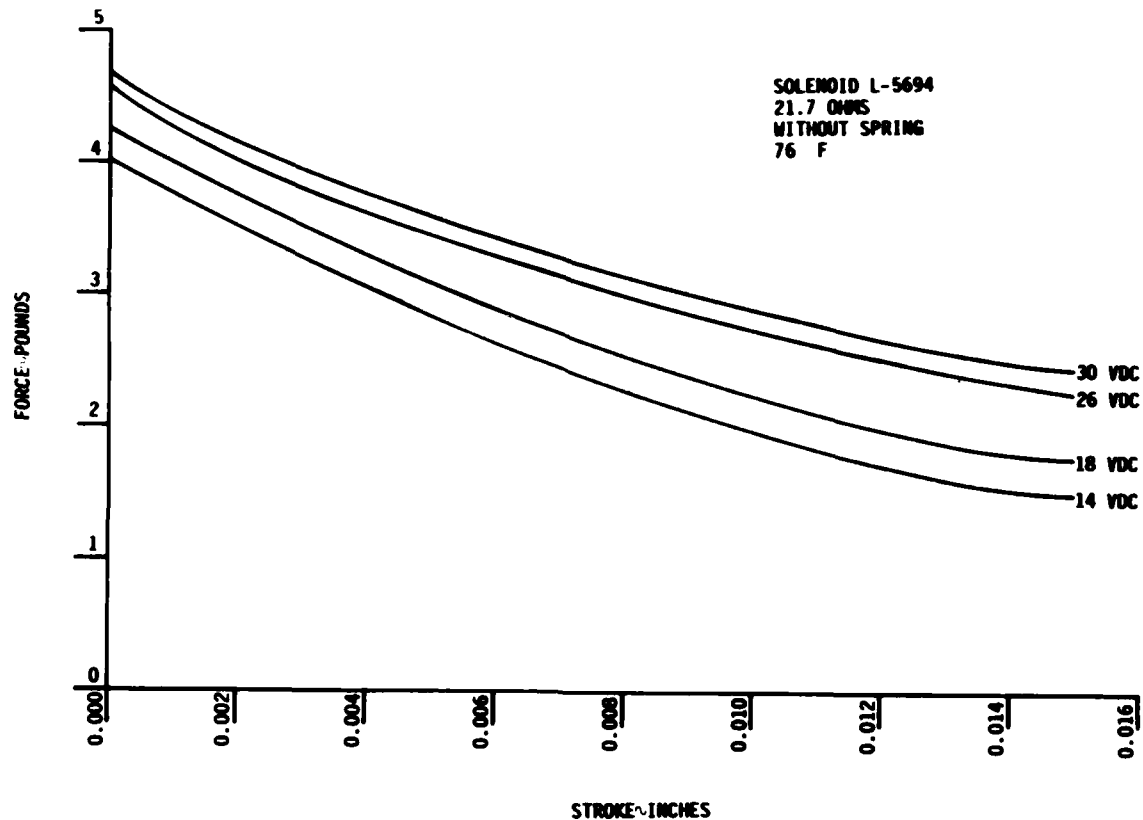


Figure 17. Solenoid force versus stroke.

During pre-flight testing of actuators SN-007 and SN-009, it was discovered that the charge valves had an occasional tendency to stick partially open causing excessive gas consumption. The following analysis was performed in an attempt to determine the cause of this problem. When the valve begins to close, it is possible that unbalanced pressure forces could cause the ball to contact the seating surface as shown in Figure 18. This would result in forces acting on the ball as shown in Figure 19. For static equilibrium to exist along the Y-axis requires that,

$$\sum F_y = F_{ss} \cos \alpha - F_{pr} \cos \alpha - \frac{1}{2} F_{ss} \sin \alpha - \frac{1}{2} R = 0 \quad (19)$$

Since static equilibrium must exist along the X-axis, this requires that,

$$\Sigma F_x = F_{pr} \sin \alpha - F_{ss} \sin \alpha - \mu_1 F_{ss} \cos \alpha + R = 0 \quad (20)$$

Multiplying equation (20) by μ_2 and rearranging terms results in,

$$\mu_2 R = \mu_2 F_{ss} (\mu_1 \cos \alpha + \sin \alpha) - \mu_2 F_{pr} \sin \alpha \quad (21)$$

Assuming that $\mu_1 = \mu_2 = \mu$ and combining equation (19) and (21) results in,

$$F_{pr} = \frac{F_{ss}}{(\cos \alpha - \mu \sin \alpha)} \left\{ (1 - \mu^2) \cos \alpha - 2 \mu \sin \alpha \right\} \quad (22)$$

which is an expression for the pressure force required to cause the ball valve to stick open. Substituting known parameters $F_{ss} = 2.0$ lb and $\alpha = 50^\circ$ into equation (22) reveals that zero pressure force (F_{pr}) is required to maintain static equilibrium for $\mu \geq 0.36$. The initial valve design used a stainless steel seat and a tungsten carbide ball, which unlubricated has a friction coefficient greater than that required to cause stiction. In order to correct this problem without changing the valve geometry, it is necessary to reduce the friction coefficient. This was done by coating the valve seat and solenoid push rod with a heat curing teflon and lubricating the ball with a light weight oil, which should reduce the friction coefficient to $\mu = 0.08$.

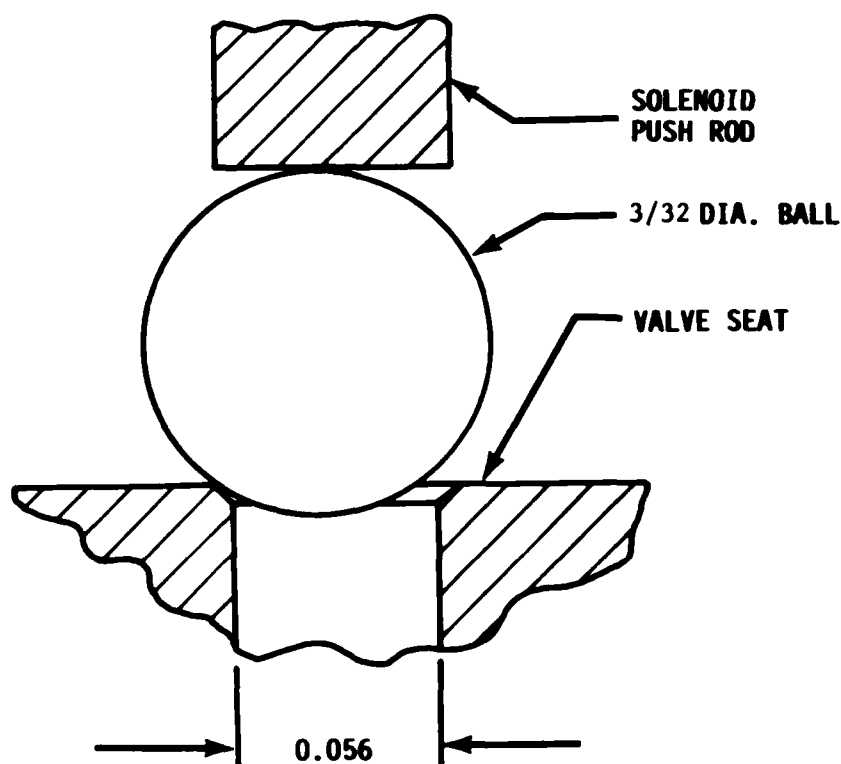


Figure 18. Ball valve stuck in open position.

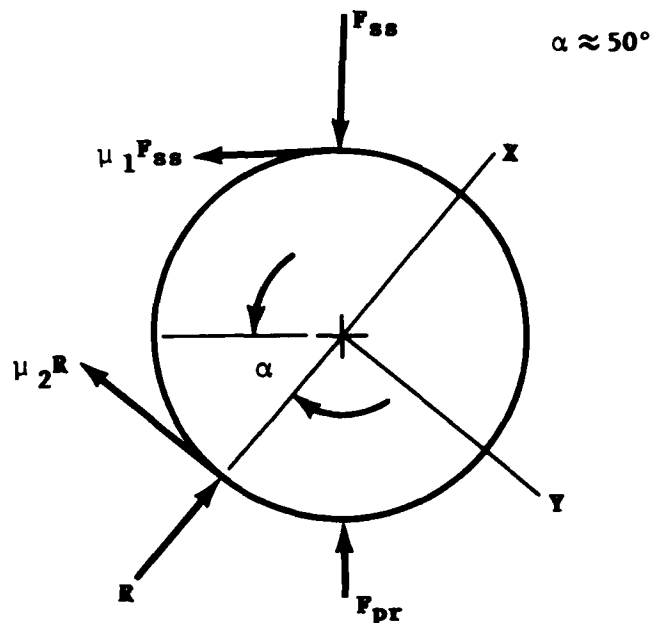


Figure 19. Ball freebody diagram.

Substituting this into equation (22) reveals that a pressure force of $F_{pr} = 1.78$ lb is required to maintain static equilibrium. Since the maximum pressure force possible is 1.0 lb, the ball valve should not be able to stick open.

Further testing of actuators SN-007 and SN-009 with the modified valves, revealed that the ball stiction problem was eliminated.

G. Housing Design

The actuator housing incorporates the previously described hardware into a single unit which must interface with the missile and operate as described in paragraph II.B. The final detailed design is fabricated according to drawing FOG-RGC-13-1076. The housing is attached to the missile by a single #8-32 fastener threaded into a pad which is epoxied to the missile exterior skin as shown in Figure 10. A 1/8 inch diameter nylon tube, which is connected to the housing with a modified Legris LF-3000 cartridge fitting, supplies gas at a regulated pressure of 400 psig.

An analysis to determine the proposed actuator mounting safety is performed based on the specified minimum 15 lbs shear and 60 in-lbs bending capability. From the freebody diagram in Figure 20, where reaction forces R_1 and R_2 represent fastener loads, it is evident that,

$$\begin{aligned} R_1 &= 15 \text{ lbs} \\ R_2 &= R_3 = 105 \text{ lbs} \end{aligned}$$

Since the resulting fastener stresses caused by these loads are 7,500 psi tensile and 1,300 psi shear a SAF grade 1 fastener will provide the necessary strength for this application.

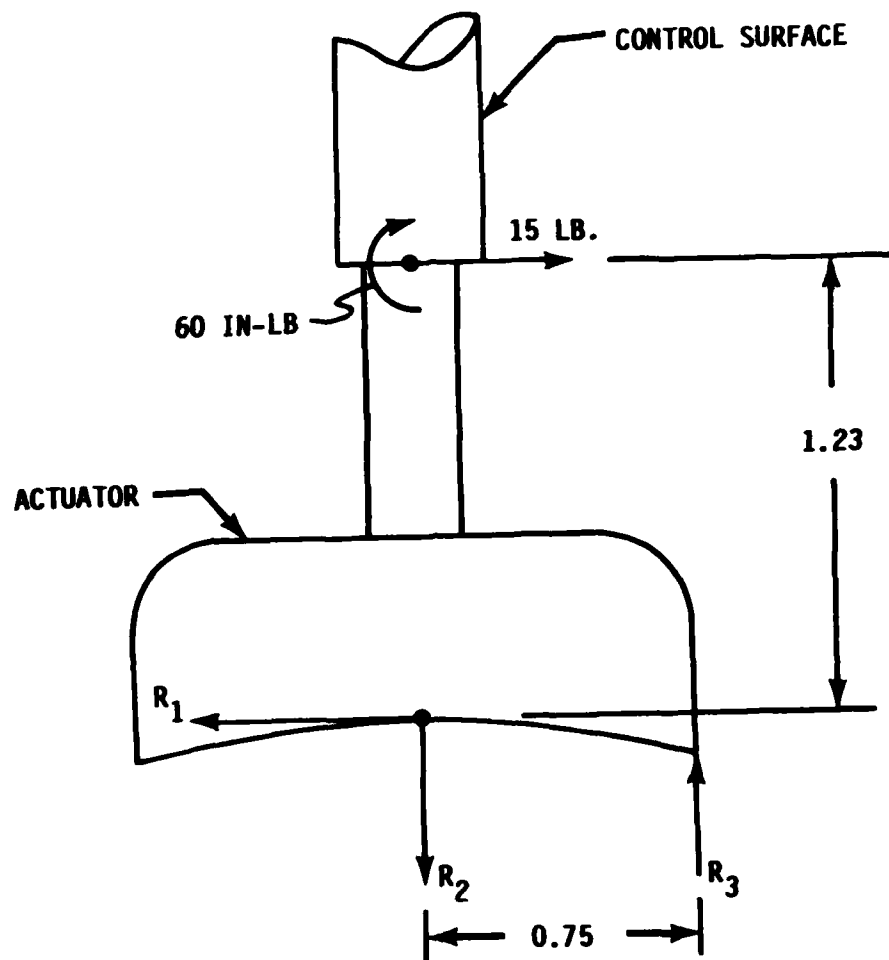


Figure 20. Actuator structural loads.

IV. TEST RESULTS

The second generation FOG-M actuator unit SN-018 was tested at the nominal operating conditions to verify that the preliminary design requirements listed in paragraph II.B. were satisfied. A summary of the actuators performance is presented in Table 4. A diagram of the test setup is shown in Figure 21 along with a photograph of the actual hardware in Figure 22. A schematic of the electronic control circuit is shown in Figure 23. The actuators slew rates were measured as shown in Figures 24 and 25 using a 30° P-P square wave input command at 1 Hz. The actuators hysteresis was measured as shown in Figure 26 using a 2° P-P sine wave input command at 1 Hz. The actuators frequency responses at peak-to-peak amplitudes of 1°, 3° and 6° are shown in Figures 27, 28 and 29 respectively. The actuator has an electrical gain of 2.0 due to the difference between the input and output scale factors. Therefore the frequency response magnitude curves should be normalized at approximately 6dB. Typical responses to a sine wave at various input amplitudes and frequencies are shown in Figures 30 through 38. Typical responses to a 1 Hz square wave input at various amplitudes are shown in Figures 34 through 42.

Environmental testing was performed over the specified -25 °F to +140 °F temperature range. The actuator and pneumatic power supply were subjected to the temperature controlled environment with the electronic control unit maintained at room temperature. The supply pressure and solenoid voltage were set at the nominal values of 400 psig and 28V. The actuator deadzone was set to 0.10 degrees. A summary of the results from testing of actuator SN-002 is presented in Table 5 with example data shown in Figures 43 through 52. This actuator used a housing which had been anodized and then sealed with a Sodium Dicromate solution. Notice from the test results in Table 5 that the 1° P-P bandwidth is below the preliminary design requirement of 6 Hz at the colder temperatures. The suspected cause of this problem was an increase in piston seal friction caused by changes in the piston seal lubrication (Parker Super-O-Lube) properties. In an attempt to improve this condition, a second actuator SN-002-T was tested. This actuator used a housing which had been hard anodized and then sealed with a teflon solution. Testing was done with no load slew rates between 1300 - 1500 Deg/S and a 0.10 degree deadzone. A summary of the results from testing of actuator SN-002-T is presented in Table 6 with example data shown in Figures 53 through 58. Notice the improvement in 1° P-P bandwidth at the colder temperatures.

The gas consumption of actuator SN-002 was measured using a sinewave input at various amplitudes and frequencies with a 0.10 degree and 0.50 degree deadzone. Results from these measurements are listed in Tables 7 and 8 along with an estimate of the bottle volume required to sustain four actuators for a 100 second flight. This estimate assumes that the stored gas remains at a constant temperature and is reduced from an initial pressure of 4700 psig to a final pressure of 800 psig.

The static stiffness of actuator SN-002 with a 0.50 degree deadzone is shown in Figures 59, 60 and 61 for supply pressures of 300 psig, 350 psig and 400 psig respectively. From these figures, it is seen that the actuator reaches the required stall torque of 6 in-lb at a ± 0.25 degree deflection angle.

A total of 15 second-generation FOG-M actuators have been assembled and performance tested at the nominal operating conditions with a 0.10 degree deadzone. A summary of the performance test data is presented in Tables 9 and 10. Actuator serial numbers 002, 003, 004 and 005 were used as workhorse units for hardware-in-the-loop simulations. They performed without problems for an excess of 75 simulated flights with an average gas consumption per 60 sec flight of 0.80 in³ at 5000 psig. Actuator serial numbers 006, 007, 008 and 010 were used on FOG-M flight MIL-5. They performed successfully until a 50 Hz, 40° P-P control surface flutter occurred at approximately 2 secs into the flight. Possible causes for this problem were discussed in the shaft/bearing revisions of section III.A. Actuator serial numbers 011, 013, 015 and 018 were prepared for use on FOG-M flight MIL-6 but were not used because the exact cause of the flutter problem had not been determined.

TABLE 4. Actuator SN-018 Performance Summary.

<u>Parameter</u>	<u>Performance</u>	<u>Figure</u>
Charge Slew Rate	1376°/sec	4-2
Discharge Slew Rate	1440°/sec	4-3
Hysteresis	0.10°	4-4
<u>Frequency -3dB</u>		
1° P-P	9.0 Hz	4-5
3° P-P	13.5 Hz	4-6
6° P-P	15.0 Hz	4-7
<u>Frequency -90° Phase</u>		
1° P-P	8.9 Hz	4-5
3° P-P	13.5 Hz	4-6
6° P-P	15.5 Hz	4-7
Stall Torque	12.0 Hz	4-38

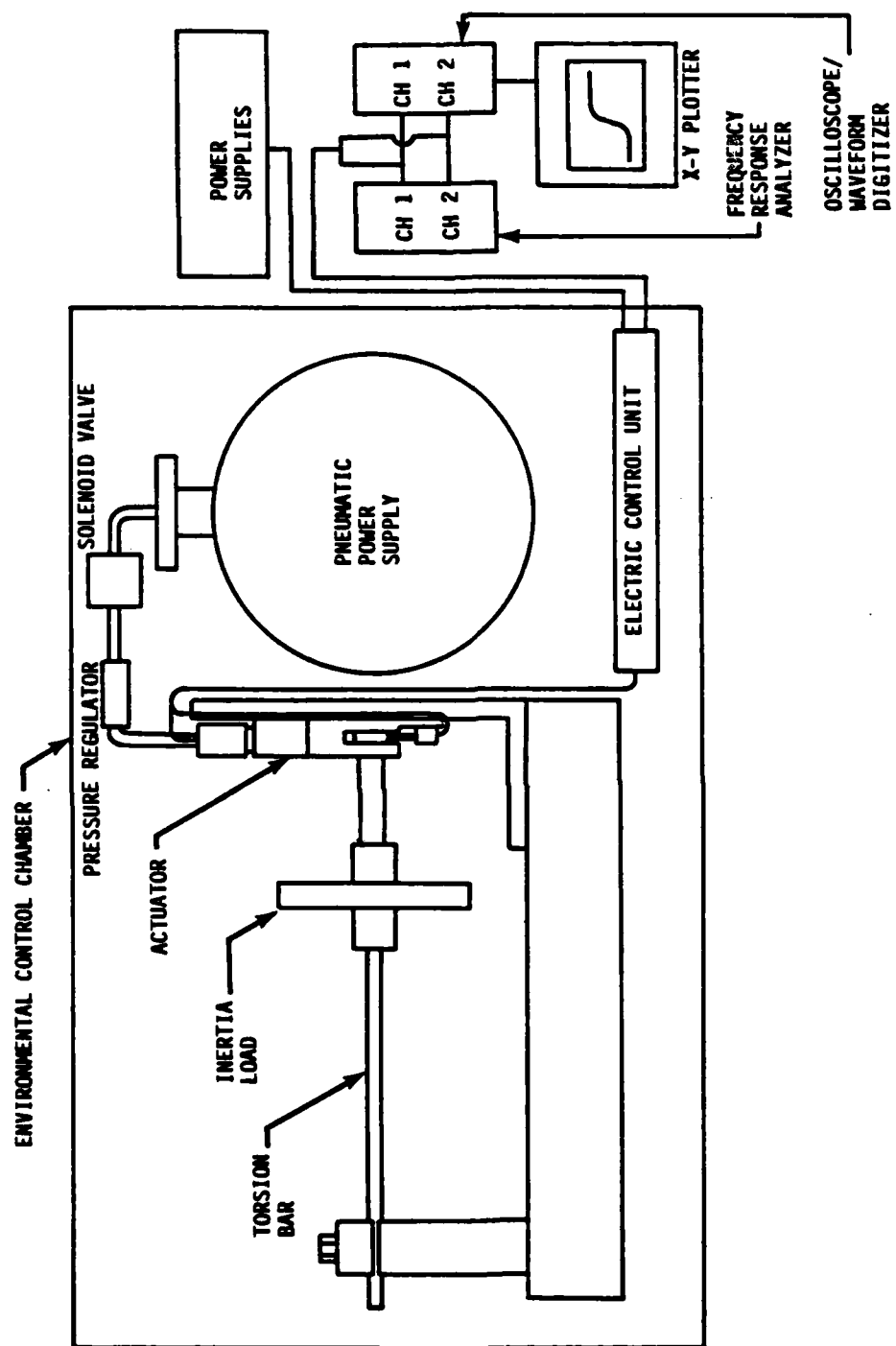


Figure 21. Actuator test set-up.

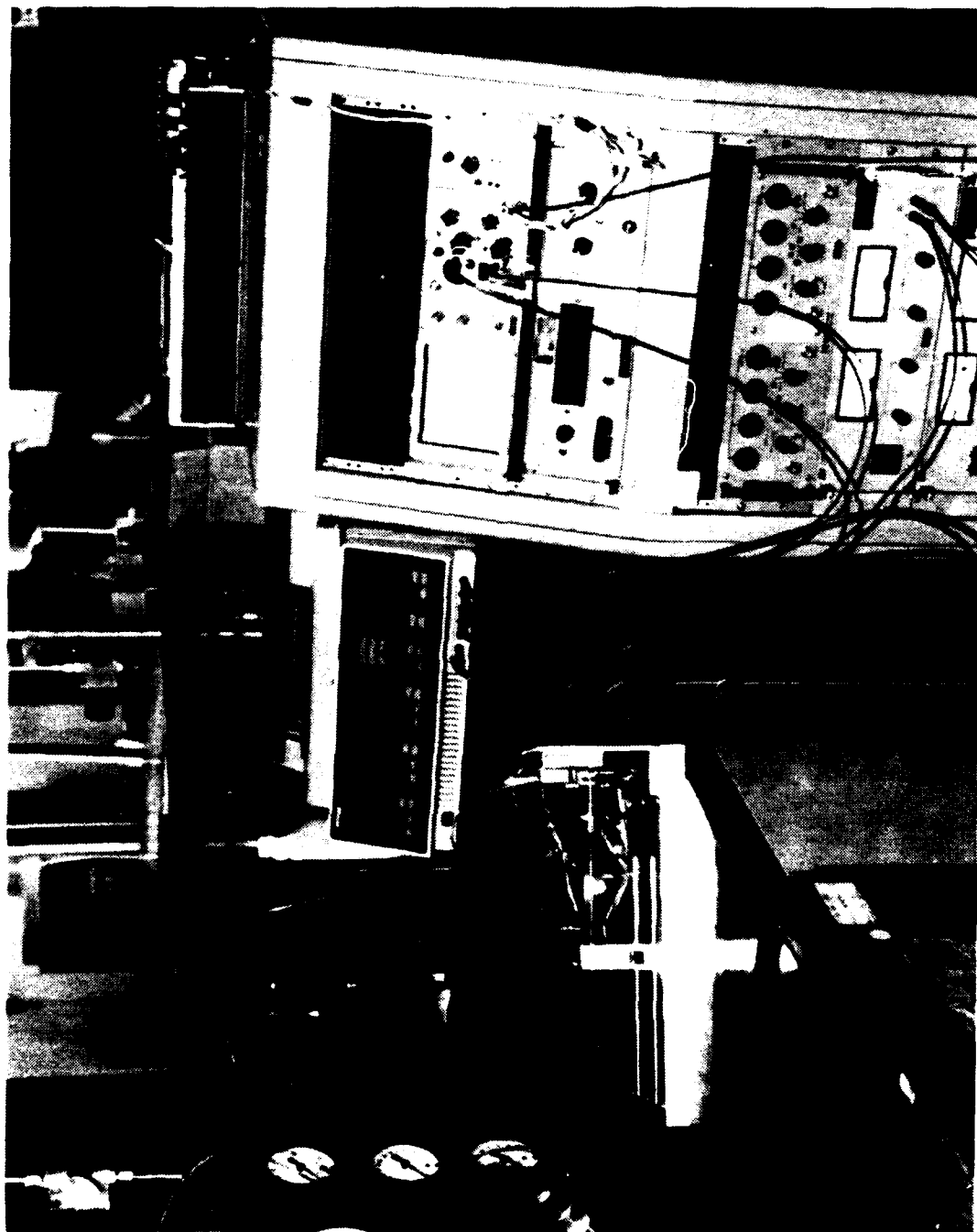
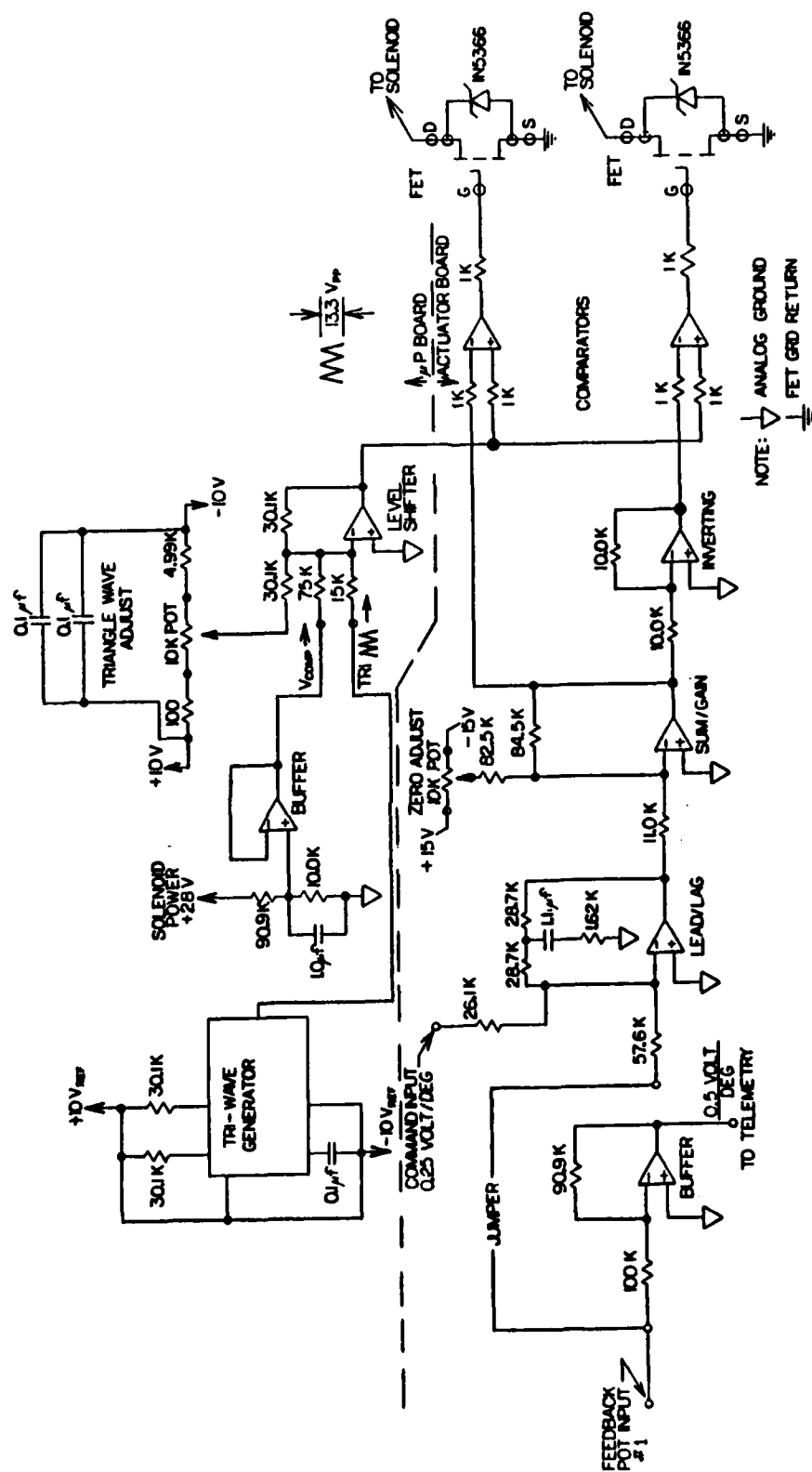


Figure 22. Actuator Test Set-Up.



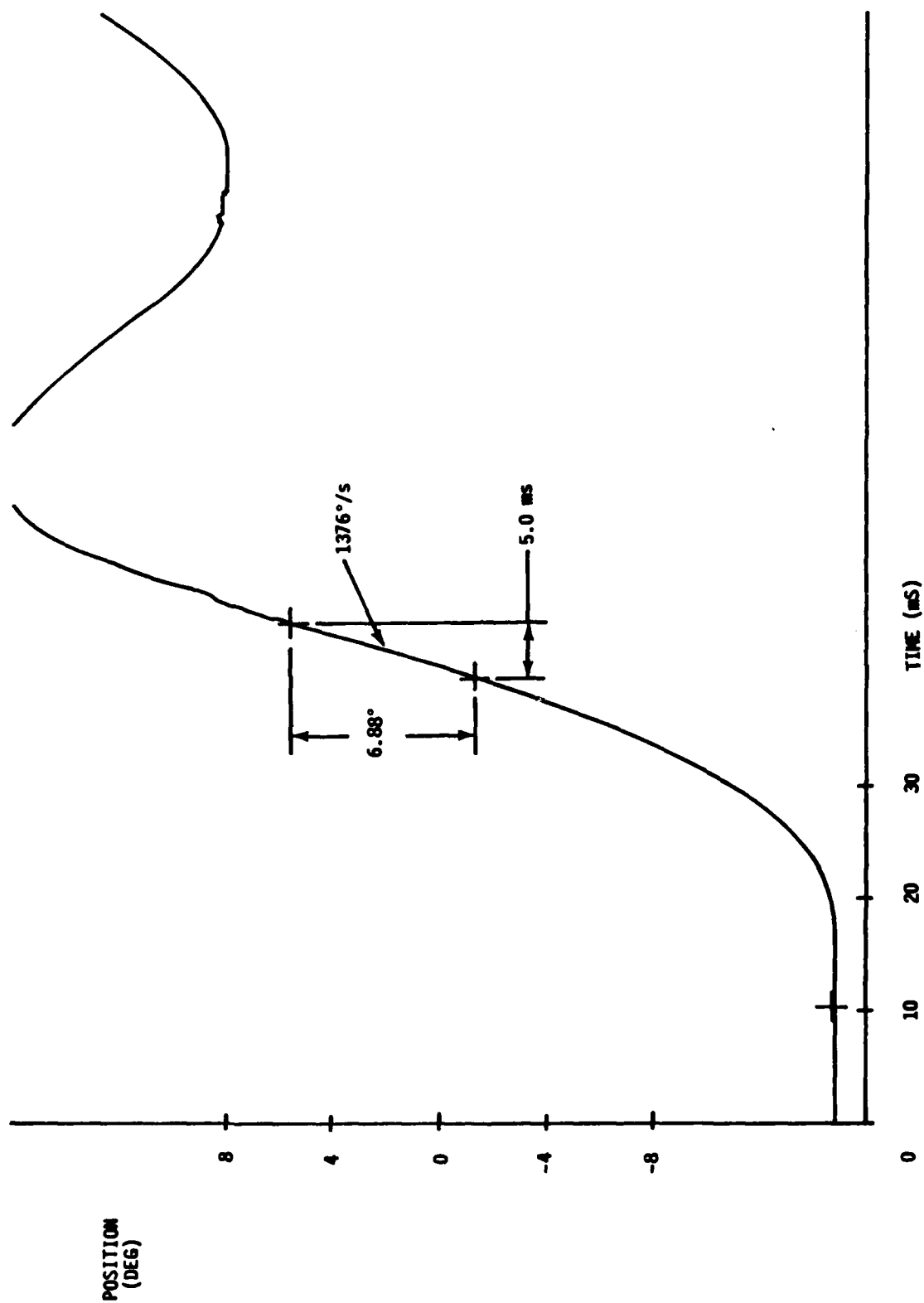


Figure 24. Charge slew rate actuator SN-018 -
0.62 in²-lb inertia load.

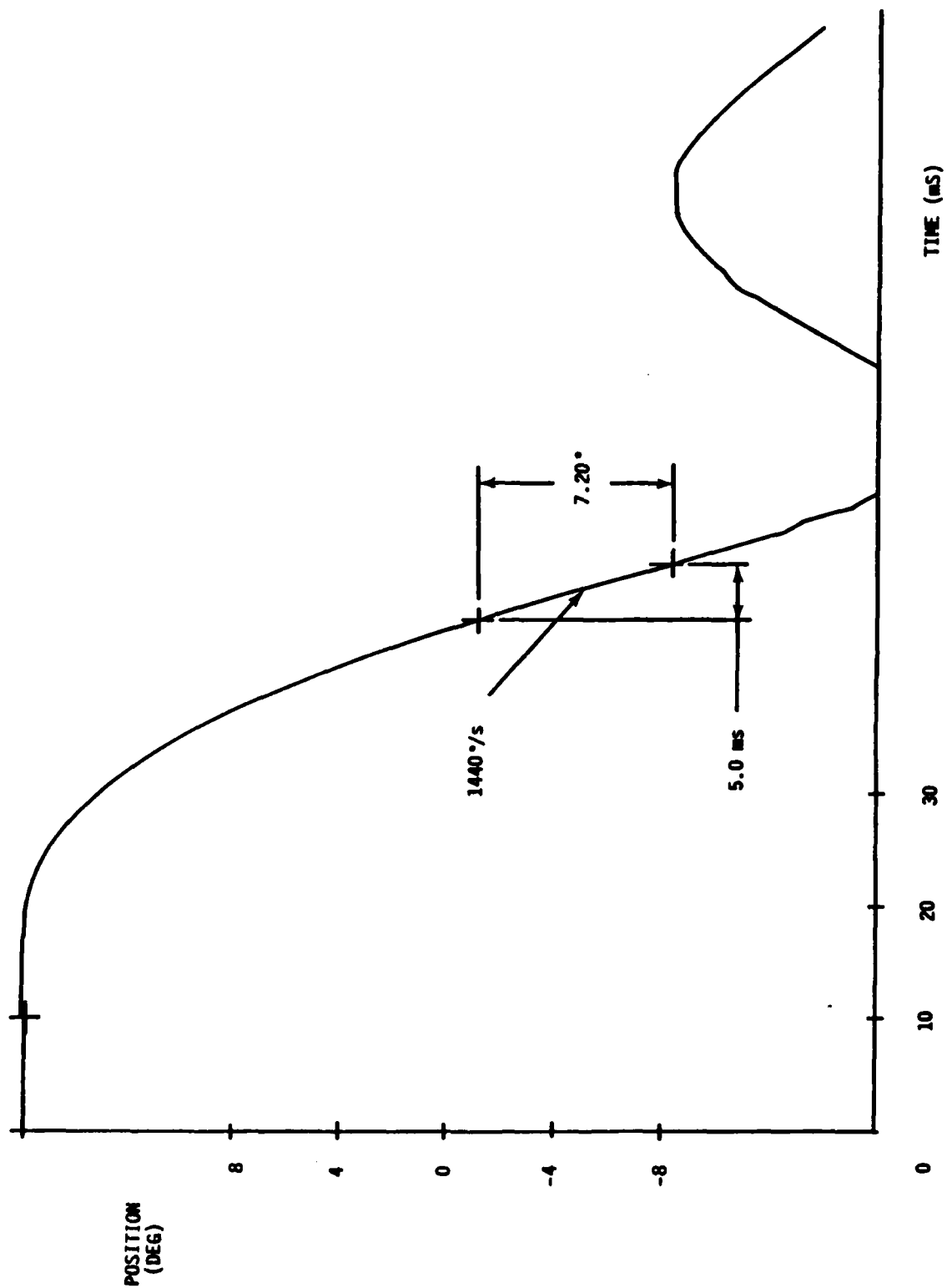


Figure 25. Discharge slew rate actuator SN-018 -
0.62 in²-lb inertia load.

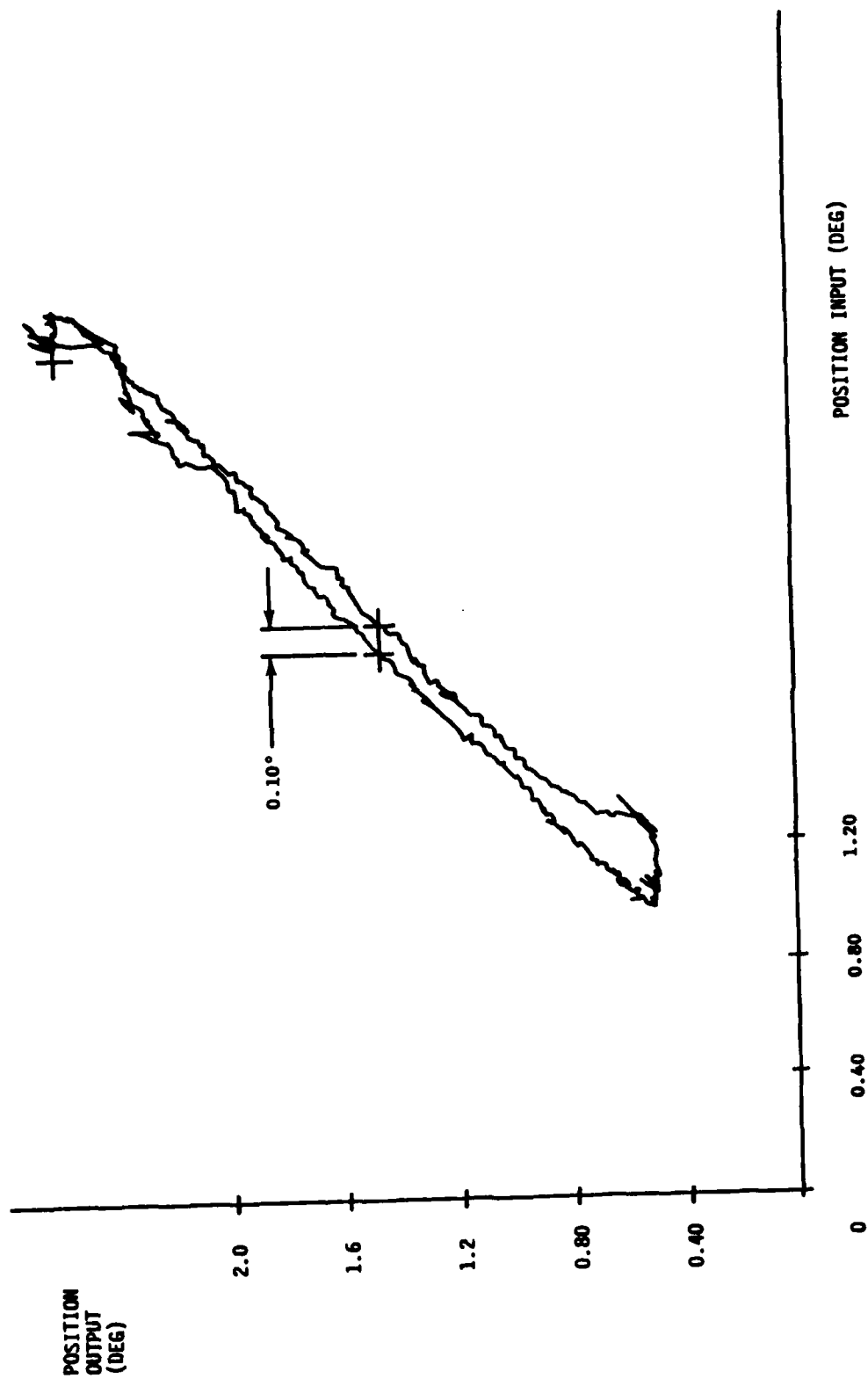


Figure 26. Hysteresis actuator SN-018 -
0.62 in²-lb inertia load,
0.30 in-lb/deg hinge load.

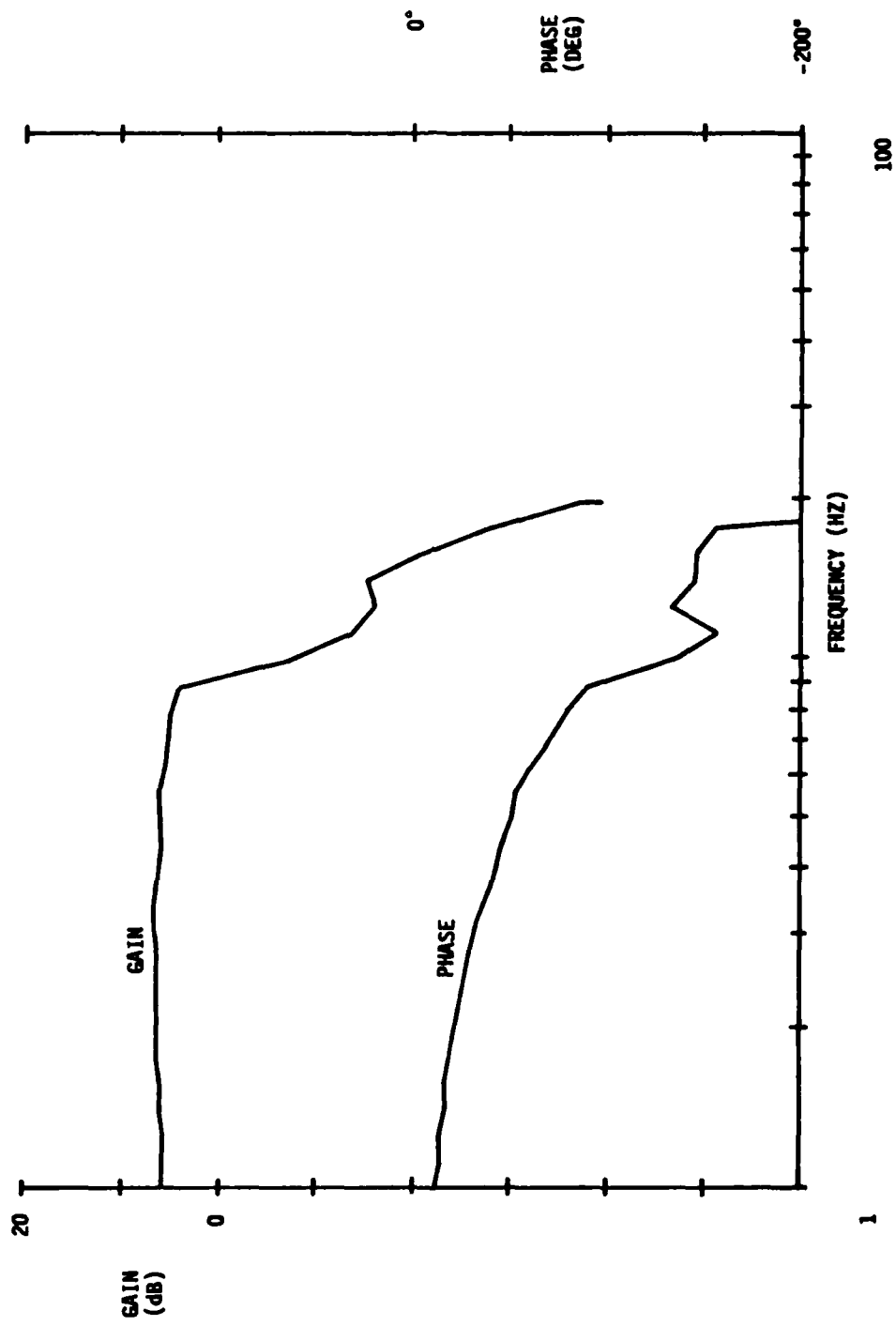


Figure 27. 1° P-P frequency response actuator SN-018 -
 0.62 in²-lb inertia load,
 0.30 in-lb/deg hinge load.

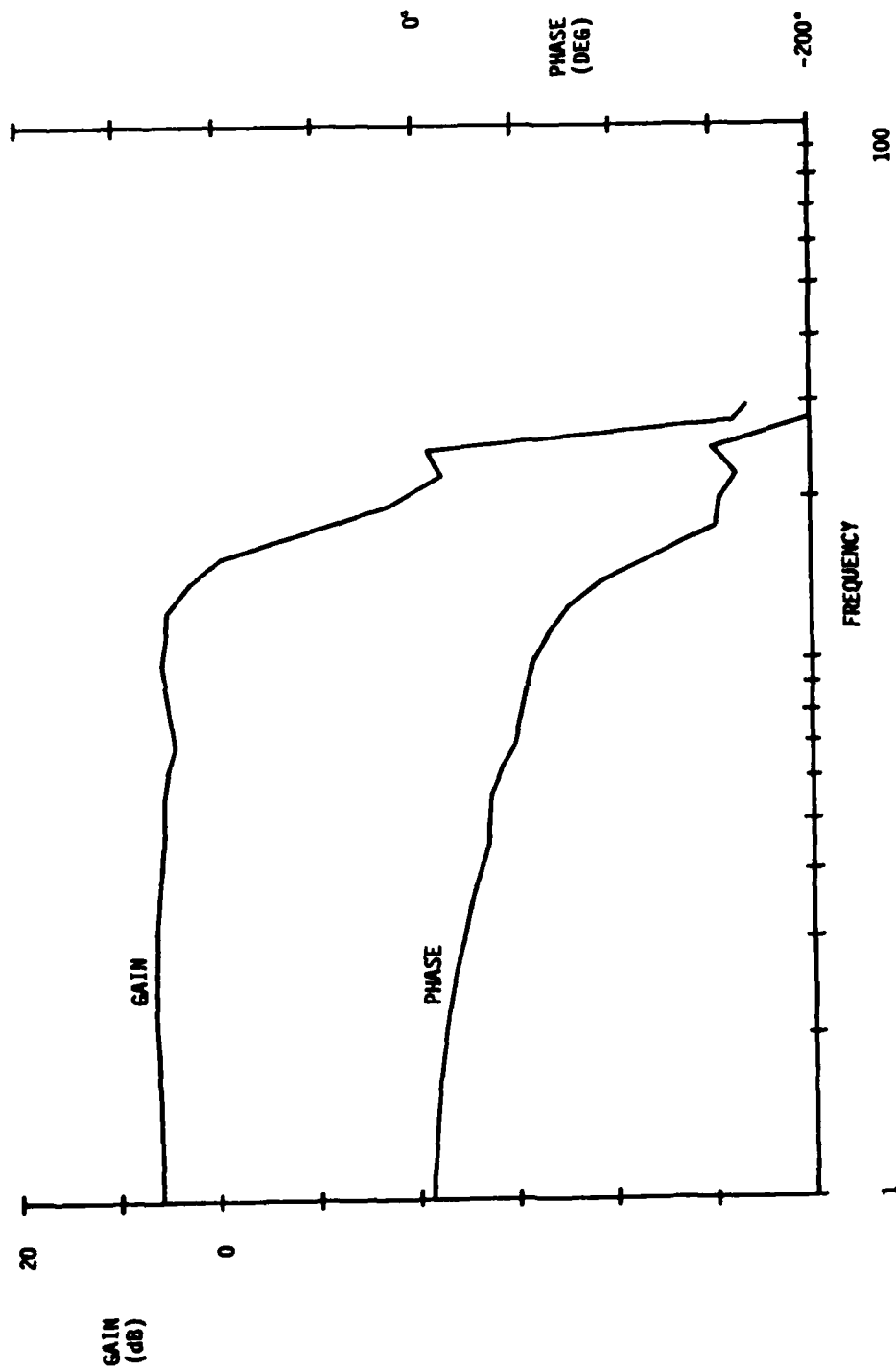


Figure 28. 3° P-P frequency response actuator SN-018 -
0.62 in-lb inertia load,
0.30 in-lb/deg hinge load.

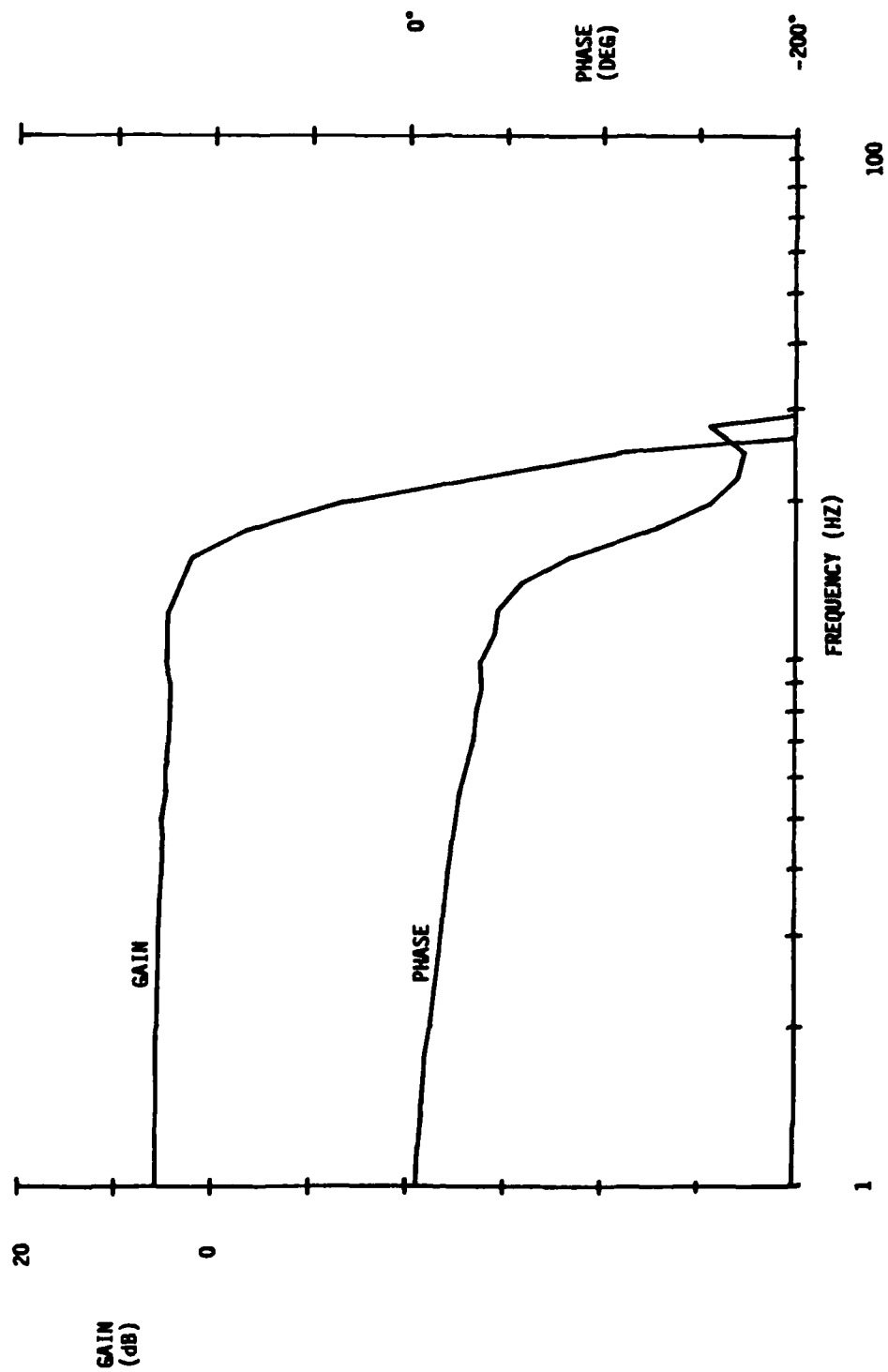


Figure 29. 6° P-P frequency response actuator SN-018 -
0.62 in²-lb inertia load,
0.30 in-lb/deg hinge load.

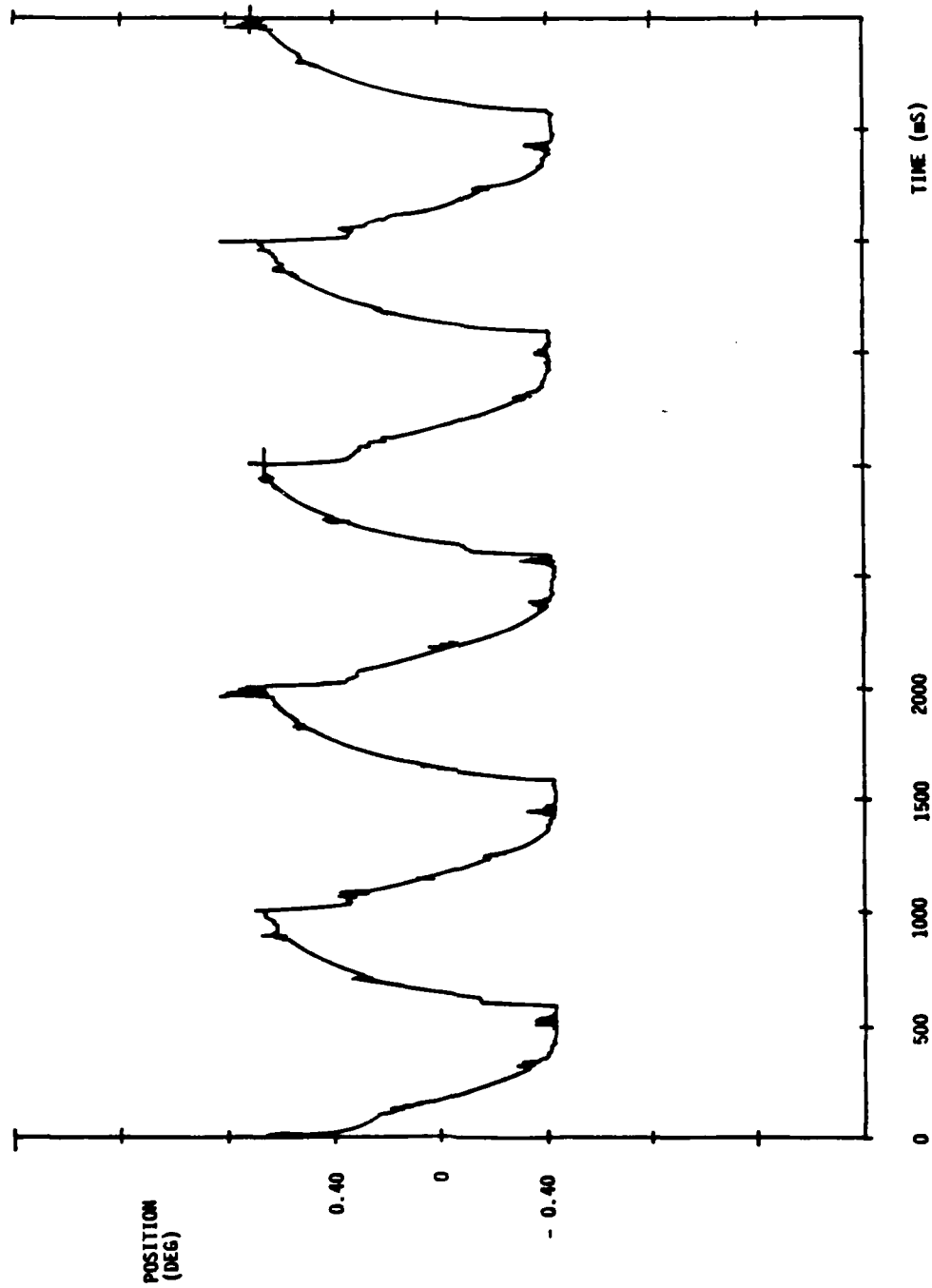


Figure 30. 1° P-P sine wave output at 1 Hz actuator SN-018 -
0.62 in²-lb inertia load,
0.30 in-lb/deg hinge load.

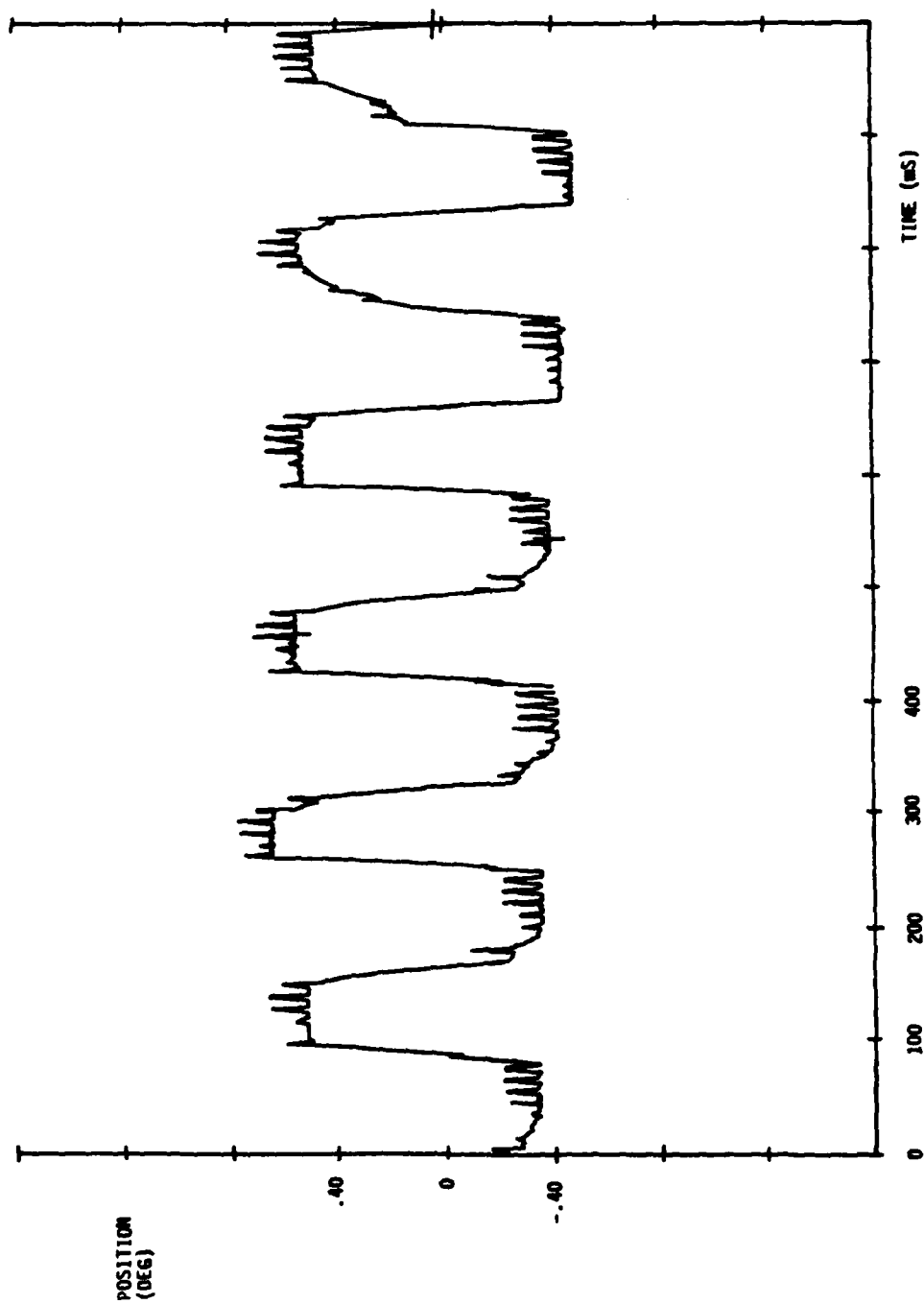


Figure 31. 1° P-P sine wave output at 6 Hz actuator SN-018 -
0.62 in²-lb inertia load,
0.30 in-lb/deg hinge load.

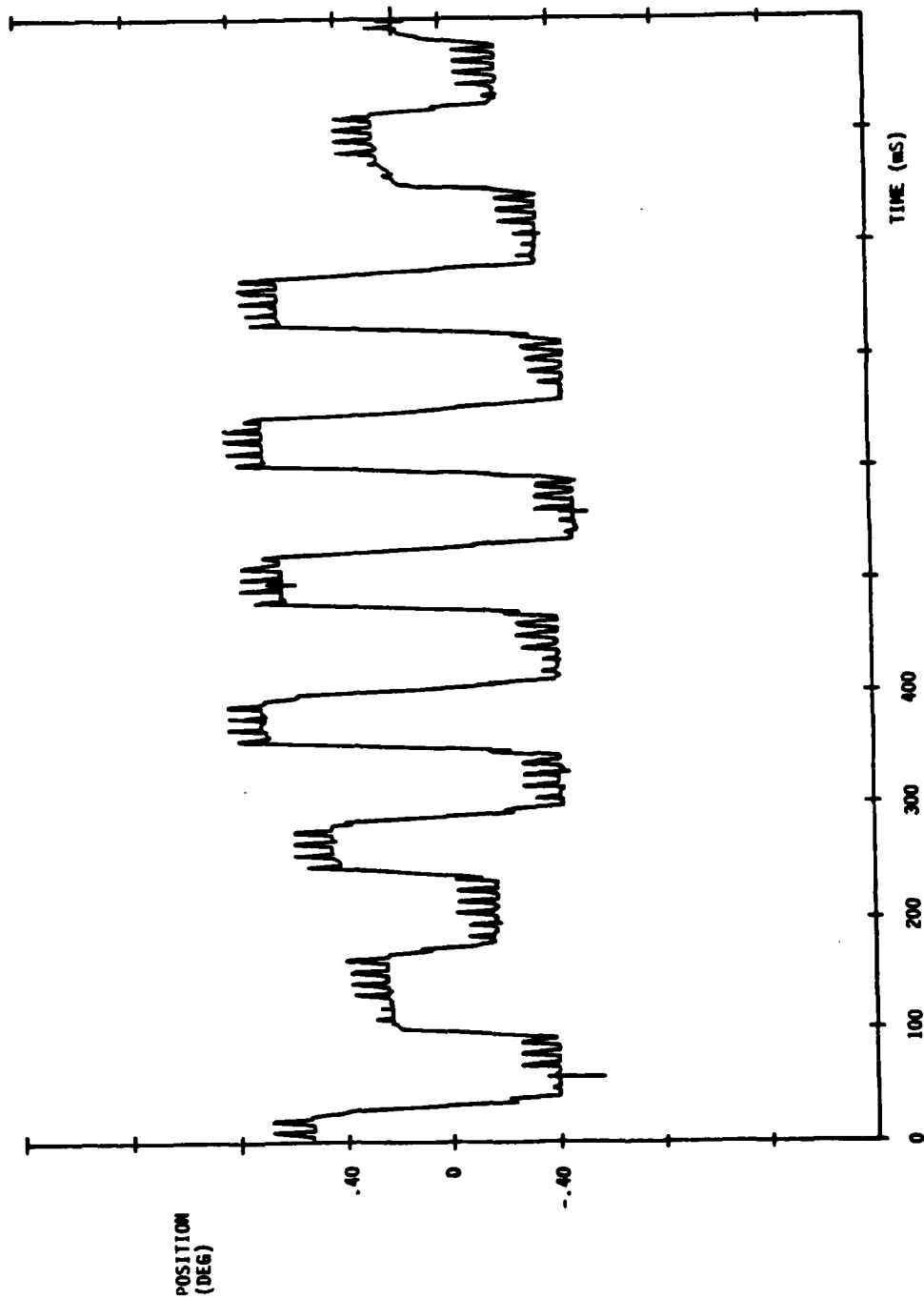


Figure 32. 1° P-P sine wave output at 8 Hz actuator SN-018 -
0.62 in²-lb inertia load,
0.30 in-lb/deg hinge load.

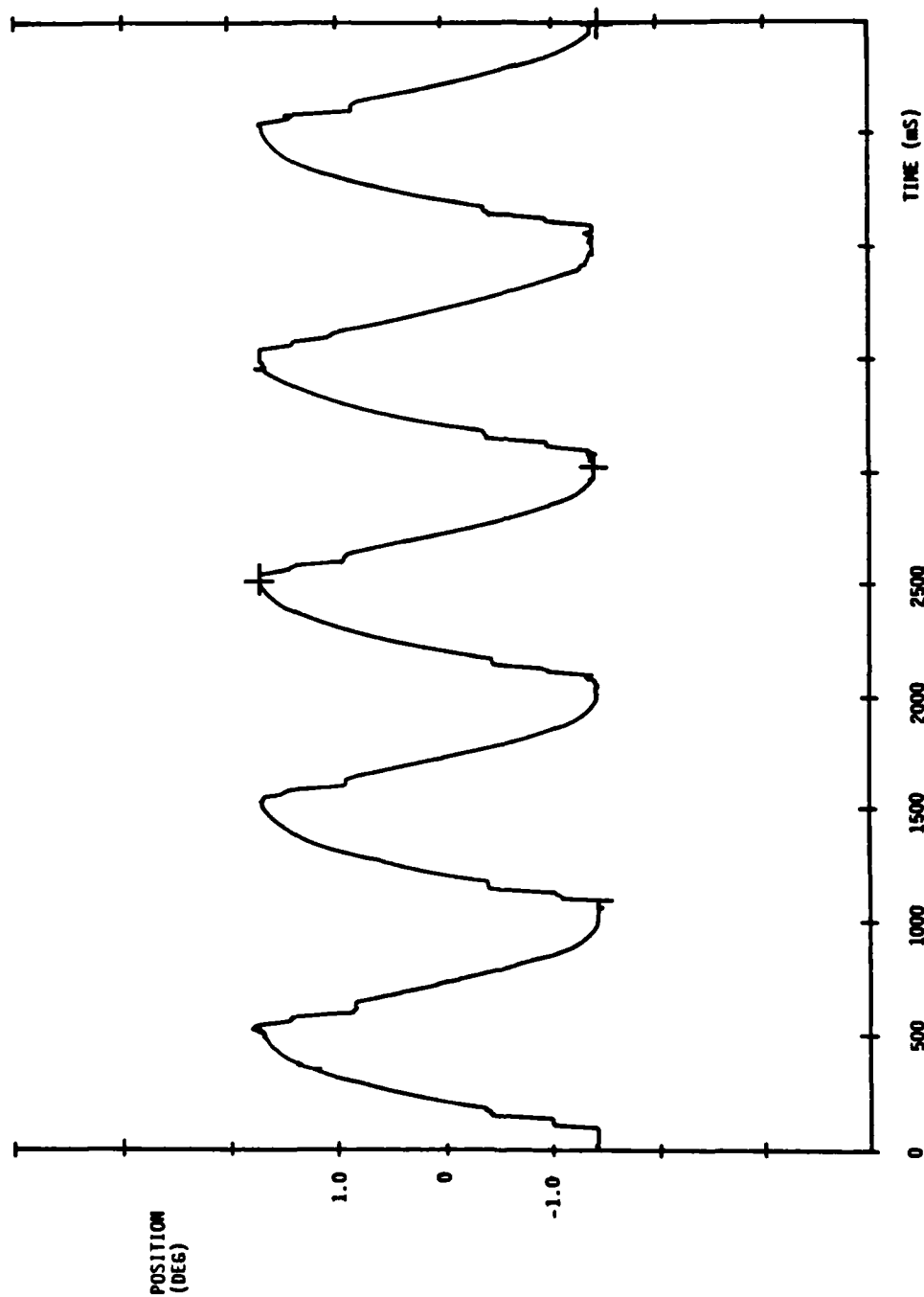


Figure 33. 3° P-P sine wave output at 1 Hz actuator SN-018 -
0.62 in-lb inertia load,
0.30 in-lb/deg hinge load.

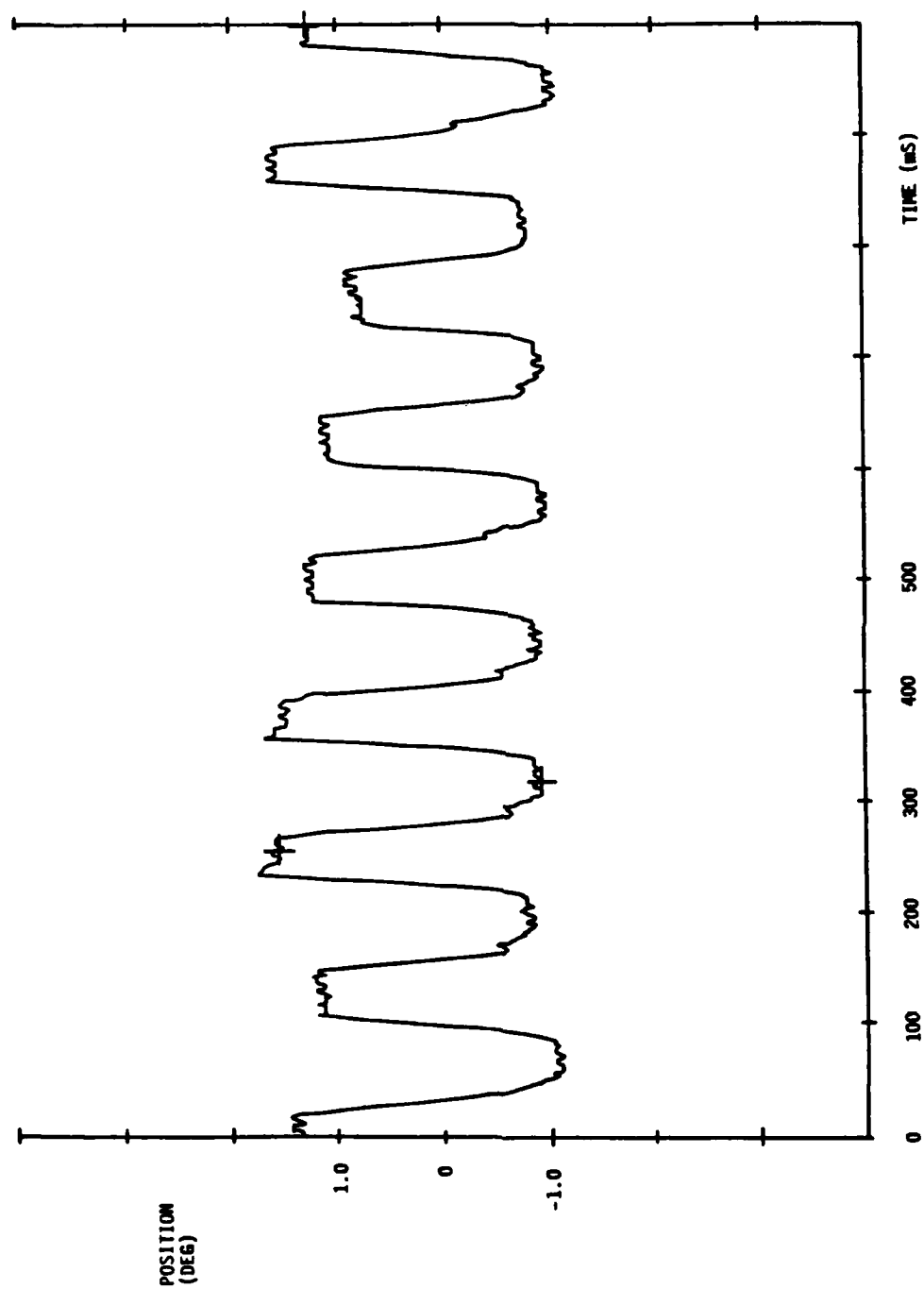


Figure 34. 3° P-P sine wave output at 8 Hz actuator SN-018 -
0.62 in²-lb inertia load,
0.30 in-lb/deg hinge load.

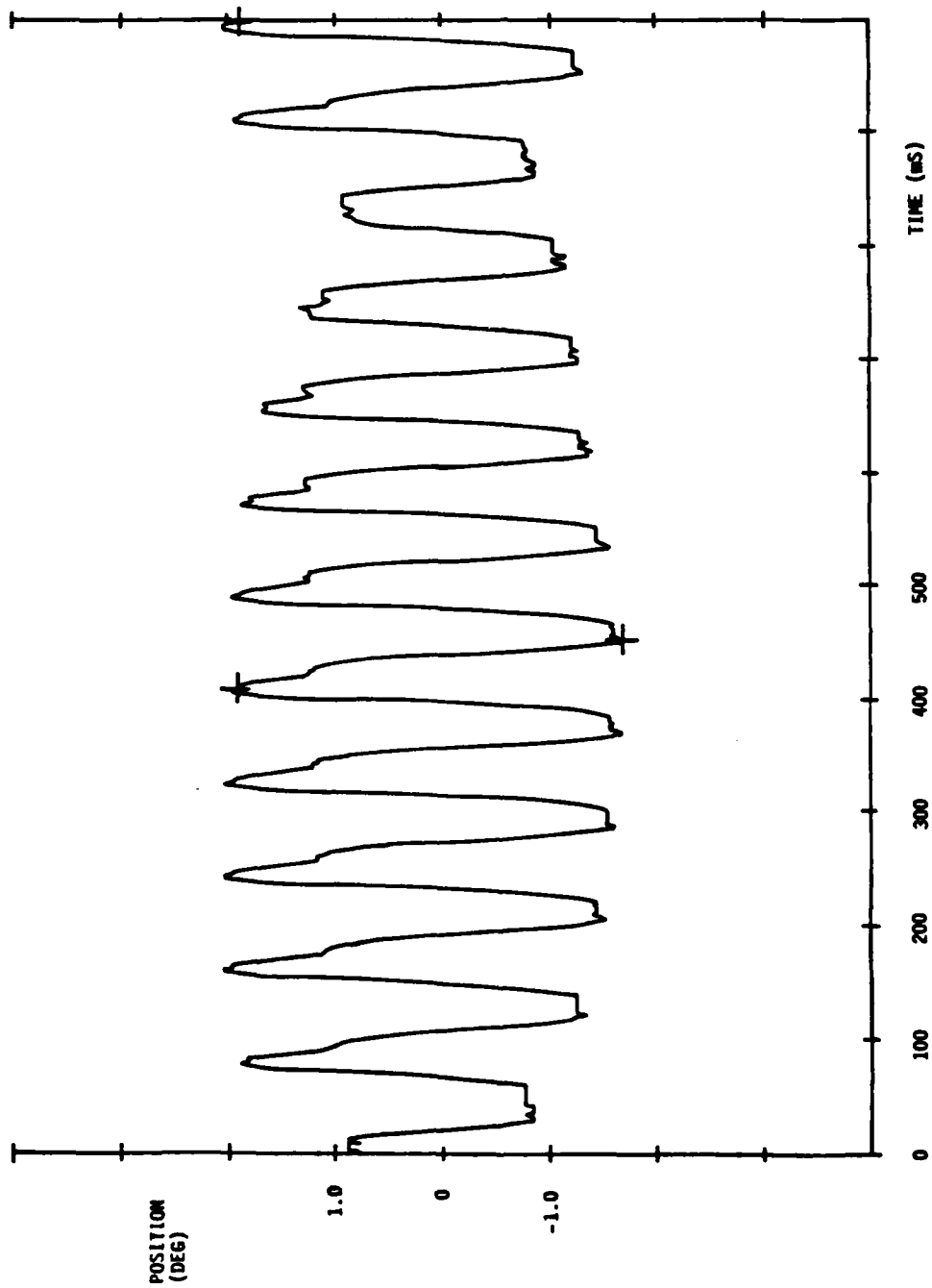


Figure 35. 3° P-P sine wave output at 12 Hz actuator SN-018 -
0.62 in²-lb inertia load,
0.30 in-lb/deg hinge load.

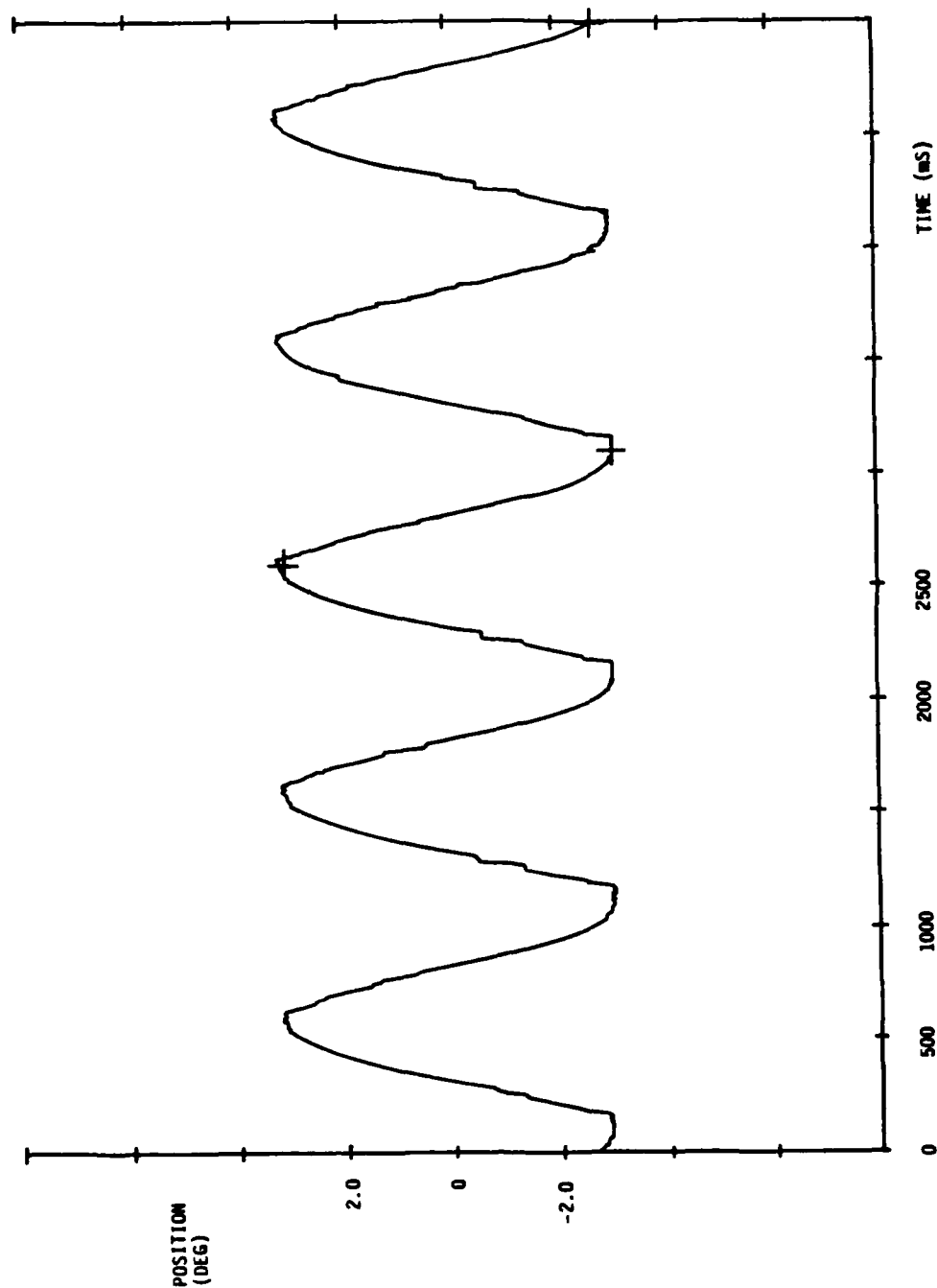


Figure 36. 6° P-P sine wave output at 1 Hz actuator SN-018 -
0.62 in²-lb inertia load,
0.30 in-lb/deg hinge load.

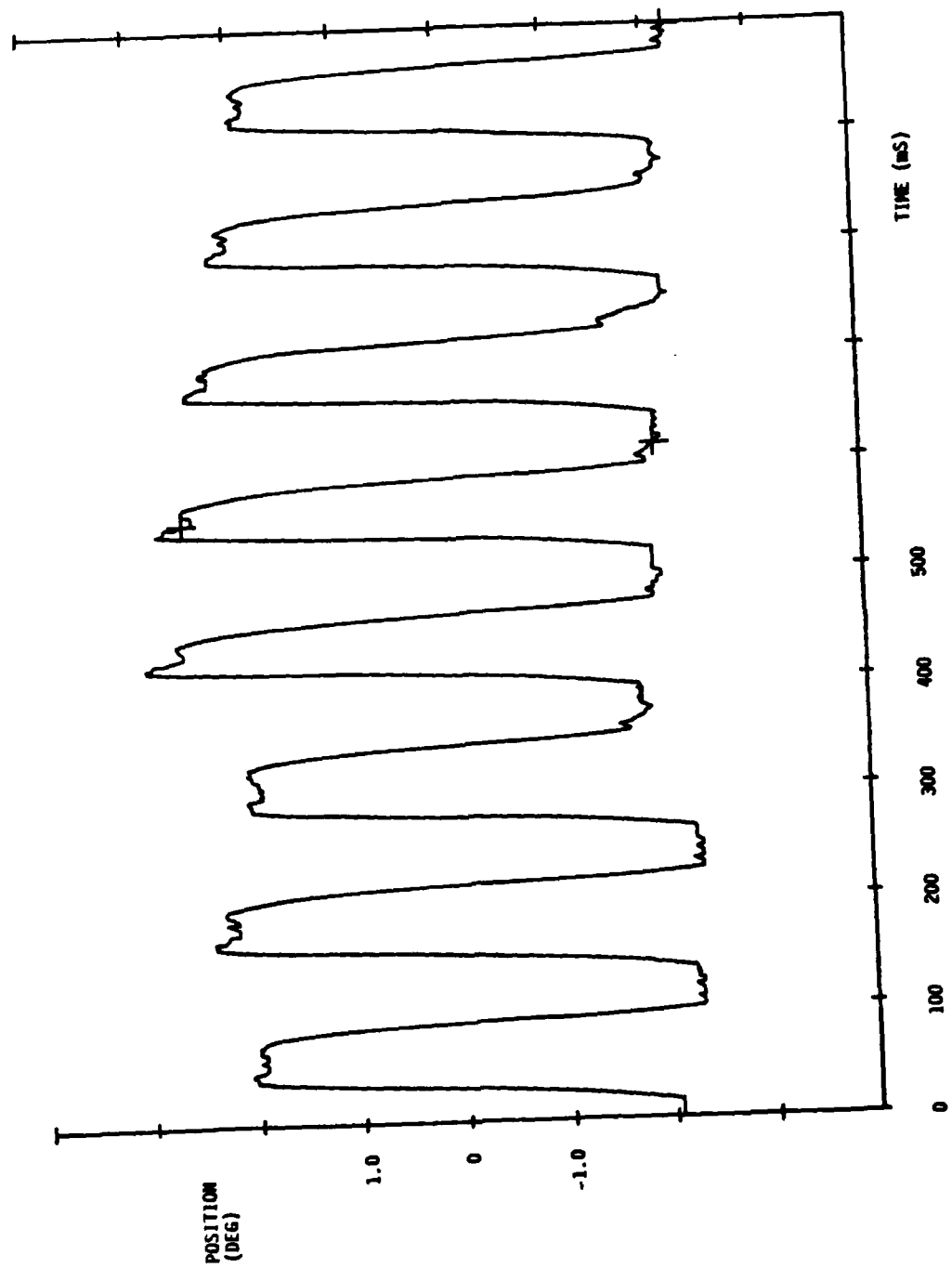


Figure 37. 6° p-p sine wave output at 8 Hz actuator SN-018 -
0.62 in²-lb inertia load,
0.30 in-lb/deg hinge load.

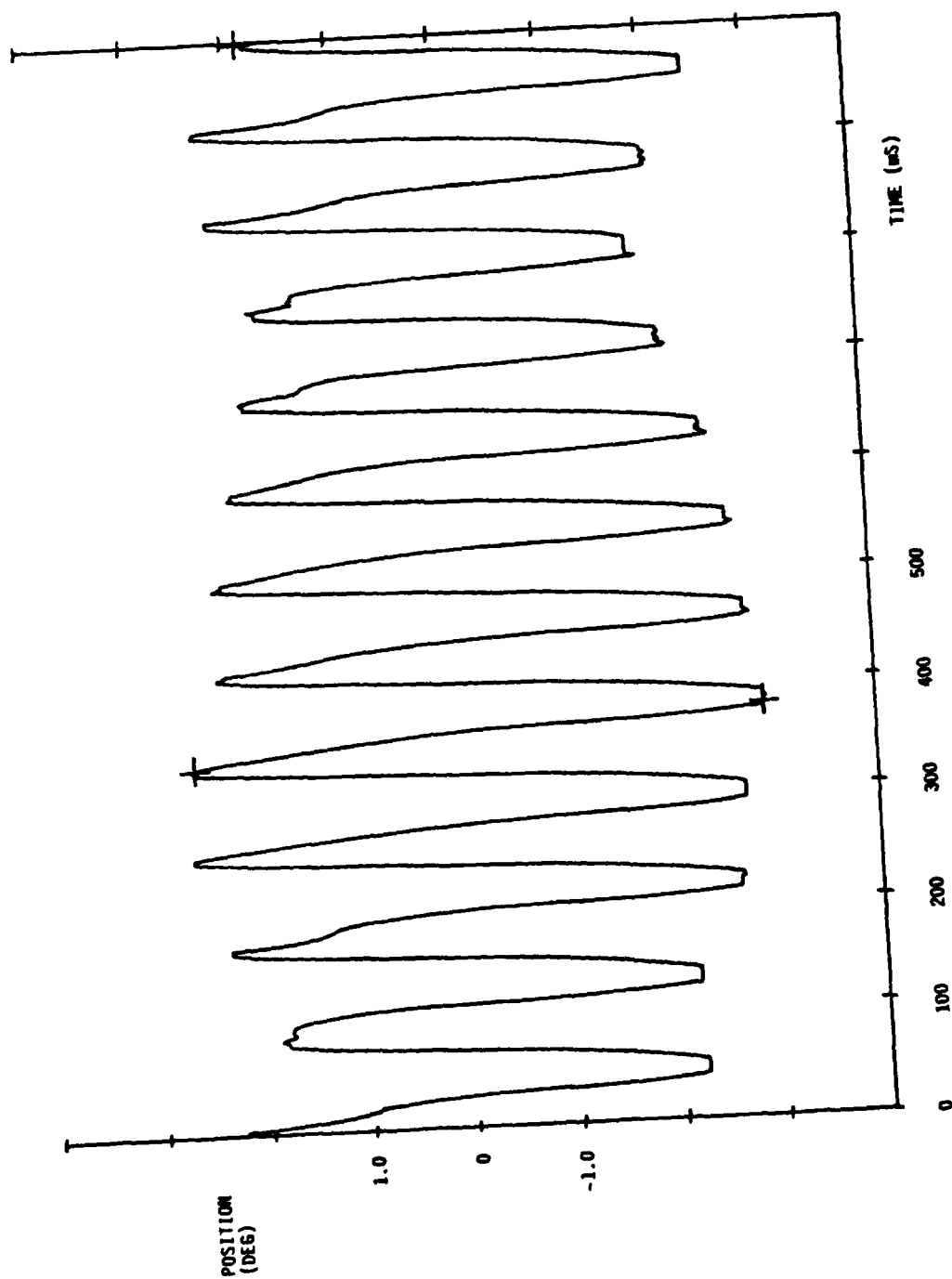


Figure 38. 6° p-p sine wave output at 12 Hz actuator SN-018 -
0.62 in -lb inertia load,
0.30 in-lb/deg hinge load.

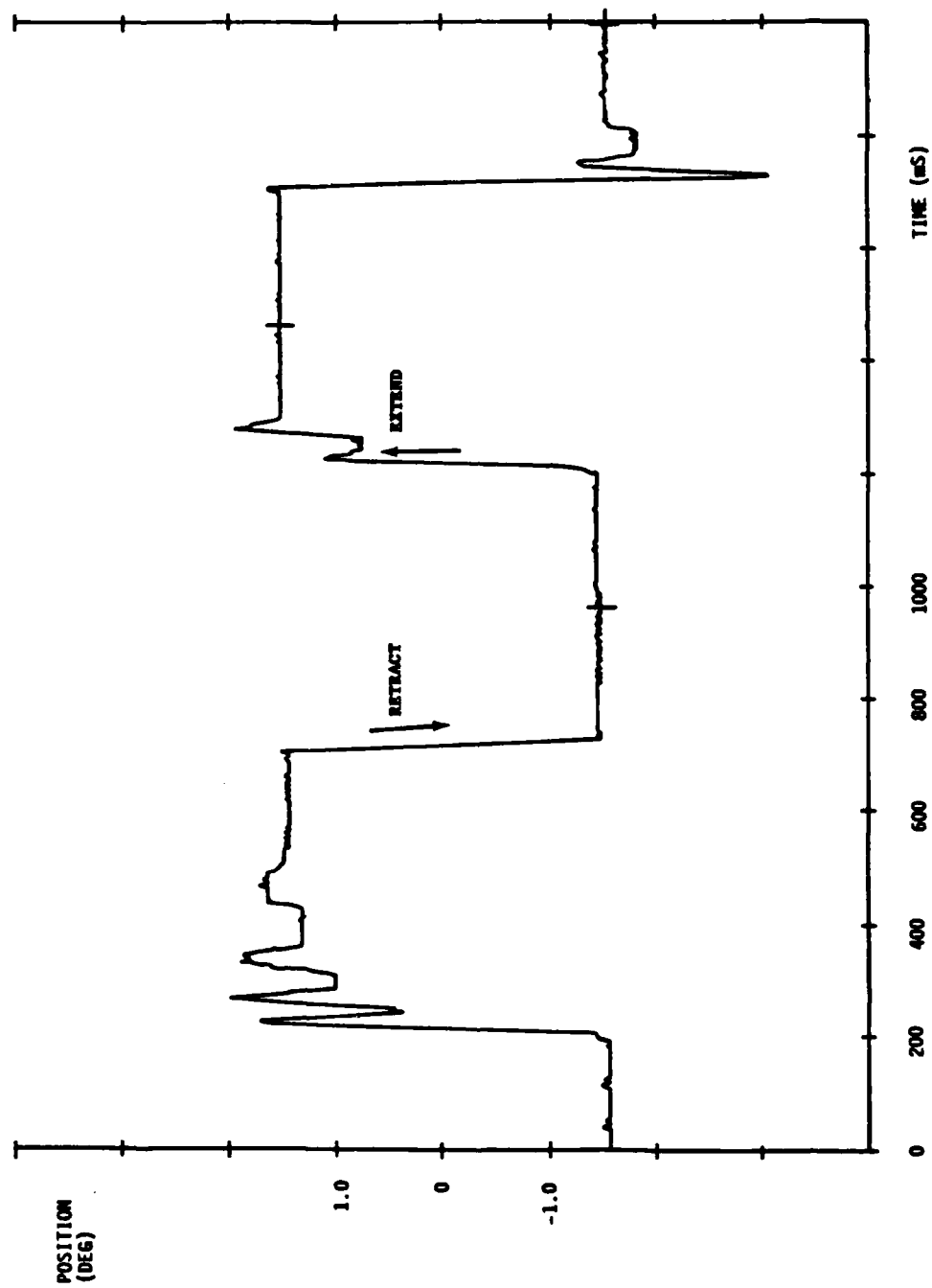


Figure 39. 3° P-P square wave output at 1 Hz actuator SN-018 -
0.62 in²-lb inertia load.

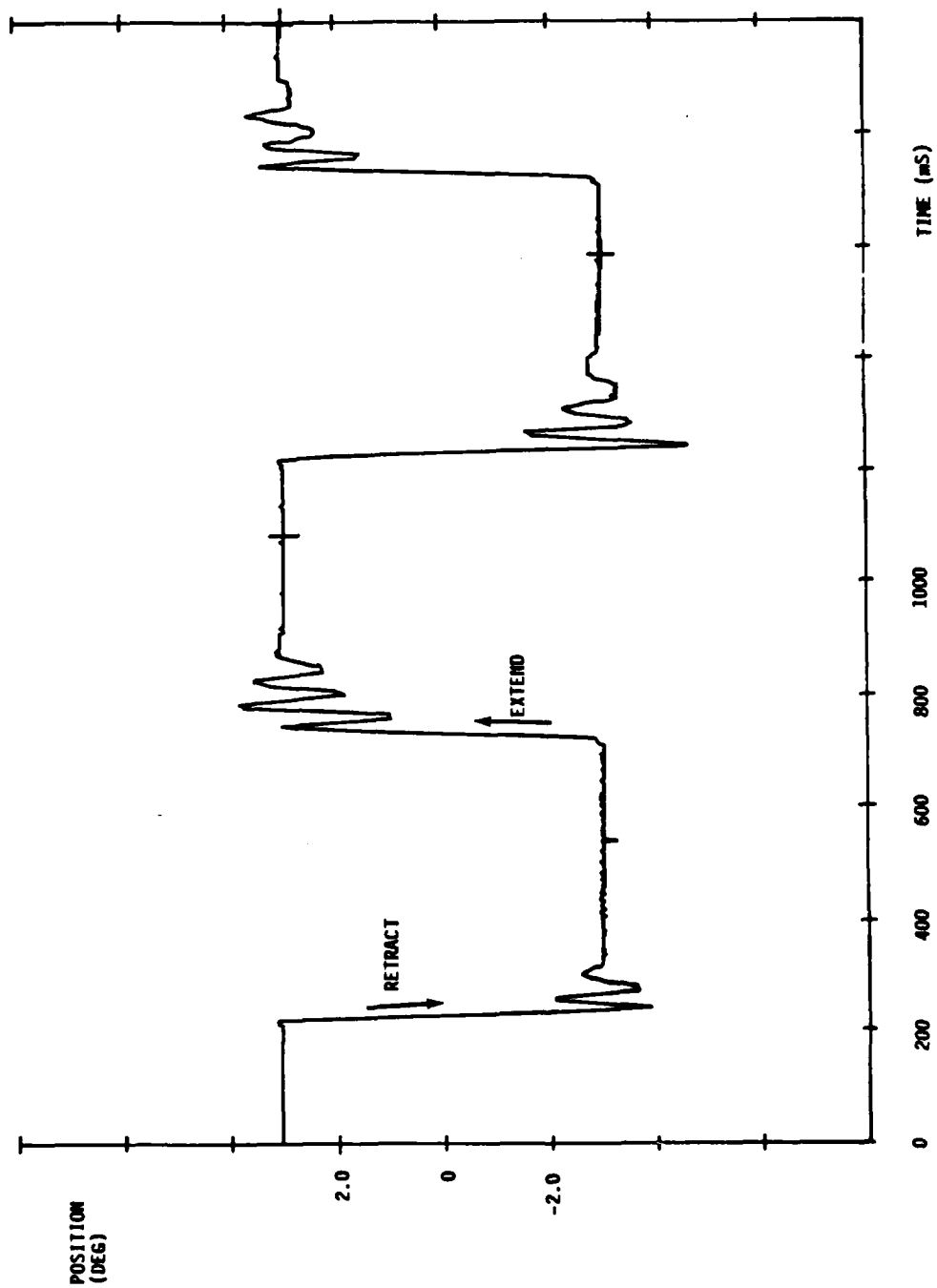


Figure 40. 6° P-P square wave output at 1 Hz actuator SN-018 -
0.62 in²-lb inertia.

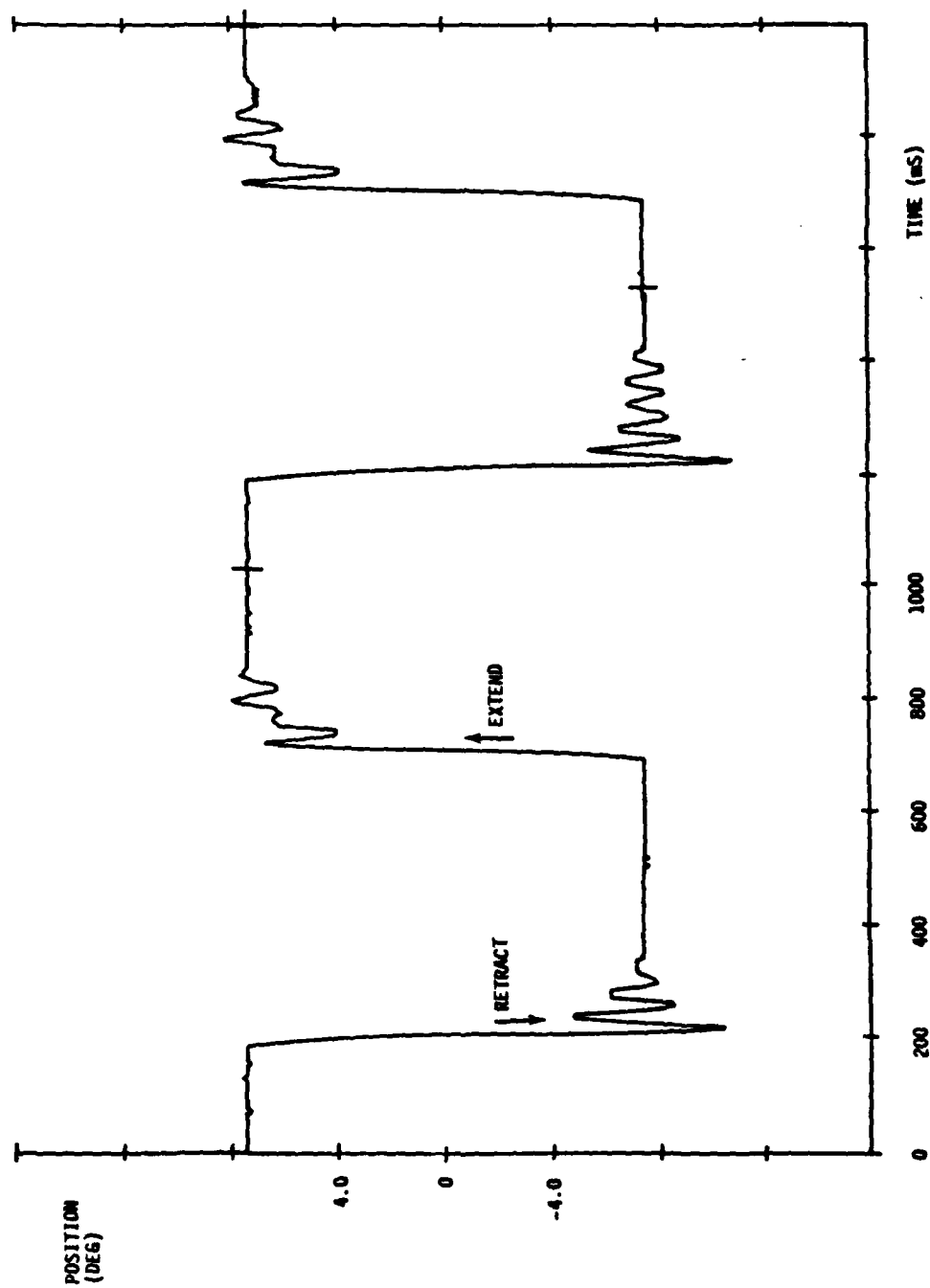


Figure 41. 15° p-p square wave output at 1 Hz actuator SN-018 -
0.62 in²-lb inertia.

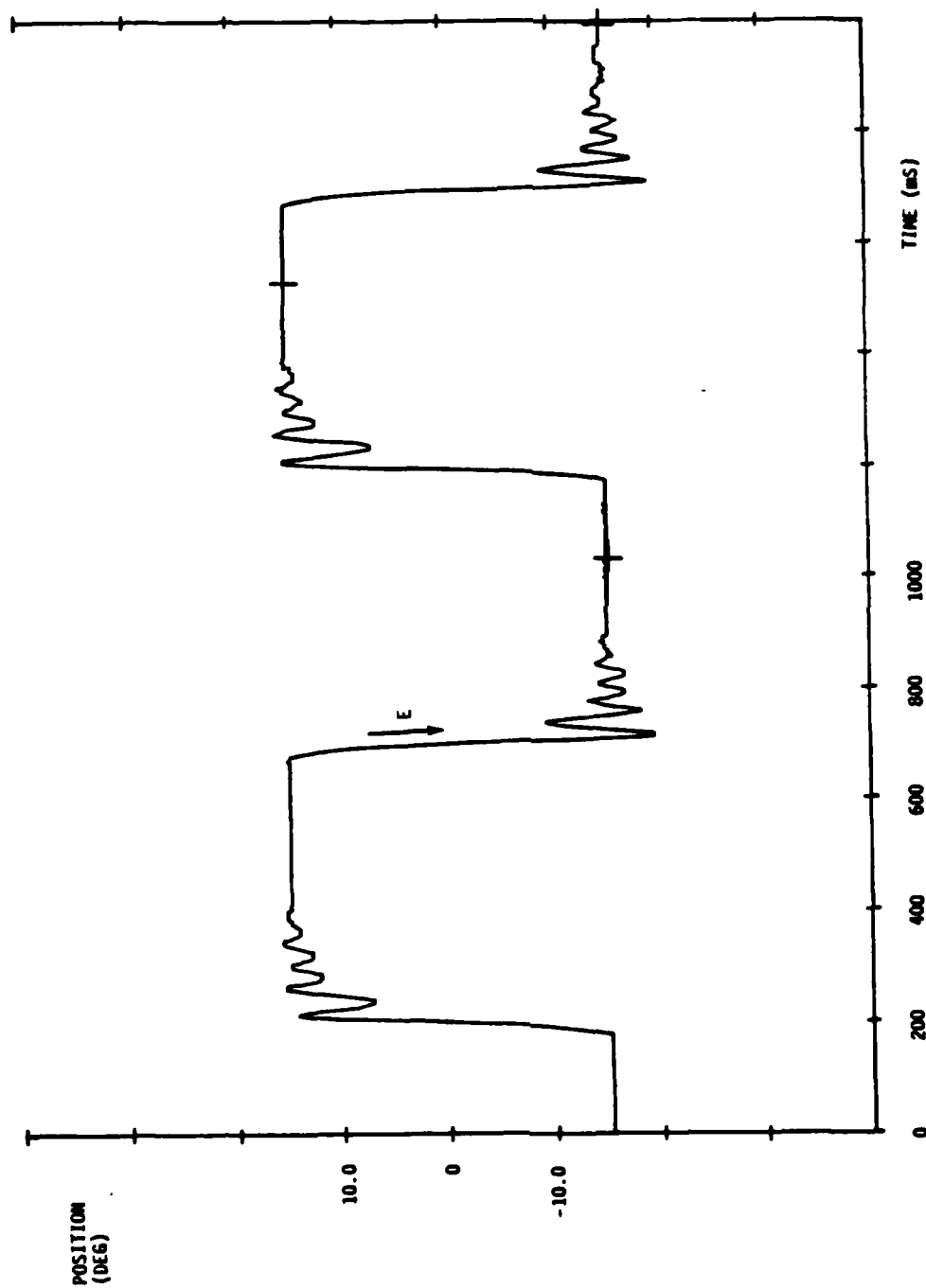


Figure 42. 30° P-P square wave output at 1 Hz actuator SN-018 -
0.62 in²-lb inertia.

TABLE 5. Environmental Test Results Actuator SN-002 (Anodized Housing).

Temperature (°F)	No Load Slew Rate (1)		Frequency Response (1)(2)			
	Charge (Deg/sec)	Discharge (Deg/sec)	Frequency -3dB		Frequency -90° Phase	
			1° P-P (Hz)	6° P-P (Hz)	1° P-P (Hz)	6° P-P (Hz)
-25	1344	1344	3.1	12.0	2.7	11.5
-5	--	--	4.1	21.0	3.4	22.0
35	--	--	8.0	18.0	7.8	18.0
68	1440	1248	14.5	23.0	14.3	23.2
100	--	--	11.0	25.0	11.5	24.0
140	1500	1280	8.3	24.0	8.8	24.0

- (1) 0.62 in²-lb Inertia Load
(2) 0.30 in-lb/deg Hinge Load

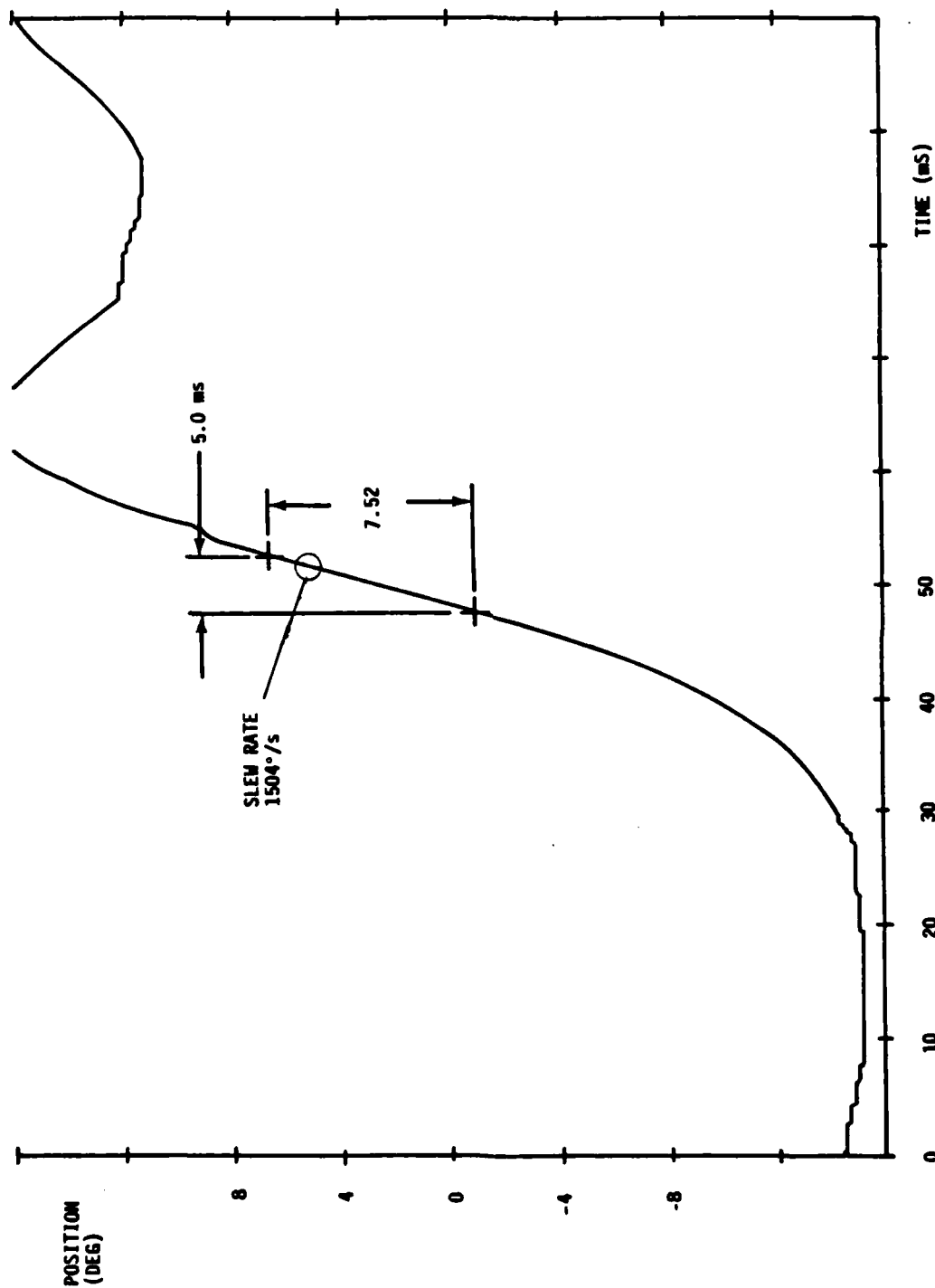


Figure 43. Charge slew rate, 140 °F actuator SN-002 -
0.62 in²-lb inertia load, no hinge load.

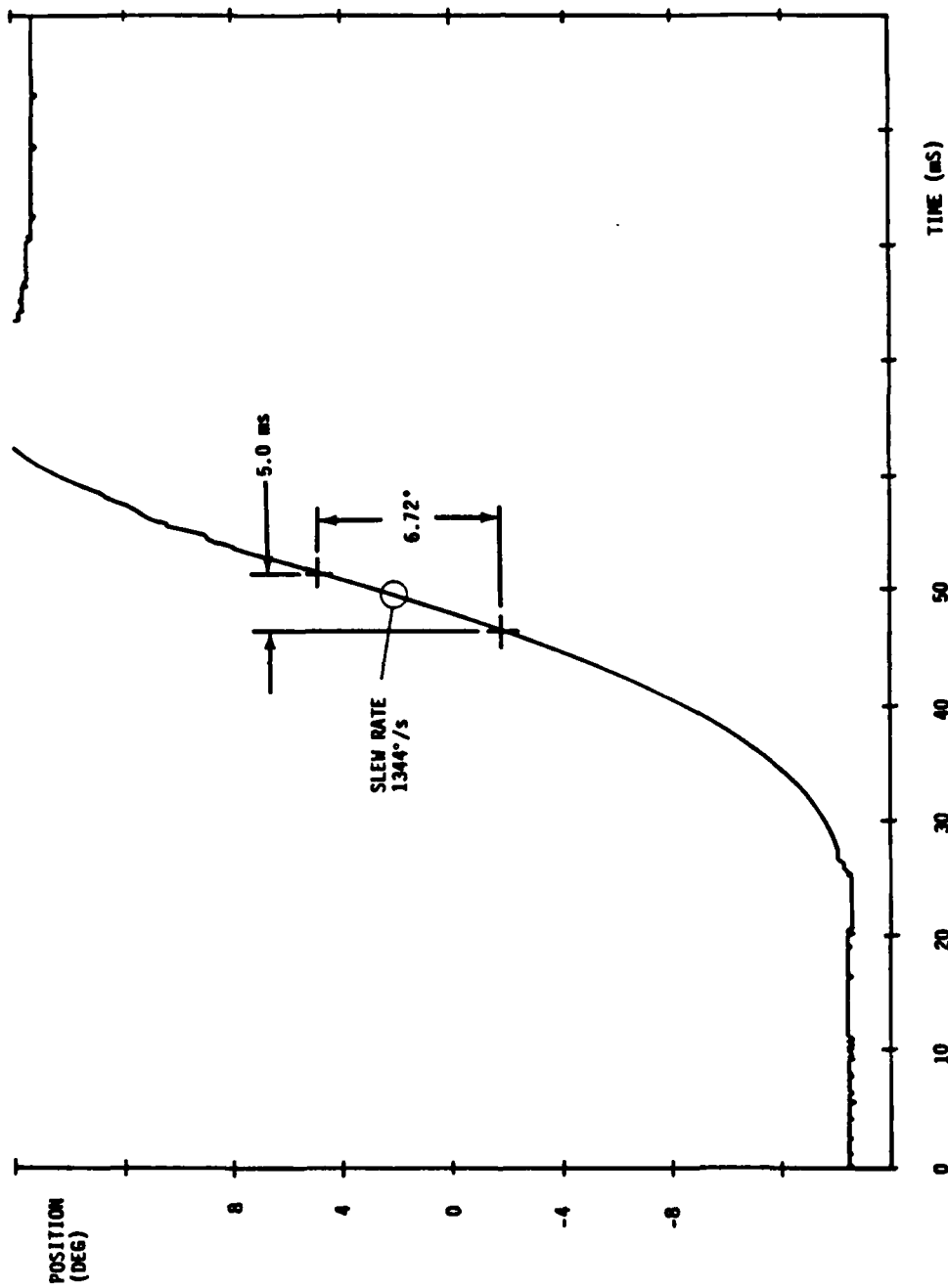


Figure 44. Charge slew rate, -25 °F actuator SN-002 -
0.62 in²-lb inertia load, no hinge load.

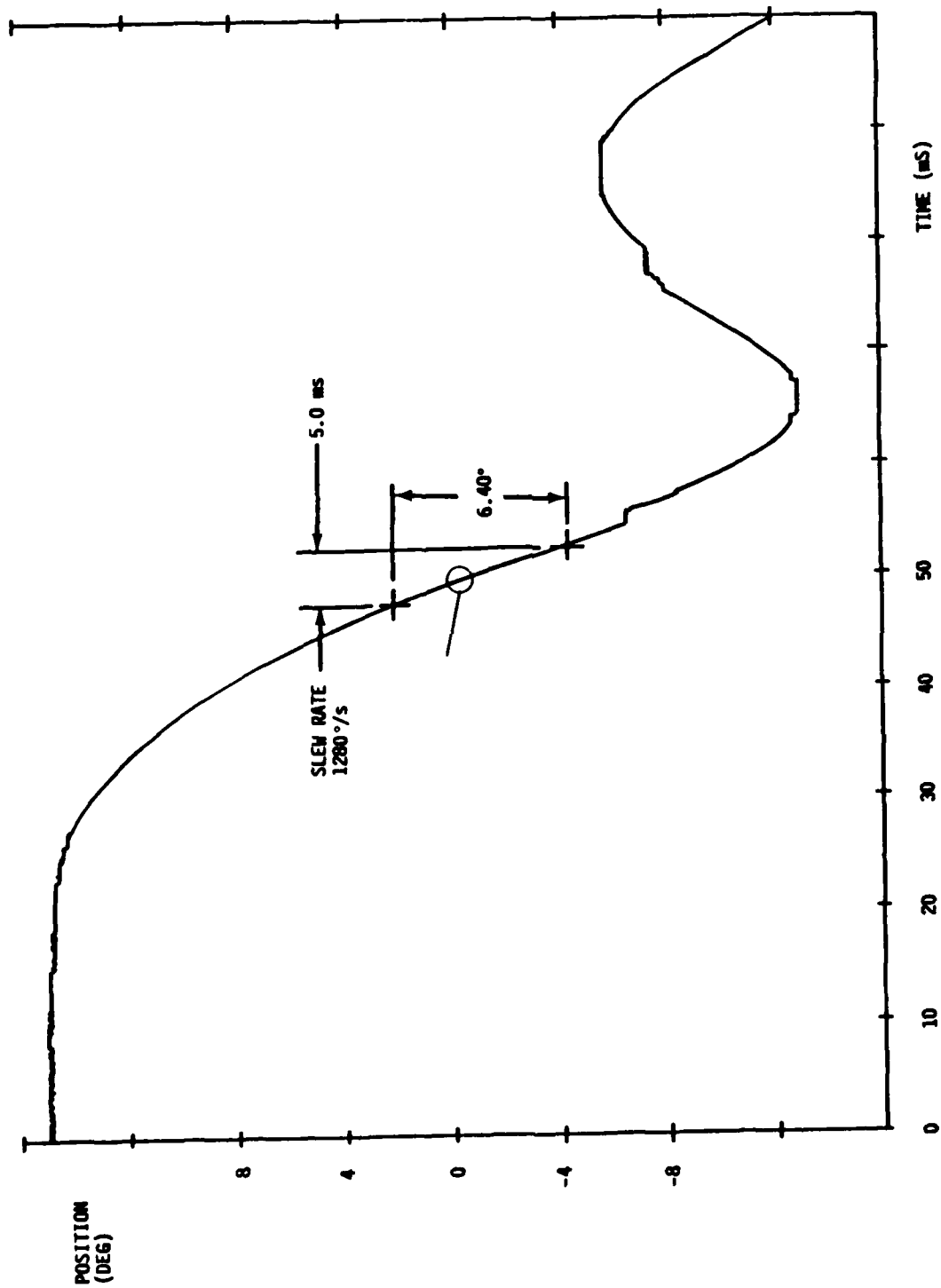


Figure 45. Discharge slew rate, 140 °F actuator SN-002 -
0.62 in²-lb inertia load, no hinge load.

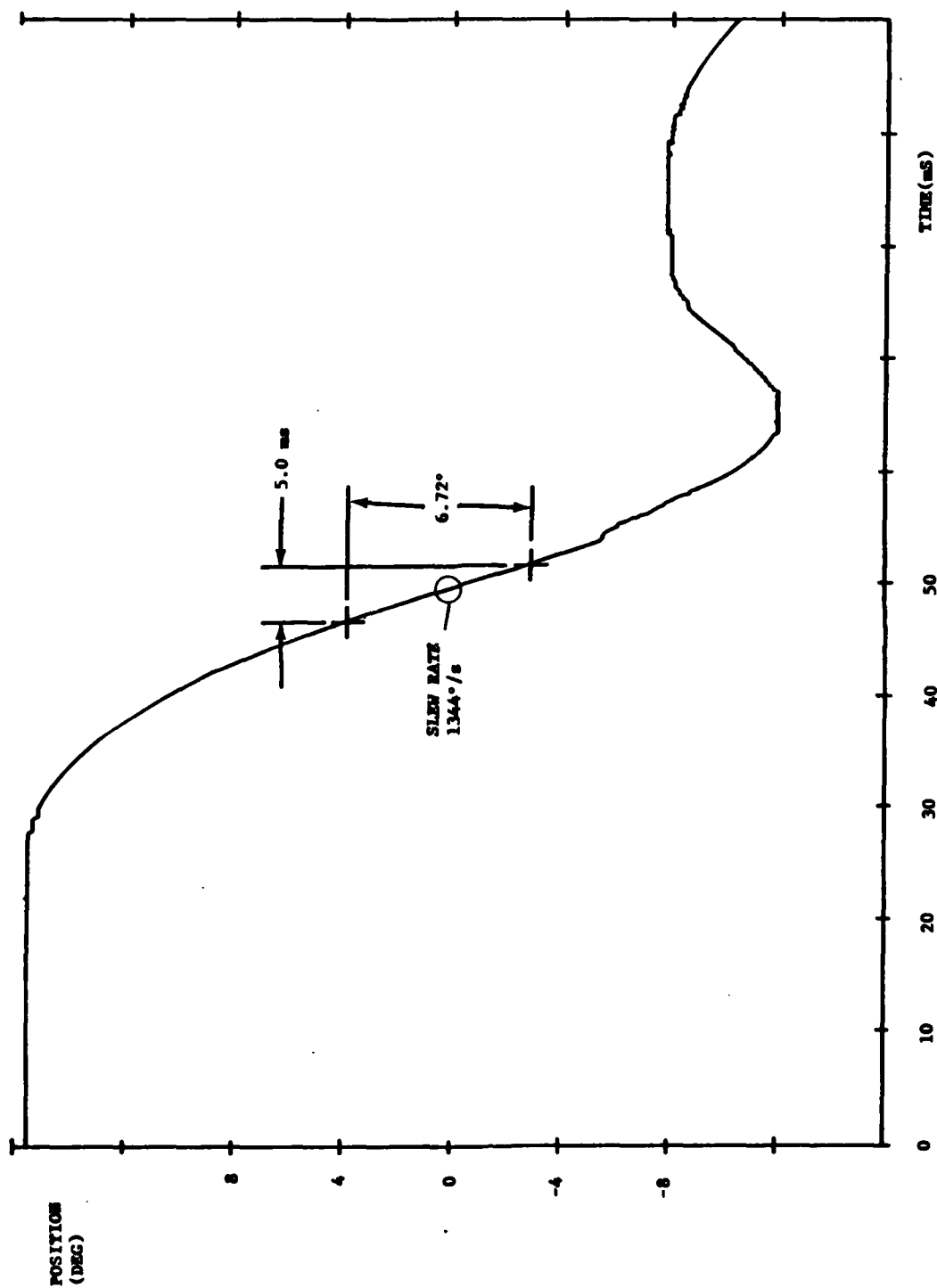


Figure 46. Discharge slew rate, -25 °F actuator SN-002 -
0.62 in²-lb inertia load, no hinge load.

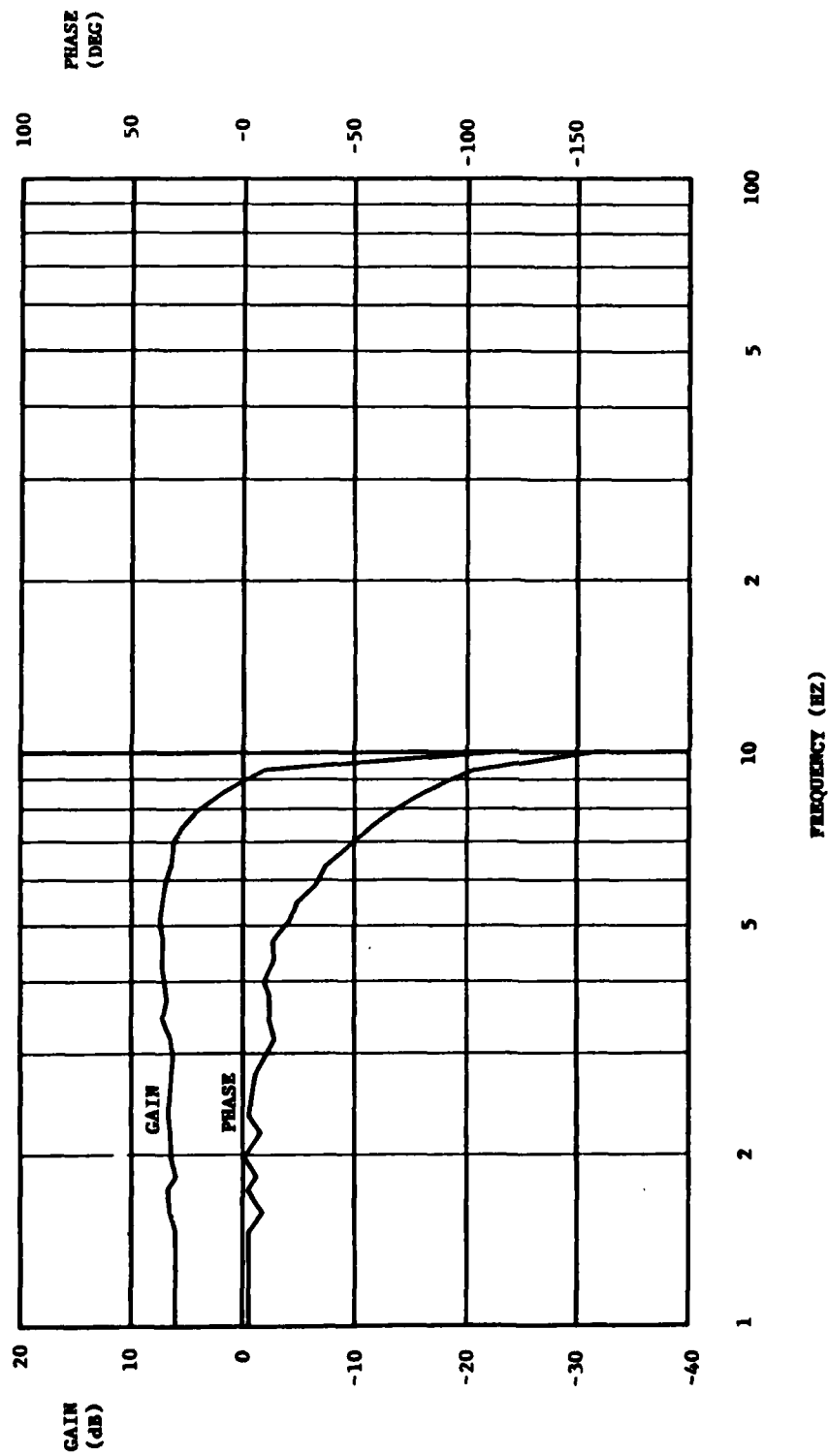


Figure 47. 1° P-P frequency response, 140 °F actuator SN-002 -
 0.62 in²-lb inertia load,
 0.30 in-lb/deg hinge load.

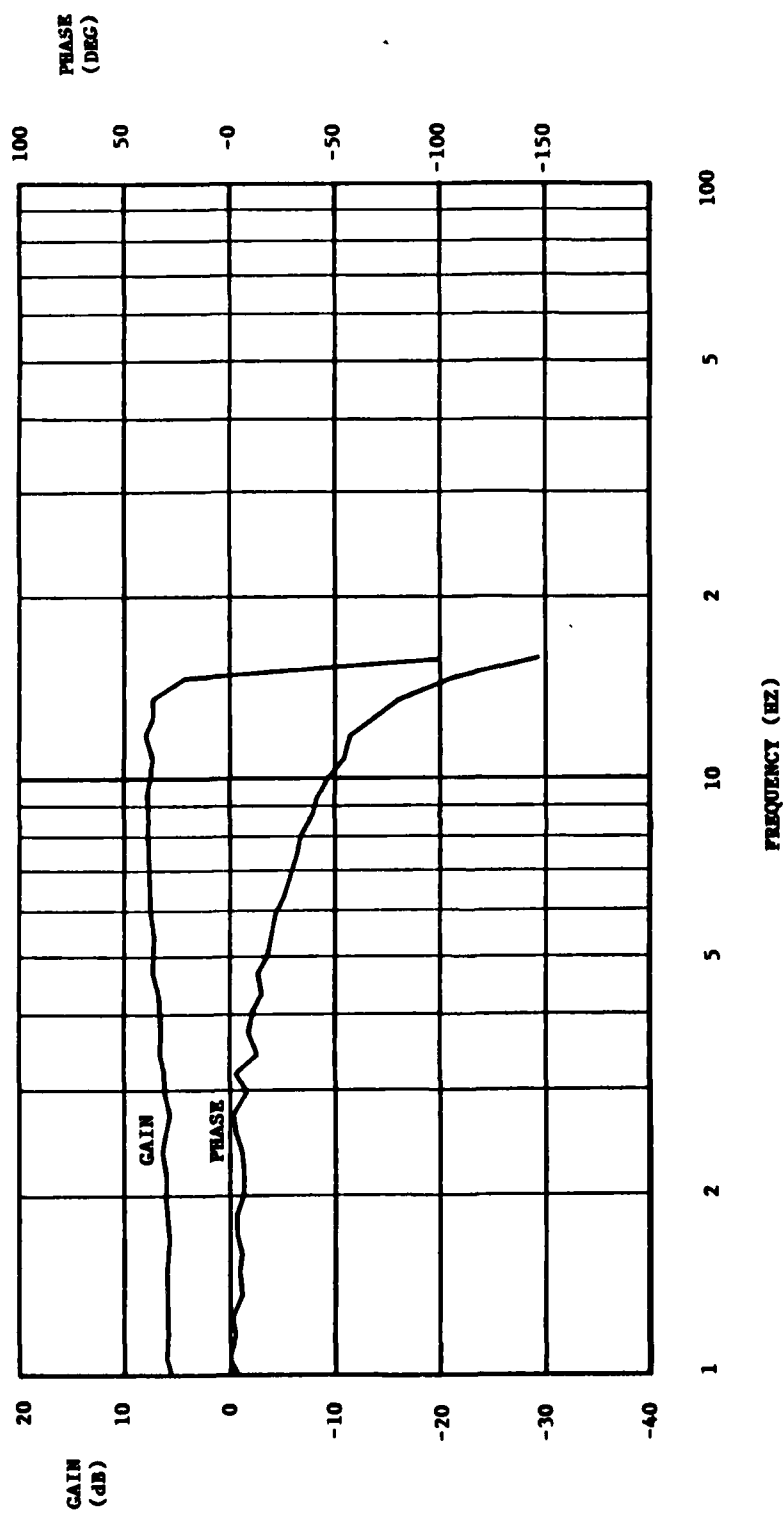


Figure 48. 1° P-P frequency response, 68 °F actuator SN-002 -
0.62 in²-lb inertia load,
0.30 in-lb/deg hinge load.

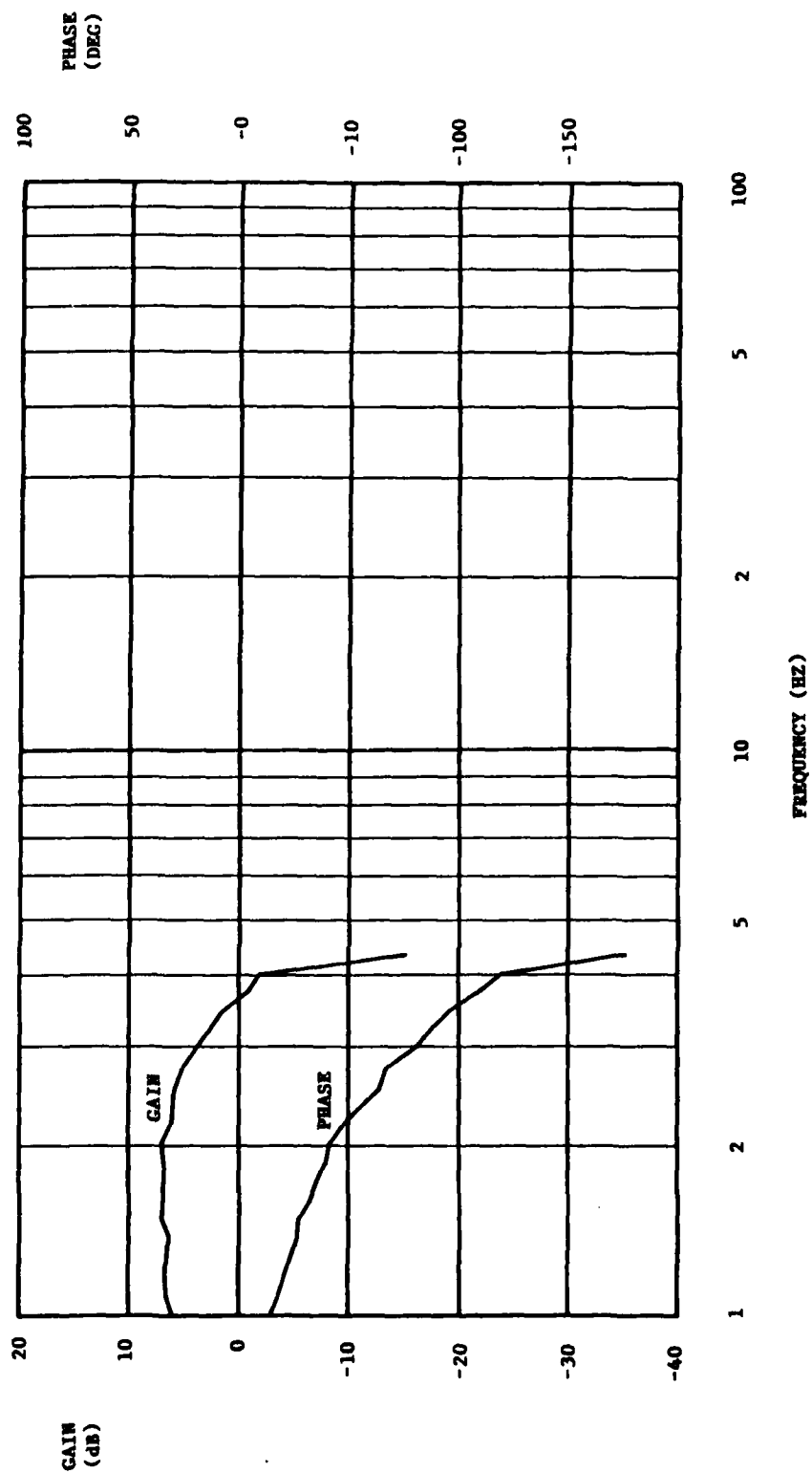


Figure 49. 1° P-P frequency response, -25 °F actuator SN-002 -
 0.62 in²-lb inertia load,
 0.30 in-lb/deg hinge load.

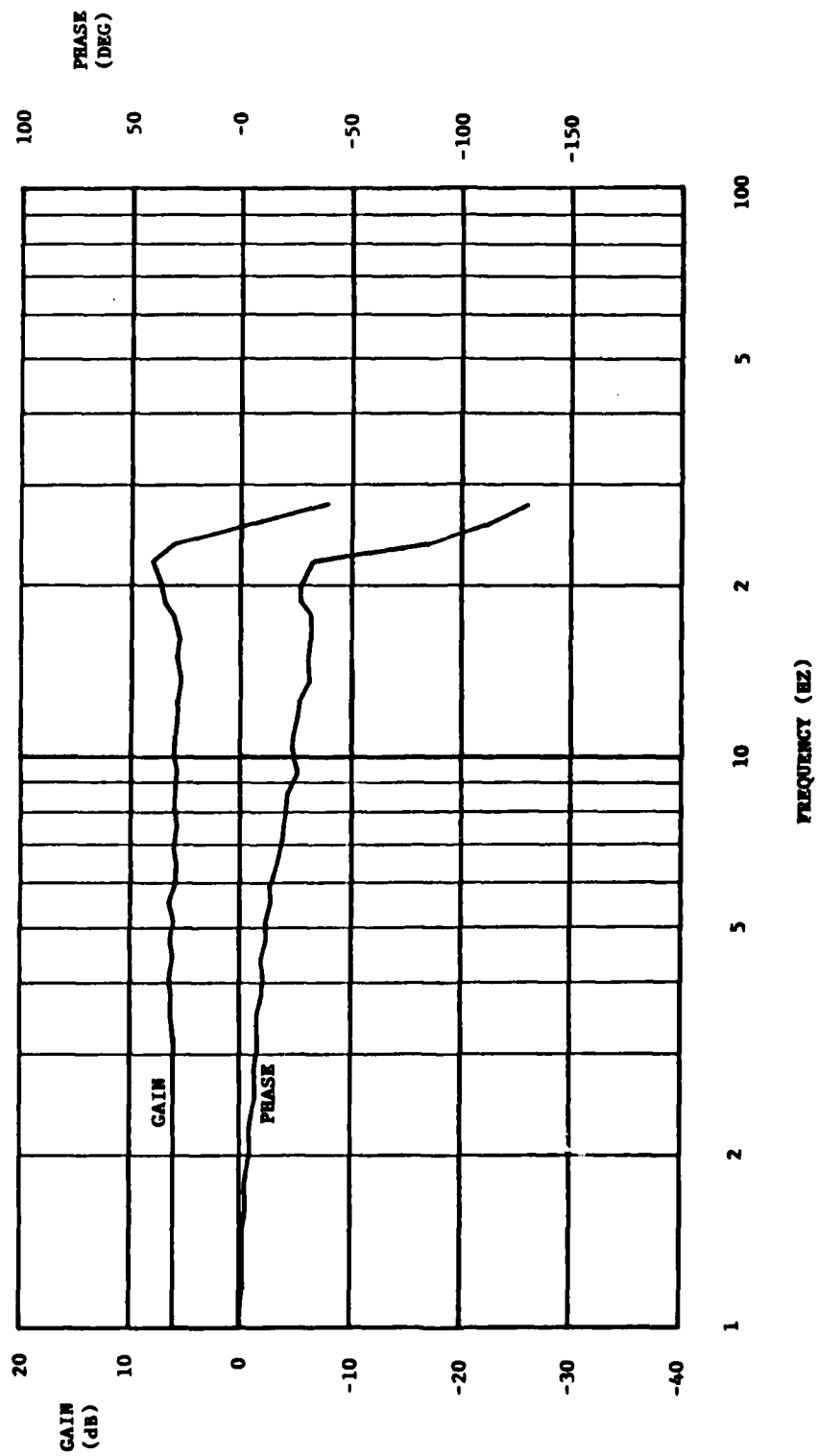


Figure 50. 6° P-P frequency response, 140 °F actuator SN-002 -
 0.62 in²-lb inertia load,
 0.30 in-lb/deg hinge load.

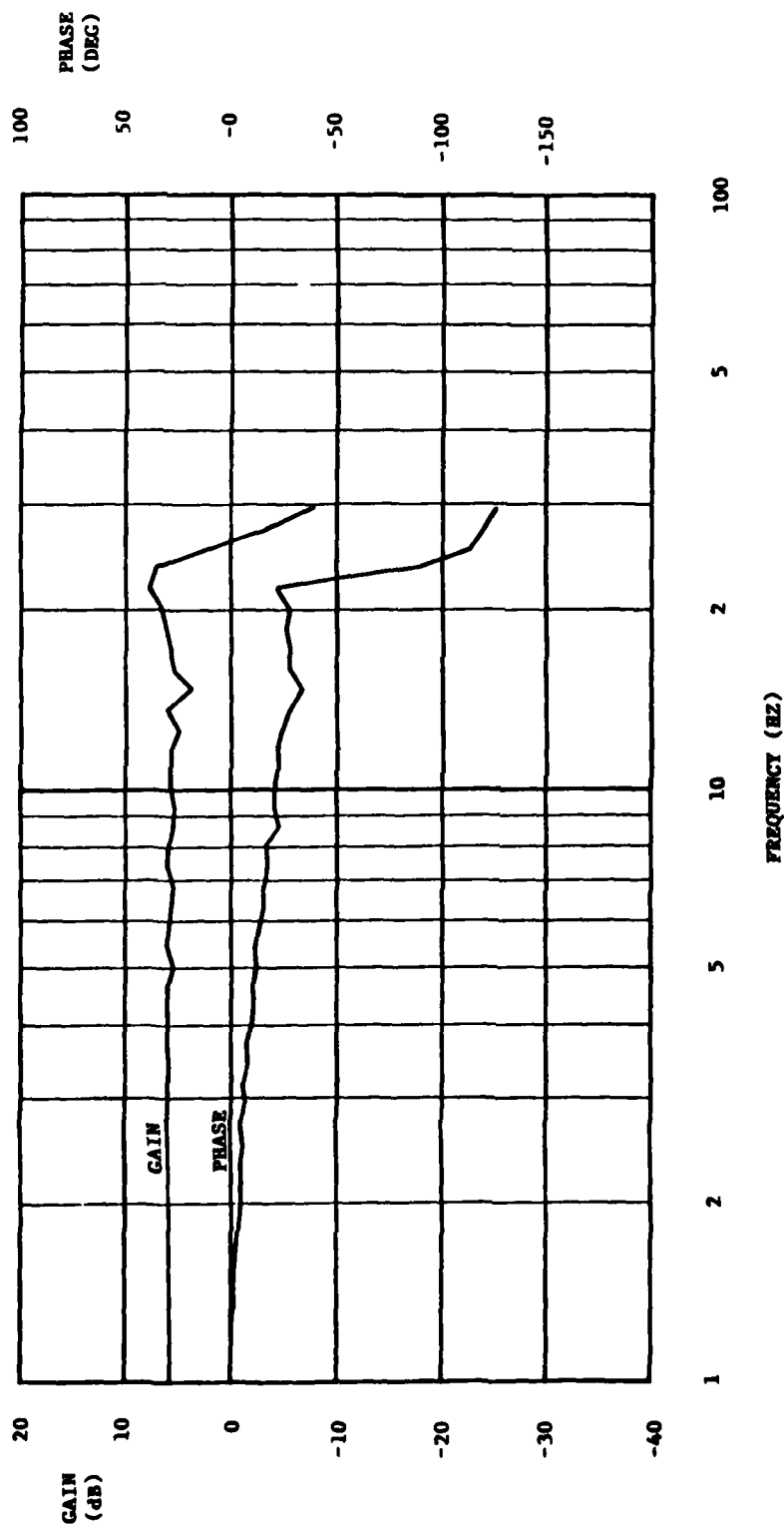


Figure 51. 6° p-p frequency response, 68 °F actuator SN-002 -
0.62 in²-lb inertia load,
0.30 in-lb/deg hinge load.

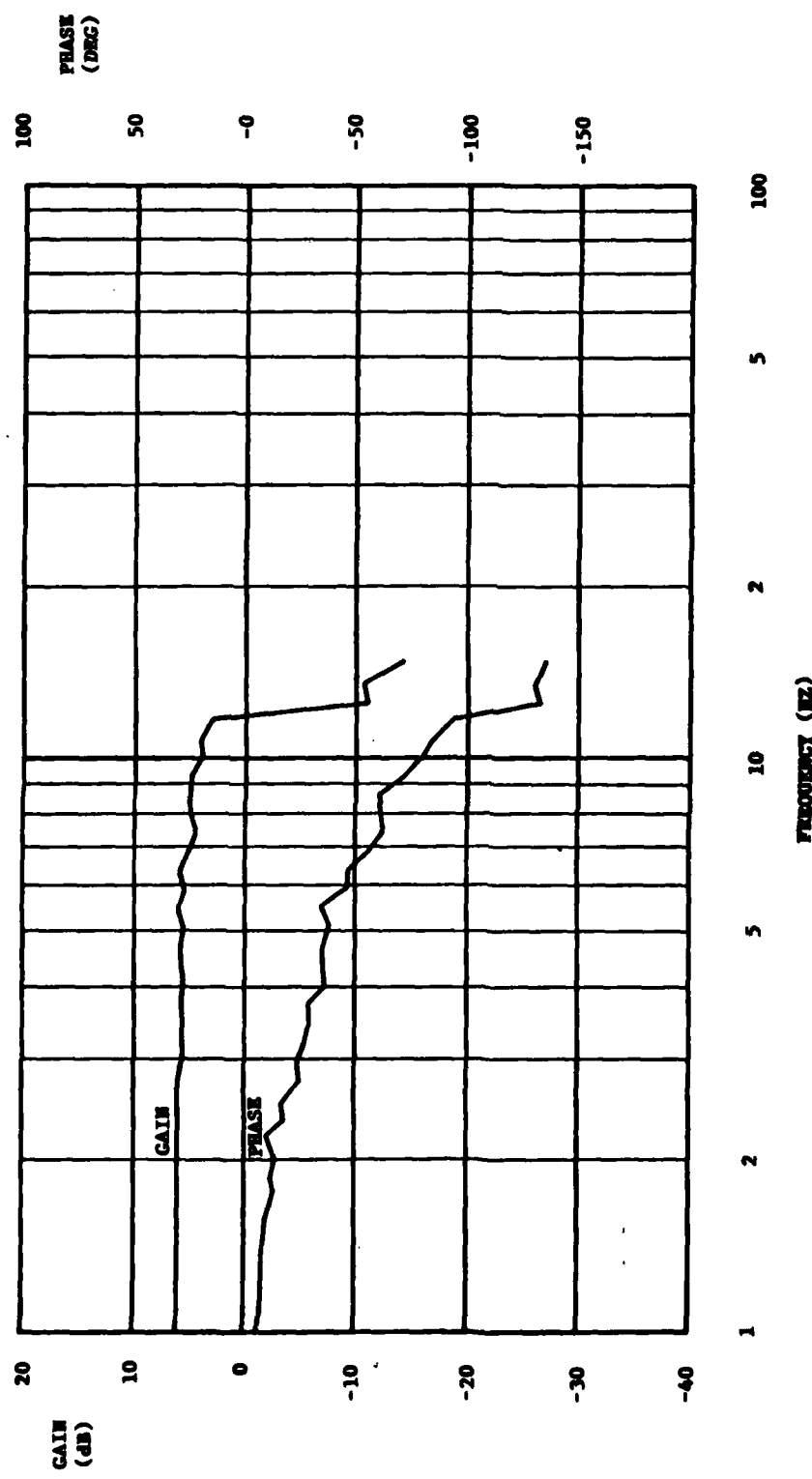


Figure 52. 6° P-P frequency response, -25 °F actuator SN-002 -
0.62 in²-lb inertia load,
0.30 in-lb/deg hinge load.

TABLE 6. Environmental Test Results Actuator SN-002 (Tiodized Housing).

Temperature (°F)	Frequency Response (1)(2)			
	Frequency -3dB		Frequency -90° Phase	
	1° P-P (Hz)	6° P-P (Hz)	1° P-P (Hz)	6° P-P (Hz)
-25	7.8	7.9	8.5	10.5
0	12.5	14.5	11.5	14.5
68	18.0	24.5	17.5	23.0
120	14.0	23.0	13.5	23.0
140	16.0	24.0	16.0	23.5

(1) 0.62 in²-lb Inertia Load

(2) 0.30 in-lb/deg Hinge Load

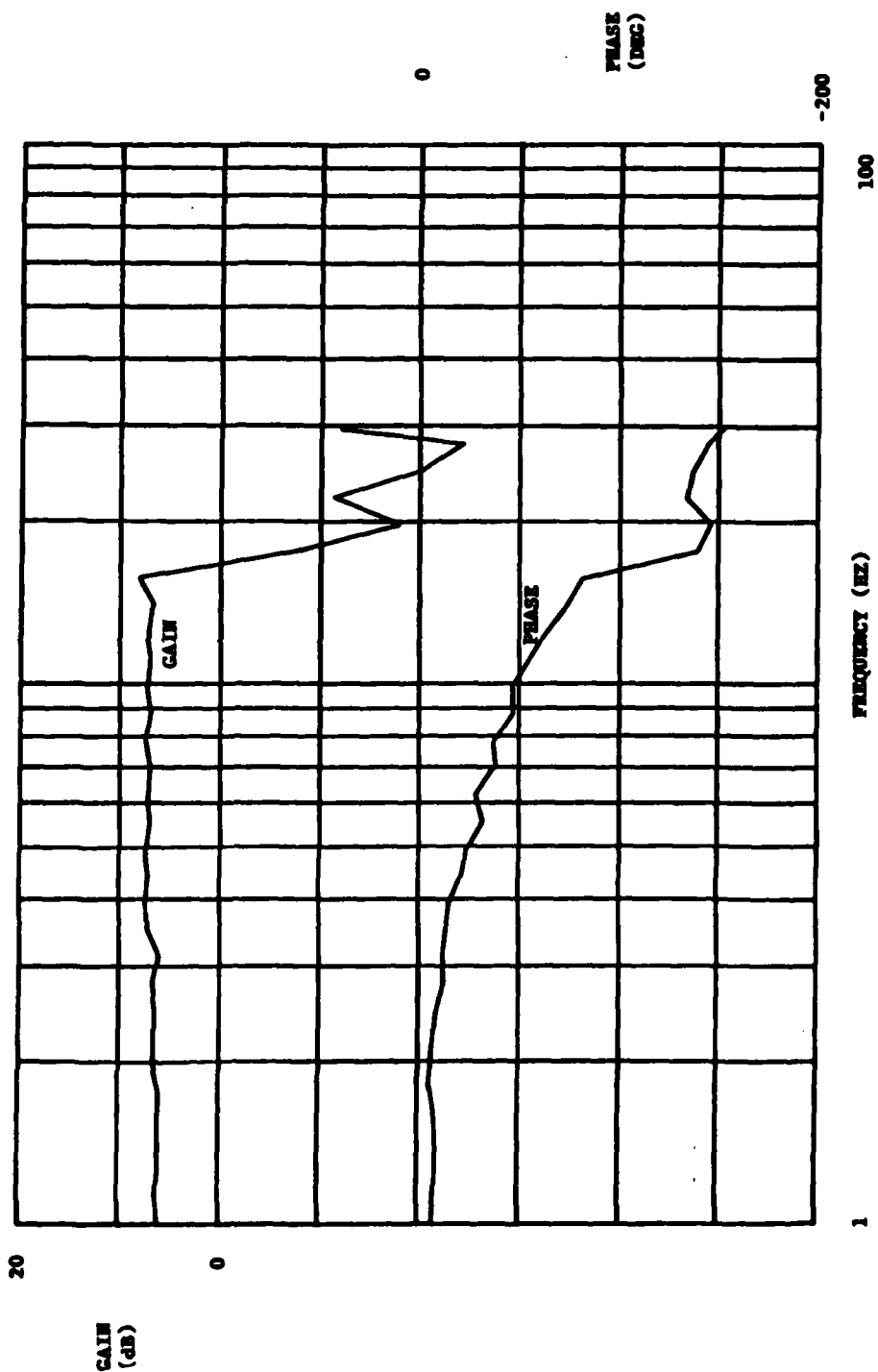


Figure 53. 1° P-P frequency response, 140 °F actuator SN-002-T -
0.62 in²-lb inertia load,
0.30 in-lb/deg hinge load.

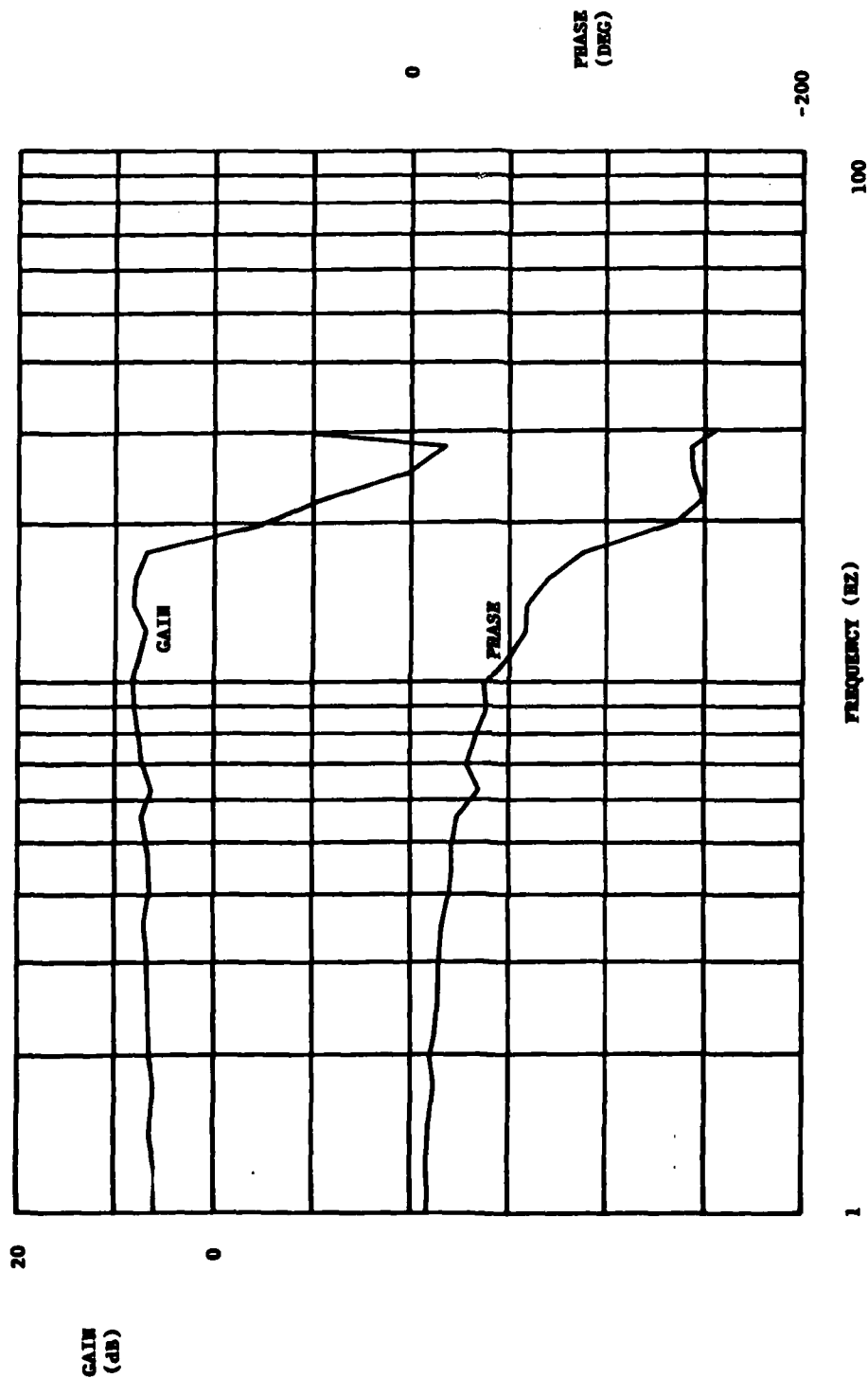


Figure 54. 1° P-P frequency response, 68 °F actuator SN-002-T -
0.62 in²-lb inertia load,
0.30 in-lb/deg hinge load.

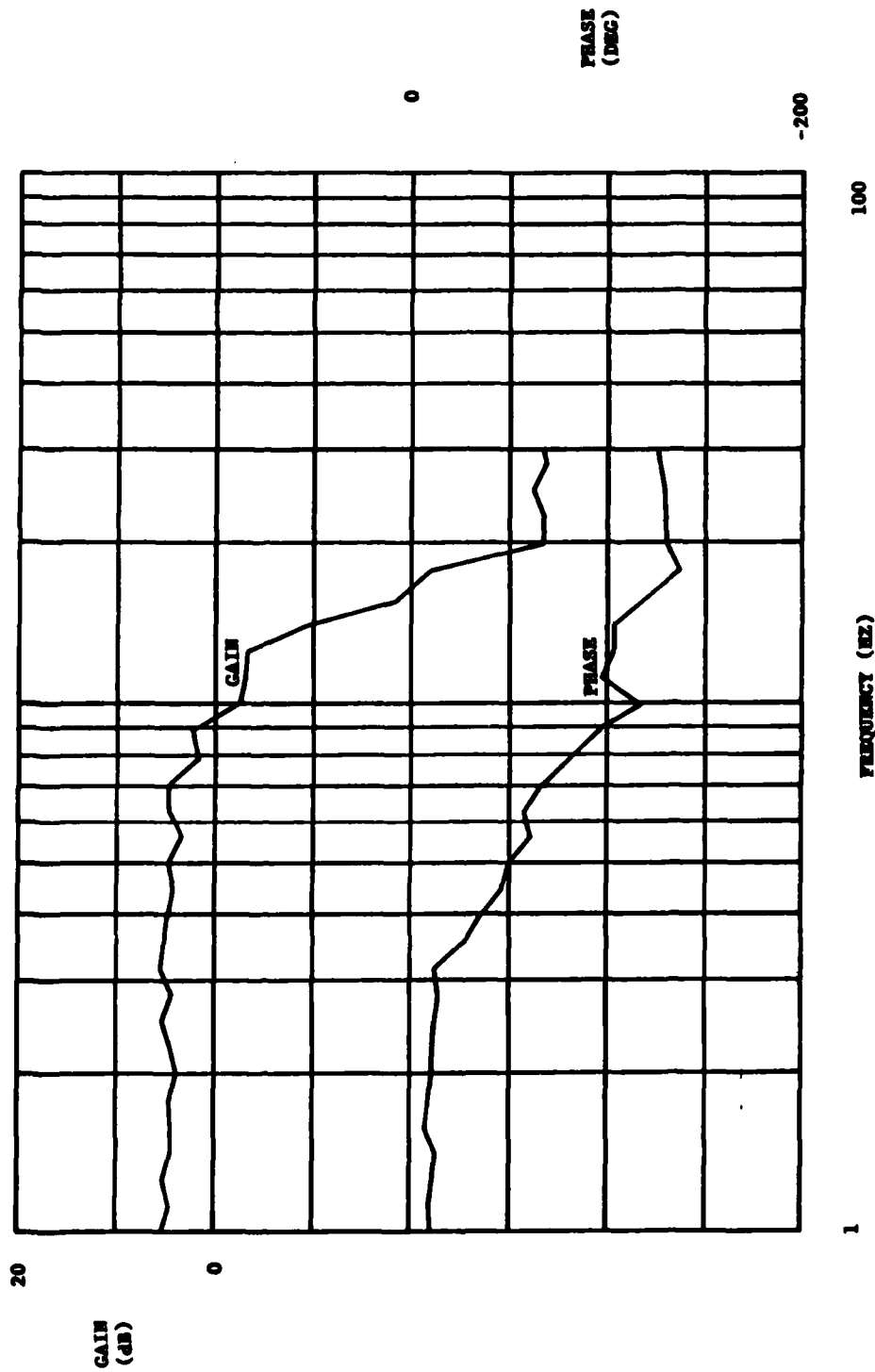


Figure 55. 1° P-P frequency response, -25 °F actuator SN-002-T -
 0.62 in²-lb inertia load,
 0.30 in-lb/deg hinge load.

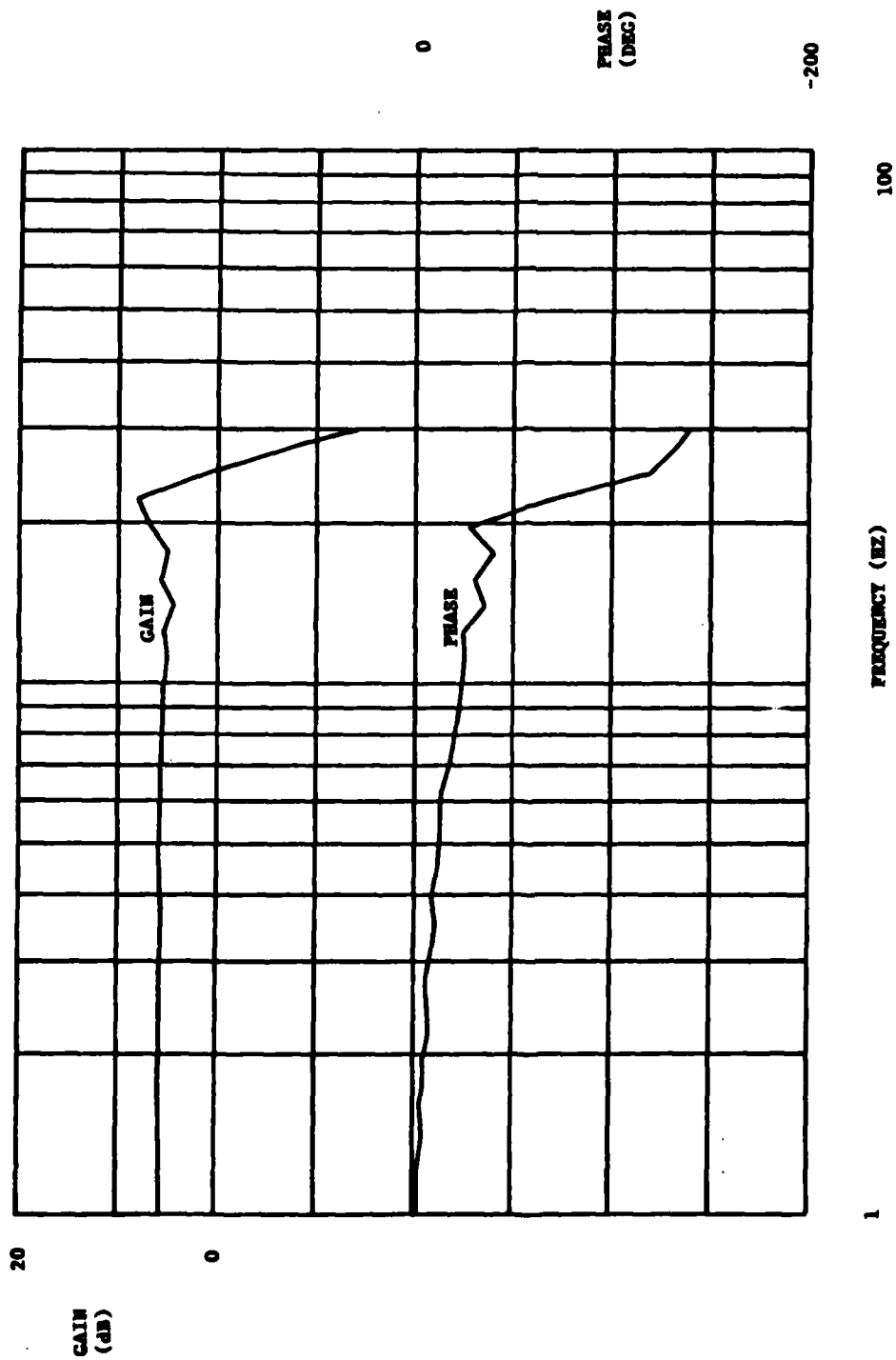


Figure 56. 6° P-P frequency response, 140 °F actuator SN-002-T -
0.62 in²-lb inertia load,
0.30 in-lb/deg hinge load.

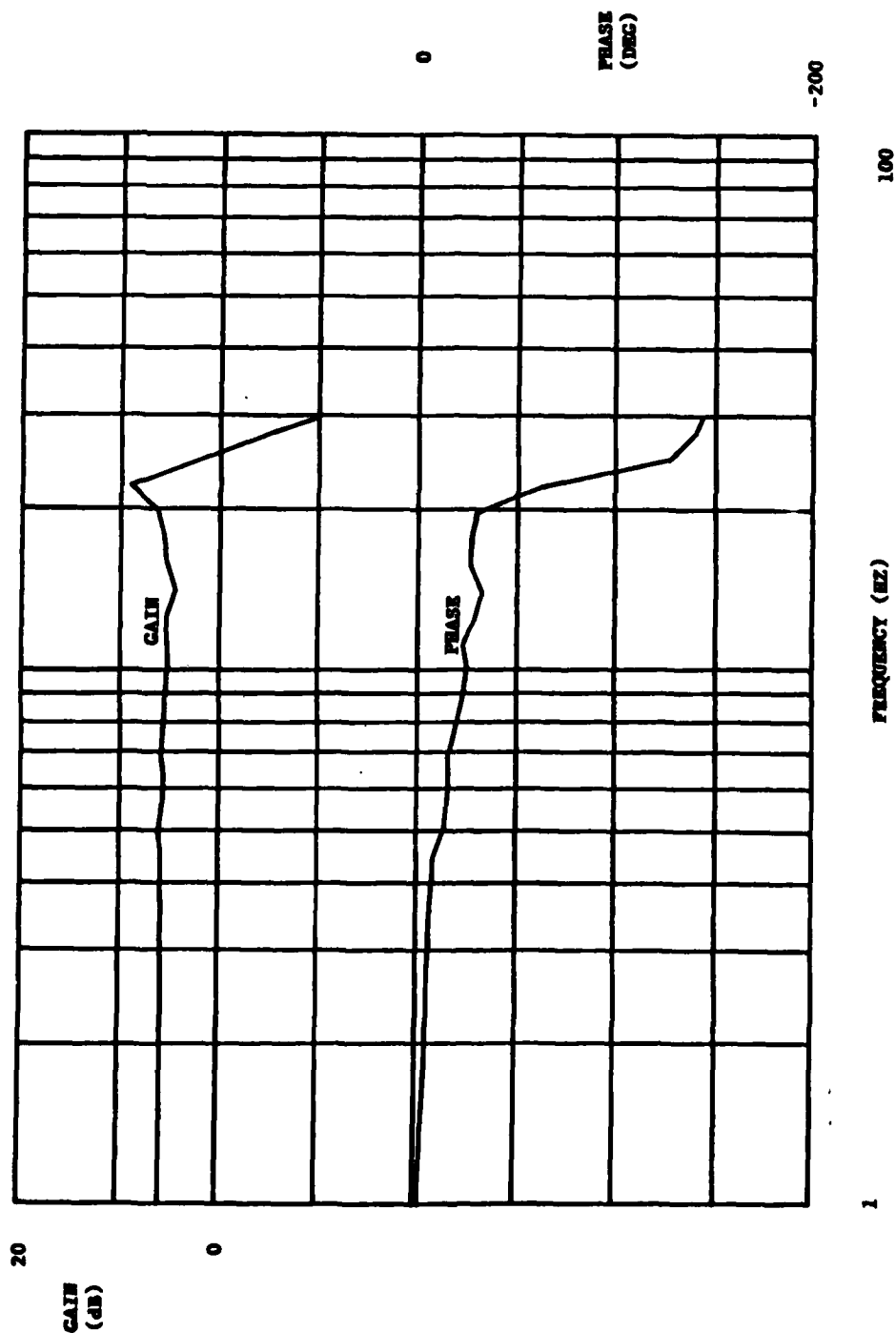


Figure 57. 6° P-P frequency response, 68 °F actuator SN-002-T -
0.62 in²-lb inertia load,
0.30 in-lb/deg hinge load.

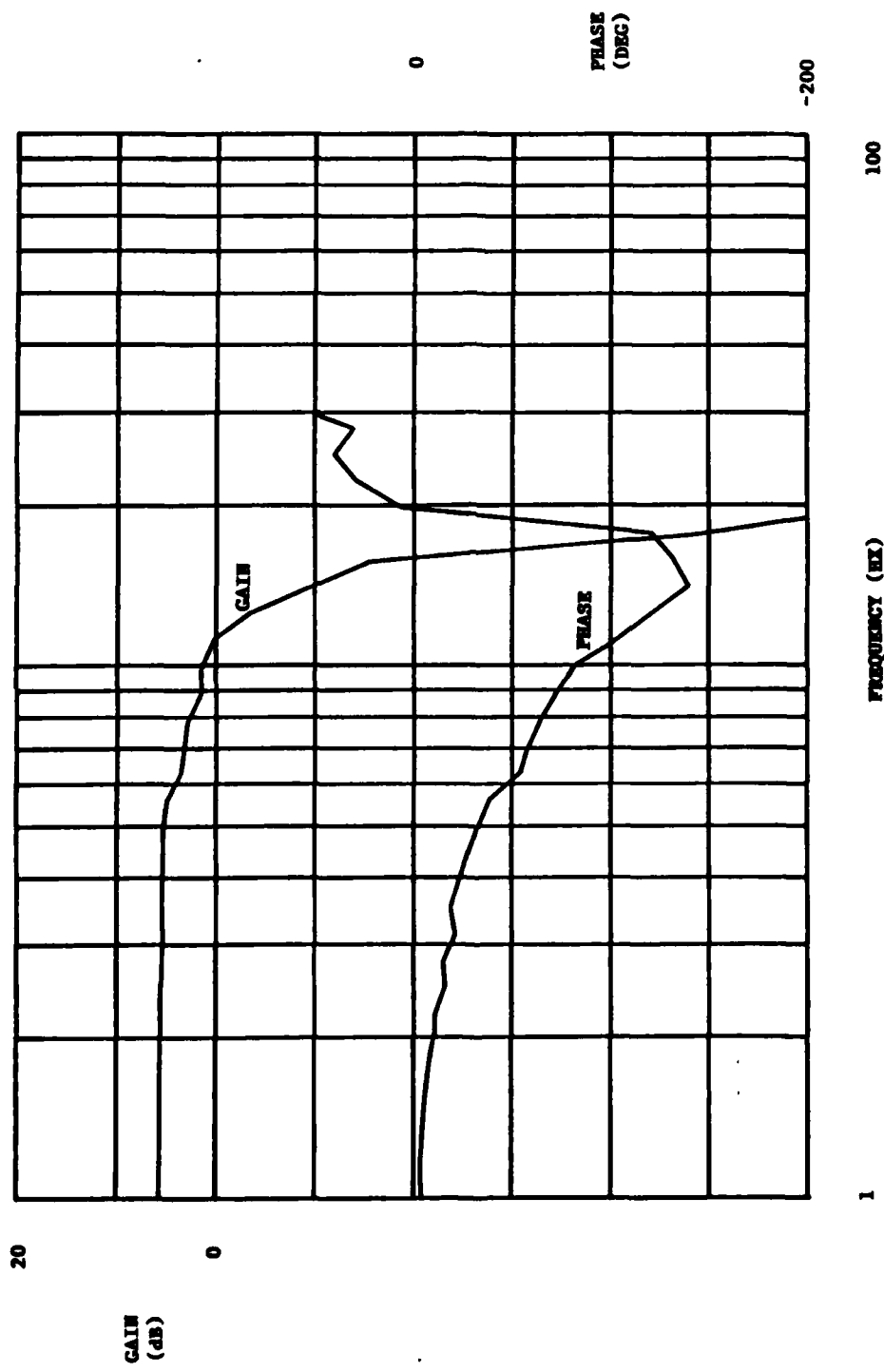


Figure 58. 6° P-P frequency response, -25 °F actuator SN-002-T -
0.62 in²-lb inertia load,
0.30 in-lb/deg hinge load.

TABLE 7. Gas Consumption Test Results Actuator SN-002.

SINE WAVE INPUT		MEASURED GAS Consumption (Std. in ³ /sec)	REQUIRED GAS Bottle Volume (in ³ at 500 psig)
FREQUENCY (Hz)	AMPLITUDE (deg P-P)		
1.0	1.0	0.37	0.56
	2.0	0.55	0.83
	4.0	0.68	1.02
	6.0	0.80	1.21
3.0	1.0	0.95	1.43
	2.0	1.42	2.15
	4.0	1.68	2.53
	6.0	1.93	2.91
6.0	1.0	1.68	2.53
	2.0	2.24	3.37
	4.0	2.49	3.76
	6.0	3.00	4.52

0.10 Degree Deadzone
0.62 in²-lb Inertia Load
0.30 in-lb/deg Hinge Load

TABLE 8. Gas Consumption Test Results Actuator SN-002.

SINE WAVE INPUT		MEASURED GAS Consumption (Std. in ³ /sec)	REQUIRED GAS Bottle Volume (in ³ at 500 psig)
FREQUENCY (Hz)	AMPLITUDE (deg P-P)		
1.0	1.0	0.32	0.48
	2.0	0.32	0.48
	4.0	0.32	0.48
	6.0	0.32	0.48
3.0	1.0	0.86	1.30
	2.0	0.93	1.40
	4.0	1.17	1.76
	6.0	1.42	2.15
6.0	1.0	0.95	1.43
	2.0	1.68	2.53
	4.0	2.24	3.37
	6.0	2.27	4.14

0.50 Degree Deadzone
0.62 in²-lb Inertia Load
0.30 in-lb/deg Hinge Load

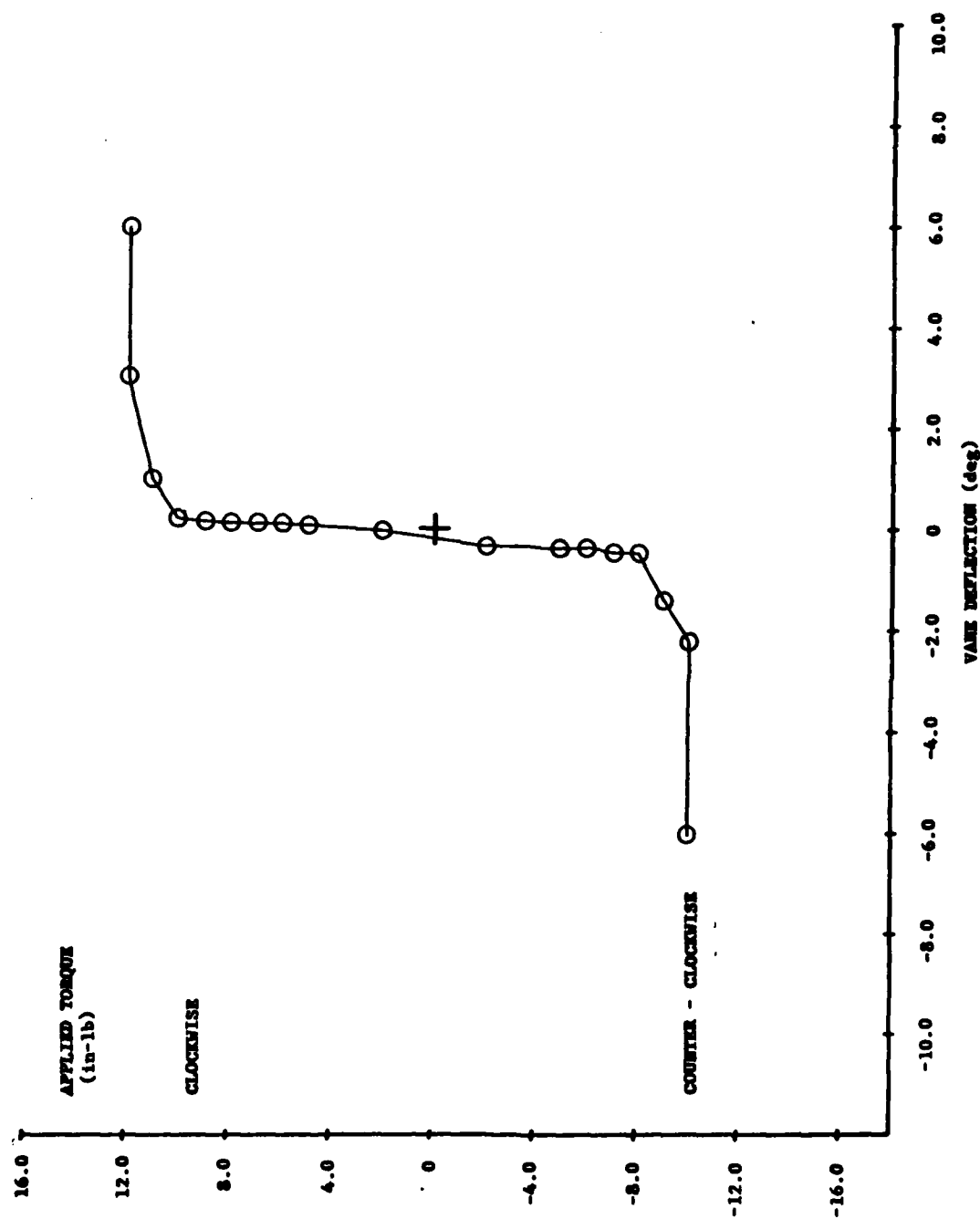


Figure 59. Applied torque versus vane deflection -
300 psig supply pressure,
0.50 degree deadzone.

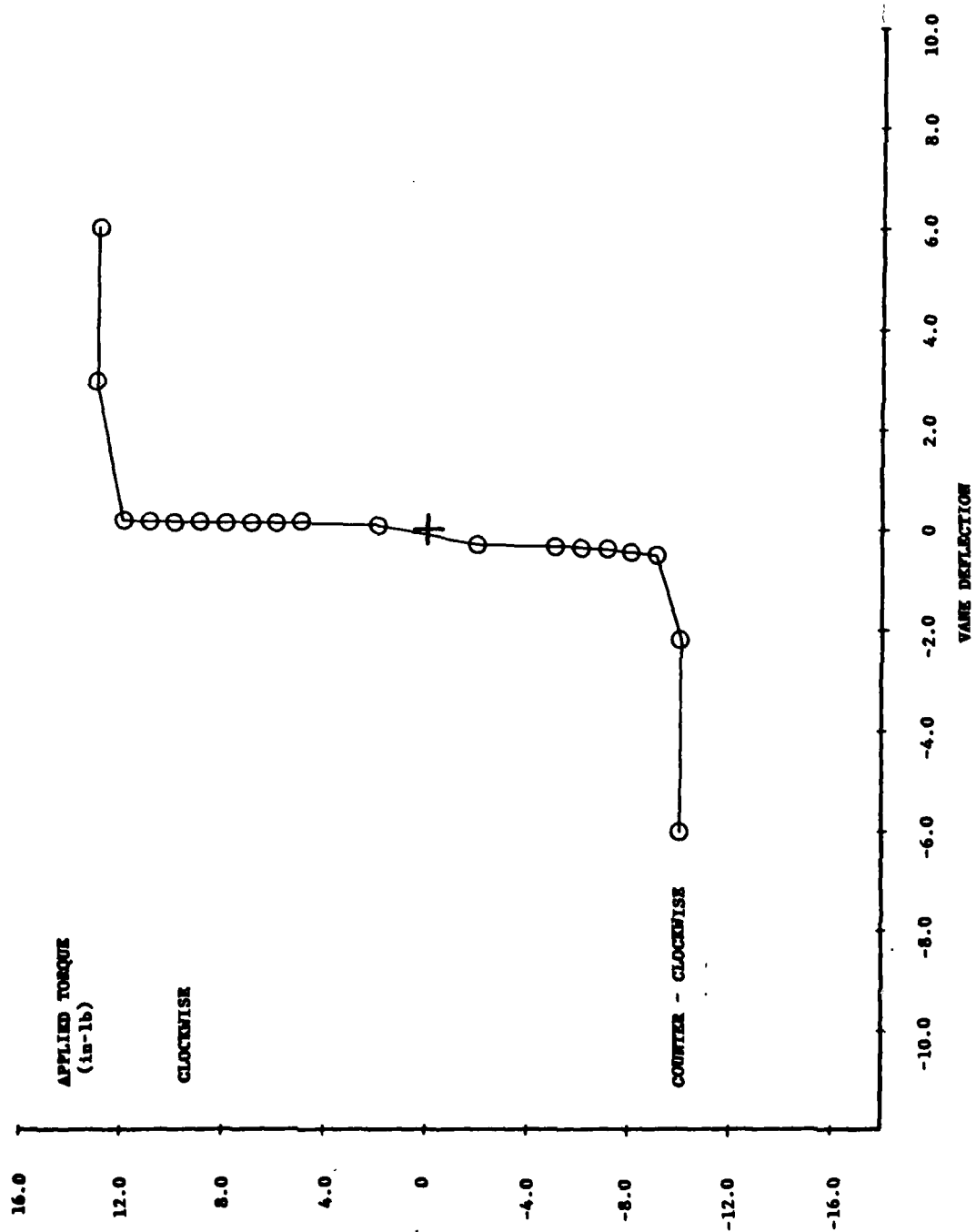


Figure 60. Applied torque versus vane deflection -
350 psig supply pressure,
0.50 degree deadzone.

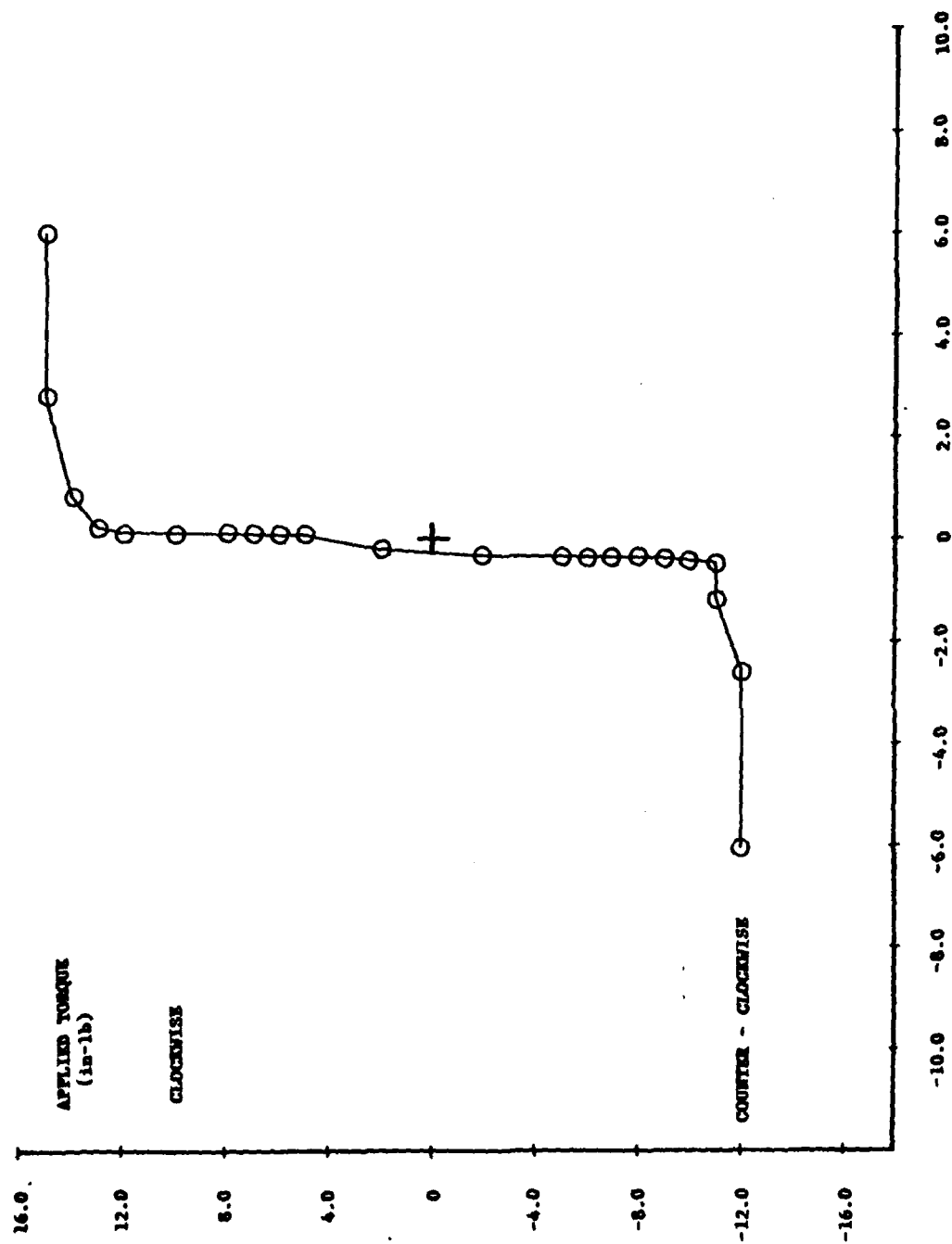


Figure 61. Applied torque versus vane deflection -
400 psig supply pressure,
0.50 degree deadzone.

TABLE 9. Actuator Performance Summary.

Actuator Serial No.	No Load Slew Rate (1)		Frequency Response (1)(2)			
	Charge (Deg/sec)	Discharge (Deg/sec)	Frequency -3dB		Frequency -90° Phase	
			1° P-P (Hz)	6° P-P (Hz)	1° P-P (Hz)	6° P-P (Hz)
SN-002	1536	1440	13.5	23.0	13.0	23.0
SN-003	1488	1472	11.5	20.0	11.0	18.0
SN-004	1376	1376	18.5	23.0	16.0	22.0
SN-005	1536	1408	14.5	20.0	14.0	21.5
SN-006	1440	1312	16.0	25.0	16.0	22.0
SN-007	1344	1280	20.0	25.0	18.0	22.0
SN-008	1376	1248	18.0	26.0	18.0	23.0
SN-009	1408	1280	11.0	22.0	11.0	22.0
SN-010	1440	1280	11.0	22.0	18.0	22.0
SN-011	1504	1472	18.5	23.5	19.0	22.5
SN-013	1472	1472	13.0	25.0	12.5	24.0
SN-014	1408	1440	29.0	29.0	29.0	24.0
SN-015	1472	1504	24.5	27.0	23.0	24.0
SN-017	1536	1440	29.0	28.5	26.0	23.5
SN-018	1504	1376	11.0	21.0	12.5	21.5

(1) 0.62 in²-lb Inertia Load

(2) 0.30 in-lb/deg Hinge Load

TABLE 10. Actuator Leakage Test Summary.

Actuator Serial No.	Leakage Flow Rate			Gas Consumption 2° P-P Sine Wave Input	
	Null Position (Std.in ³ /sec)	+20° Position (Std.in ³ /sec)	-20° Position (Std.in ³ /sec)	3Hz (Std.in ³ /sec)	6Hz (Std.in ³ /sec)
SN-006	0	0.057	0	1.17	1.93
SN-007	0	0.061	0.061	0.925	1.68
SN-008	0	0.024	0.024	0.824	1.63
SN-009	0	0	0	0.925	1.68
SN-010	0.047	0.047	0.047	1.22	1.93
SN-011	0.061	0.305	0.305	1.42	2.44
SN-013	0	0	0	1.42	2.24
SN-014	0	0	0	1.42	2.44
SN-015	0	0	0	1.42	2.24
SN-017	0	0.061	0	1.68	2.75
SN-018	0.061	0.061	0.061	1.42	2.44

V. COST ANALYSIS

A production cost analysis of the second generation FOG-M actuator resulted in an estimated total cost of \$95.50 per actuator plus the cost of assembly and performance verification. An itemized listing of the major cost items is provided in Table 11. The cost of purchased parts are budgetary estimates from the manufacturer. The cost of fabricated parts are estimates based on the most economical fabrication method and material which satisfies the parts strength and environmental requirements.

TABLE 11. Second Generation Closed Center
Pneumatic Actuator Major Cost Items.

Part Number	Nomenclature	Qty Req'd	Recommended Manufacturing Method/Material	Total Cost
L-5694	Solenoid	2	Purchase	\$48.00
FOG-RGC-13-1076	Actuator Housing	1	Die Cast - NC Machining Aluminum	20.00
FOG-RGC-13-1081	Valve Seat	2	NC Machining/17-4 PH Stainless Steel	5.00
SFP-101-1	Potentiometer	1	Purchase	5.00
FOG-RGC-13-1082	Crank	1	Powered Metal - NC Machining Stainless Steel	4.00
FOG-FGC-13-1073	Discharge Valve Housing	1	NC Machining/Aluminum	3.00
FOG-RGC-13-1074	Piston	1	NC Machining/Aluminum	3.00
FOG-RGC-13-1080	Valve Spacer	2	Injection Molded - NC Machining/Structural Plastics	4.00
PLGA1560010	Lee Plug	2	Purchase	1.10
04DU04	Bearing	2	Purchase	1.10

Total of Major Cost Items = \$94.20

Total of Minor Cost Items = 1.30

Total Cost of Actuator \$95.50

VI. RECOMMENDATIONS AND CONCLUSIONS

A closed center valve pneumatic actuator, which meets the requirements identified for the Fiber Optic Guided Missile, has been designed, fabricated and tested. The actuator design has proven to be very reliable during several months of bench testing and hardware-in-the-loop simulation testing. This report gives the complete data package from which the hardware was fabricated along with a description of the detailed hardware design.

A single flight test, using this actuator design, resulted in a control surface flutter which occurred at approximately two seconds after launch. Possible actuator related causes for this problem were the loose shaft/bearing fit, the shaft bending stiffness, and the actuator hinge stiffness. The loose shaft/bearing fit was corrected by increasing the shaft diameter, and the shaft bending stiffness was increased by reducing the shaft cantilever. The actuator was then wind tunnel tested, using a mass balanced control surface, to the maximum aerodynamic pressure expected during flight without flutter.

A comparison of this actuator design with the first generation actuator design is presented in Table 12. Notice that the second generation design has achieved a significant reduction in size and weight with only a small reduction in performance. An undesirable characteristic of the second generation actuator design is its increased cost which was a result of using smaller diameter solenoids.

The reduction in control system weight possible with the second generation actuator design is beneficial to the Fiber Optic Guided Missile. However, the reduction in actuator size was not beneficial since the use of a smaller actuator fairing caused an increase in missile drag force. Therefore it is recommended that a larger 3/4 inch diameter solenoid be used to reduce the actuator cost.

TABLE 12. Actuator Comparison

<u>Parameter</u>	<u>1st Generation Actuator Design</u>	<u>2nd Generation Actuator Design</u>
Slew Rate	1100°/sec	1400°/sec
1° P-P Bandwidth	12.5 Hz	9.0 Hz
6° P-P Bandwidth	17.0 Hz	15.0 Hz
Stall Torque	28 in-lb	12 in-lb
Hysteresis	0.50°	0.10°
Size	1.3 in X 2.3 in X 4 in length	0.6 in X 1.5 in X 4.7 in length
Weight	0.95 lbs ea	0.32 lbs ea.
Gas Consumption	0.80 in ³ @ 5000 psig per 60 sec flight	0.80 in ³ @ 5000 psig per 60 sec flight
COST	\$72.55	\$95.50 ea

REFERENCES

1. Raven, Frances H., Automatic Control Engineering, McGraw-Hill Book Company, 1968.
2. Anderson, Blaine W., and Wiley, John, and Son, Inc., The Analysis and Design of Pneumatic Systems, 1967.
3. Berry, Roger P., Design and Development of a Closed Center Valve Pneumatic Actuator for the Fiber Optic Guided Missile (FOG-M), TR-RG-85-1.
4. Dunaway, J.C., Dixon, Mark, and Landingham, George, FOG-M Wind Tunnel Flutter Test, TR-RG-30-85-RGC.

NOMENCLATURE

- σ - Normal Stress (psi)
- R_1, R_2, R_3 - Reaction Force (lb)
- F, W - Dimensions Defined in Figure 3-1 (in)
- P - Bearing Journal Pressure (psi)
- V - Bearing Sliding Velocity (fpm)
- P_c - Control Chamber Pressure (psi)
- P_s - Supply Pressure (psi)
- d_p - Piston Diameter (in)
- d_r - Rod Diameter (in)
- F_s - Piston Stall Force (lb)
- F - Piston Force (lb)
- M - Bending Moment (in-lb)
- z - Section Modulus (in³)
- ω - Slew Rate (deg/sec)
- L - Crank Lever Arm (in)
- T_c - Control Chamber Temperature (°R)
- R - Gas Constant (in-lbf)/(lbm-°R)
- W_n - Net Mass Flow Rate (lb/sec)
- W_c - Charge Valve Mass Flow Rate (lb/sec)
- W_d - Discharge Valve Mass Flow Rate (lb/sec)
- P_1 - Pressure Upstream of Orifice (psia)
- T_1 - Temperature Upstream of Orifice (°R)
- N_{12}, N_{23} - Ratio of Actual Mass Flow Rate to Sonic Mass Flow Rate
- K - Ratio of Specific Heat at Constant Pressure to That at Constant Volume

NOMENCLATURE (Concluded)

g - Gravitational Conversion Factor (in/S²)

$$C_1 - \left\{ \frac{Kg}{R} \left\{ \frac{2}{K+1} \right\}^{(K+1)/(K-1)} \right\}^{1/2}$$

A'_{12} - Upstream Orifice Flow Area Times a Discharge Coefficient. (in²)

A'_{23} - Valve Flow Area Times a Discharge Coefficient. (in²)

P_2 - Pressure Between Upstream Orifice and Valve (psia)

P_3 - Pressure Downstream of Valve (psia)

A_{23} - Valve Flow Area (in²)

d_s - Valve Seat Diameter (in)

d_B - Valve Ball Diameter (in)

X - Solenoid Travel (in)

A_{12} - Orifice Flow Area (in²)

μ_1, μ_2 - Friction Coefficient

F_{ss} - Solenoid Spring Force (lbs)

α - Ball Contact Angle (deg)

F_{pr} - Pressure Force (lbs)

M - Mass in Control Chamber (lb)

V_c - Control Chamber Volume (in³)

Y - Piston Displacement (in)

L_p, L_n - Dimension Defined in Figure A-1 (in)

θ - Actuator Deflection (deg)

t - Time (sec)

APPENDIX A

ACTUATOR EQUATIONS

ACTUATOR EQUATIONS

The purpose of the following analysis is to derive an expression which relates the actuator's slew rate to the mass flow rates through the charge and discharge valves. A schematic of the actuator is shown in Figure A-1. Conservation of mass for the control chamber requires that,

$$\frac{dM}{dt} = W_c - W_d \quad (A-1)$$

assuming that the fluid in the control chamber behaves according to the ideal gas law,

$$P_c V_c = MRT_c \quad (A-2)$$

$$M = \frac{P_c V_c}{RT_c} \quad (A-3)$$

If it is assumed that P_c and T_c are constant with respect to time, equation A-3 can be differentiated to obtain,

$$\frac{dM}{dt} = \left\{ \frac{P_c}{RT_c} \right\} \frac{dV_c}{dt} \quad (A-4)$$

since,

$$V_c = \frac{\pi}{4} d_p^2 Y \quad (A-5)$$

Combining equations A-1, A-4 and A-5

$$\left\{ \frac{\pi P_c d_p^2}{4RT_c} \right\} \frac{dY}{dt} = W_c - W_d \quad (A-6)$$

Piston displacement (Y) is related to angular displacement (θ) by,

$$Y = L_n - (L_p - L \tan \theta) \quad (A-7)$$

Differentiating equation A-7 with respect to time,

$$\frac{dY}{dt} = L \sec^2 \theta \frac{d\theta}{dt} \quad (A-8)$$

Replacing $\frac{d\theta}{dt}$ (Rad/s) with ω (Deg/S) and $s^2\theta$ with $(1/\cos^2\theta)$ results in,

$$\frac{dY}{dt} = \left\{ \frac{\pi}{180} \right\} \frac{L\omega}{\cos^2\theta} \quad (A-9)$$

Combining equations A-6 and A-9 and solving for ω ,

$$\omega = \left\{ \frac{720 RT_c \cos^2\theta}{\pi^2 P_c d_p^2 L} \right\} (W_c - W_d) \quad (A-10)$$

or,

$$\omega = \left\{ \frac{720 RT_c \cos^2\theta}{\pi^2 P_c d_p^2 L} \right\} W_n \quad (A-11)$$

Where W_n represents the net mass flow rate into the control chamber.

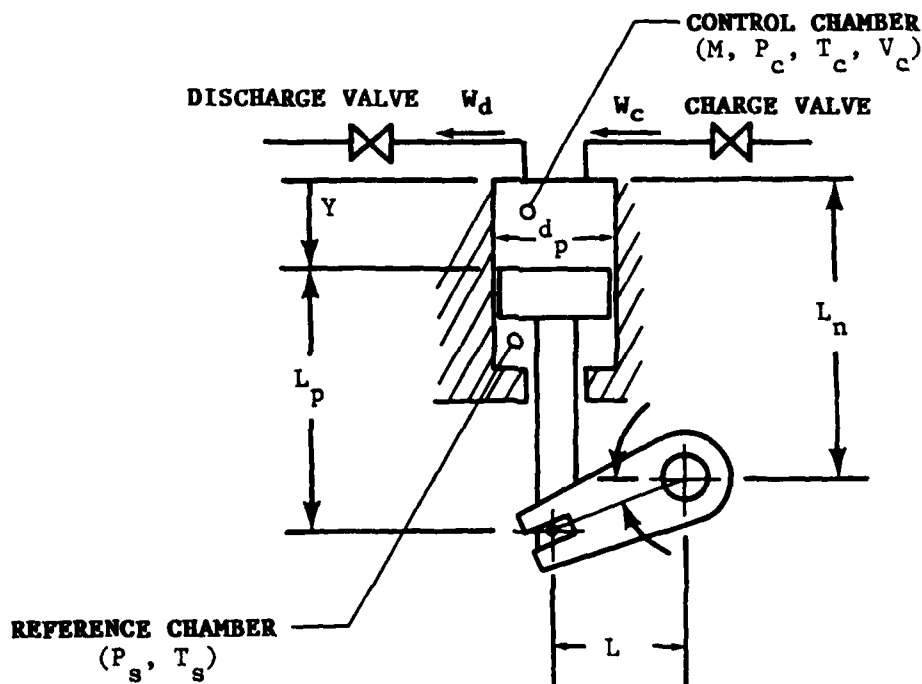


Figure A-1. Actuator schematic.

APPENDIX B

ACTUATOR DETAILED DRAWINGS

ENGINEERING PARTS LIST
PNEUMATIC ACTUATOR ASSY
CLOSED CENTER

Drawing No. FOG-RGC-13-1091
Sheet 1 of 3

ITEM	NOMENCLATURE	PART NO.	MANUFACTURER	QTY
1	Socket Head Cap Screw	#4-40 UNC		2
2	Roll Pin	1/16"X 5/16" MBK	C.E.M. Company	1
3	Piston	FOG-RGC-13-1074-1	Fabricate	1
4	O - Ring	2-007 N674-70	Parker Seal Co.	1
5	O - Ring	2-010 N674-70	Parker Seal Co.	1
6	O - Ring	5-051 N674-70	Parker Seal Co.	1
7	3/32 Dia Tungsten Carbide	Ball, Grade 25	Industrial Telectronics	1
8	Shim-Ball Valve	FOG-RGC-13-1072	Fabricate	As Req'd
9	O - Ring	5-179 N674-70	Parker Seal Co.	1
10	Discharge Valve Assy	FOG-RGC-13-1107		1
11	Solenoid	L-5694	G.W. Lisk Co.	1
12	Tube Fitting	LF-3000	Legris Inc.	1
13	Spacer - Ball Valve	FOG-RGC-13-1080	Fabricate	1
14	Seat - Ball Valve	FOG-RGC-13-1081-1	Fabricate	1
15	Lee Plug	PLGA1560010	The Lee Company	2
16	Crank Assy	FOG-RGC-13-1126		1
17	Potentiometer	SFP-101-1	New England Instru Co.	1
18	Roll Pin	1/16 "X 7/16" MBK	C.E.M. Company	1
19	Bearing	04D004	Garlock Bearings Inc.	2
20	Shaft	FOG-RGC-13-1075	Fabricate	1
21	Washer-Tube Fitting	FOG-RGC-13-1111	Fabricate	1

AD-A166 391

DESIGN AND DEVELOPMENT OF A SECOND GENERATION CLOSED
CENTER VALVE PNEUMAT (U) ARMY MISSILE COMMAND REDSTONE
ARSENAL AL GUIDANCE AND CONTROL R P BERRY APR 85

2/2

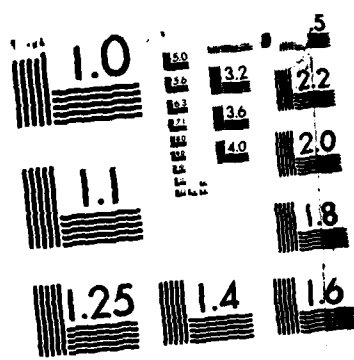
UNCLASSIFIED

ANSMI/RG-85-14-TR SBI-AD-E950 823

F/G 13/7

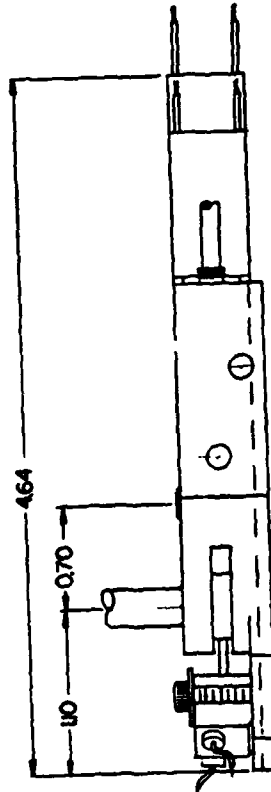
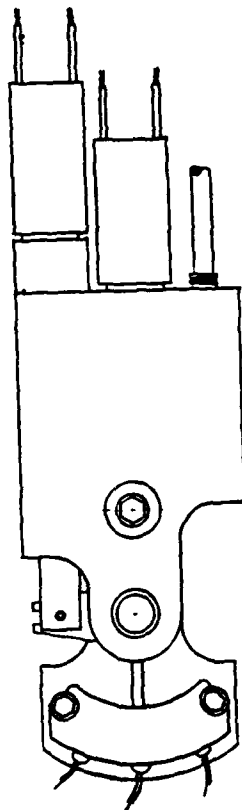
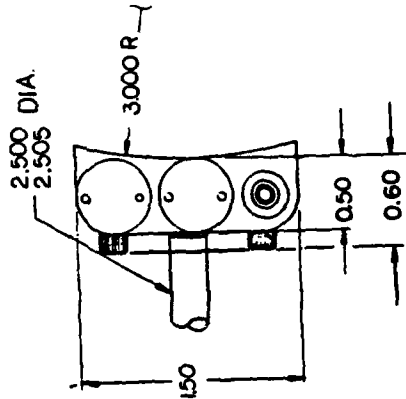
NL





MICROCOPY RESOLUTION TEST CHART
NATIONAL BUREAU OF STANDARDS-1963-A

DATE	DESCRIPTION	DATE APPROVAL



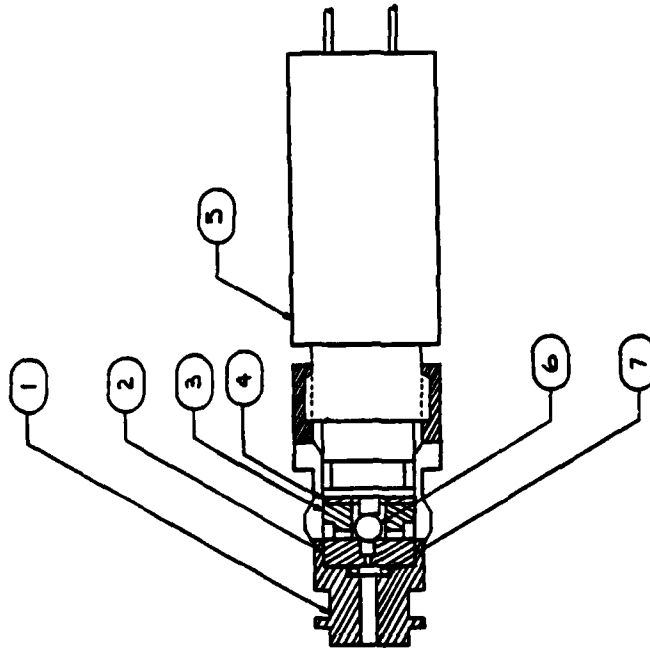
U.S. ARMY MISSILE RESEARCH & DEVELOPMENT COMMAND REDSTONE ARSENAL, ALABAMA		PNEUMATIC ACTUATOR ASSEMBLY CLOSED CENTER 0.313 IN. DIA.	
DATE 11 MAR 60	PREPARED BY [Signature]	SIZE C	FIGURE NO. 55717
CHECKED BY [Signature]	ENGINEER [Signature]	FOG-RGC-13-1091	SHEET 3 OF 3
APPROVED BY [Signature]		APPROVED BY [Signature]	
TEST UNIT		APPLICATOR	

**ENGINEERING PARTS LIST
DISCHARGE VALVE ASSEMBLY**

Drawing No. FOG-RGC-13-1107
Sheet 1 of 2

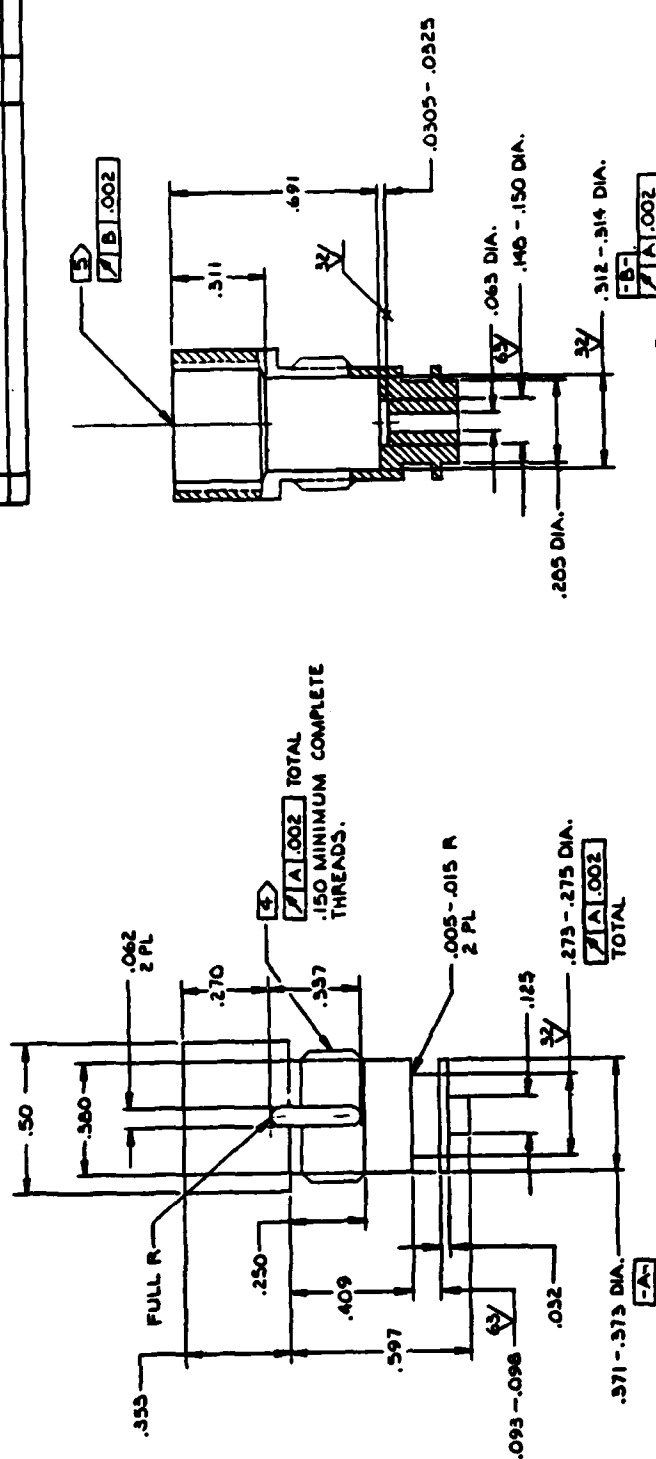
<u>ITEM</u>	<u>NOMENCLATURE</u>	<u>PART NO.</u>	<u>MANUFACTURER</u>	<u>QTY</u>
1	Discharge Valve Housing	FOG-RGC-13-1073	Fabricate	1
2	Seat - Ball Valve	FOG-RGC-13-1081-2	Fabricate	1
3	Spacer - Ball Valve	FOG-RGC-13-1080	Fabricate	1
4	Shim - Ball Valve	FOG-RGC-13-1072	Fabricate	As Required
5	Solenoid	L - 5694	G.W. Lisk Co.	1
6	3/32 Dia Tungsten Carbide Ball	Grade 25	Industrial Telectronics	1
7	O-Ring	5-051 N674-70	Parker Seal Co.	1

REV	DESCRIPTION	DATE	APPROVAL



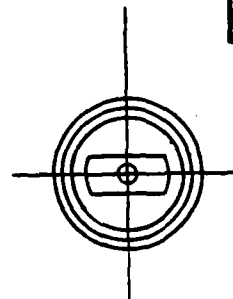
U.S. ARMY MISSILE RESEARCH AND DEVELOPMENT COMMAND REDSTONE AERONAUTICAL RANGE, ALABAMA		DISCHARGE VALVE ASSY	
DATE 3-13-68 PREPARED BY J. H. HARRIS CHECKED BY J. H. HARRIS SUBMITTED BY J. H. HARRIS	DATE 3-13-68 PREPARED BY J. H. HARRIS CHECKED BY J. H. HARRIS SUBMITTED BY J. H. HARRIS	PART NO. C 55717	DRAWING NO. FOG-RGC-13-1107
SEE PARTS LIST		SCALE 4/1	
APPLICATION -1051 BERT ASSY		SHEET 1 OF 1	

REV	DESCRIPTION	DATE	APPROVAL



SECTION E-E

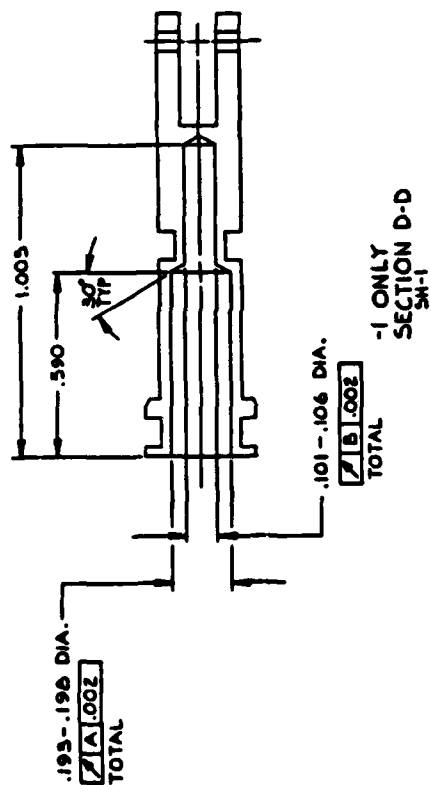
1. $\sqrt{125}$ FINISH ALL MACHINE SURFACES EXCEPT AS NOTED.
 2. ANODIZE PER MIL-A-8625, TYPE II, CLASS I, ALL OVER.
 3. DIMENSION AND FINISH APPLY AFTER ANODIZING.
- (3) .4375-26 UNEF-2A THREADS PER HANDBOOK H-26
(3) .4375-26 UNEF-2B. THREADS PER HANDBOOK H-26



U.S. ARMY MOBILE RESEARCH & DEVELOPMENT COMMAND REDSTONE ARSENAL, ALABAMA		DISCHARGE VALVE HOUSING	
DATE: 02-19-54	DESIGNED BY: J. B. B. / J. B. B.	SIZE: 1/2" DIA.	QUANTITY: 100
CONTRACT NO.	ENGINEER: J. B. B. / J. B. B.	SIZE: 1/2" DIA.	QUANTITY: 100
PROJECT NO.	ENGINEER: J. B. B. / J. B. B.	SIZE: 1/2" DIA.	QUANTITY: 100
TEST UNIT: 1107	TEST NO.: 105-M	SIZE: 1/2" DIA.	QUANTITY: 100
APPLICATION		SIZE: 1/2" DIA.	QUANTITY: 100
NEXT UNIT: 1107		SIZE: 1/2" DIA.	QUANTITY: 100
TEST NO.: 105-M		SIZE: 1/2" DIA.	QUANTITY: 100
APPLICATION		SIZE: 1/2" DIA.	QUANTITY: 100

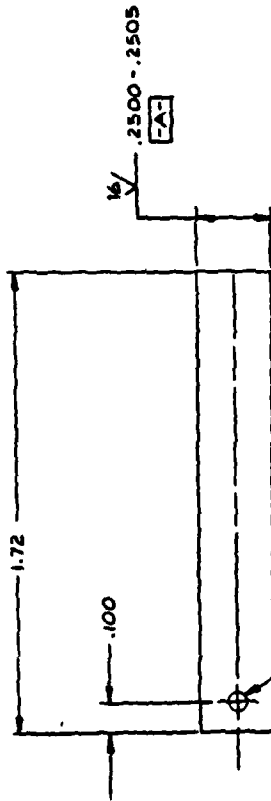
FORM 2-5 Rev 4-17-57

REVISIONS		
DATE	DESCRIPTION	APPROVAL

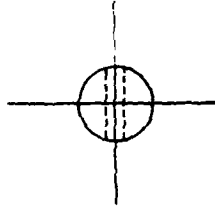


U.S. ARMY MISSILE RESEARCH & DEVELOPMENT COMMAND REDSTONE ARSENAL, ALABAMA		PISTON	
DATE: 02-27-64	PREPARED BY: R. B. B. 3/10/64	SIZE: C	PROJ. NO.: 55717
CHECKED BY: R. B. B. 3/10/64	ENGINEER: R. B. B. 3/10/64	SCALE: 4/1	DRAWING NO.: FOG-RGC-13-1074
APPROVED BY: R. B. B. 3/10/64		SHEET 2 OF 2	

REVISIONS		
REV	DESCRIPTION	DATE
1	A CHANGE SHAFT DIAMETER	1/14/60

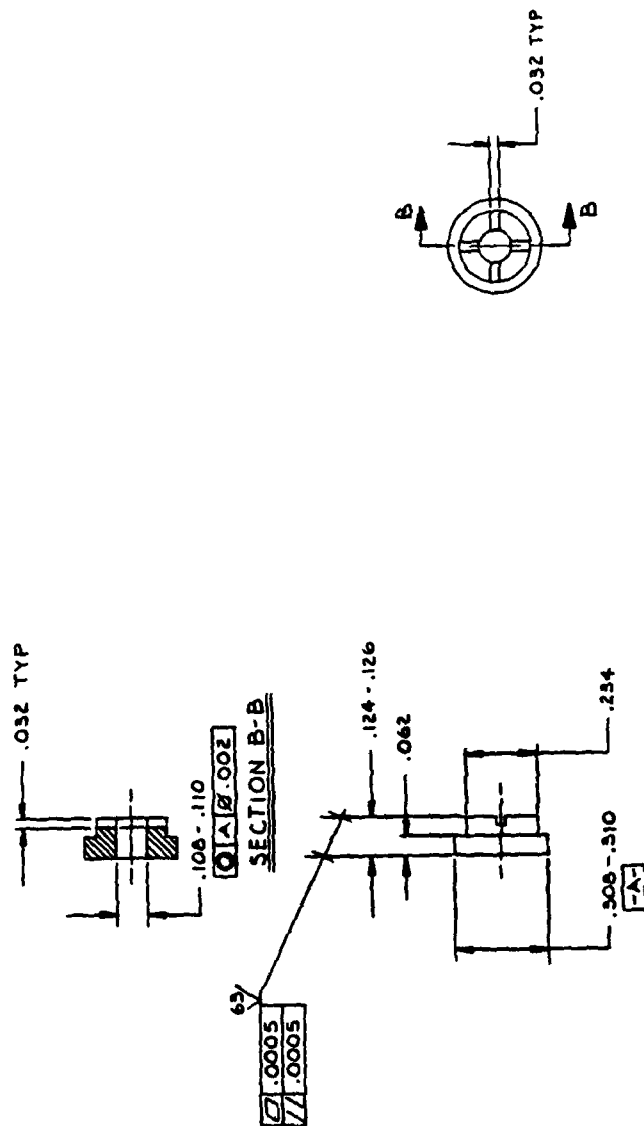


1. $\sqrt{}$ FINISH ALL MACHINE SURFACES EXCEPT AS NOTED.
2. PASSIVATE PER QQ-P-35



U.S. ARMY MISSILE RESEARCH & DEVELOPMENT COMMAND REDSTONE ARSENAL, ALABAMA		SHAFT	
DATE 06-17-63	PREPARED BY B. B. B. 10/11/63	SITE PAGE NO. C 55717	DRAWING NO. FOG-RGC-13-1075
CHECKED BY B. B. B. 10/11/63	ENGINEER BY B. B. B. 10/11/63		
MATERIAL 17-4 PH CRES PER AMS 5643		SCALE 4/1	
ITEM NO.	QUANTITY	APPROVED BY NAME OF COMMANDER	
1088	FOG-M	APPROVED BY NAME OF COMMANDER	
1091	FOG-M	APPROVED BY NAME OF COMMANDER	
1120	FOG-M	APPROVED BY NAME OF COMMANDER	
NET WT USED ON APPLICATION		SHEET 1 OF 1	

FOG-RGC-13-1075 SHAFT C

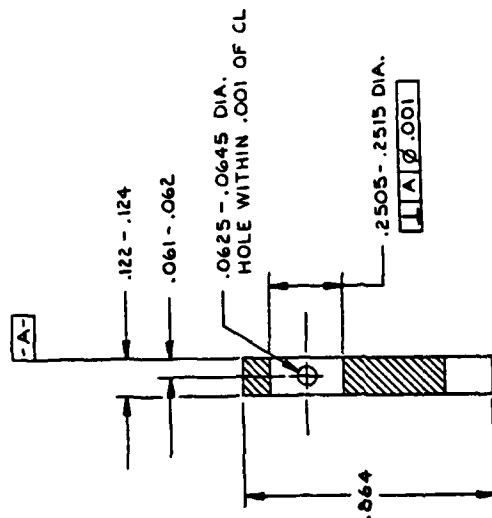
[illegible]

1. 125/✓ FINISH ALL MACHINE SURFACES EXCEPT AS NOTED.
2. ANODIZE PER MIL-A-8625, TYPE II, CLASS I ALL OVER.
3. DIMENSIONS AND FINISH APPLY AFTER ANODIZING.

Revised - 8 June 4-1, 1967

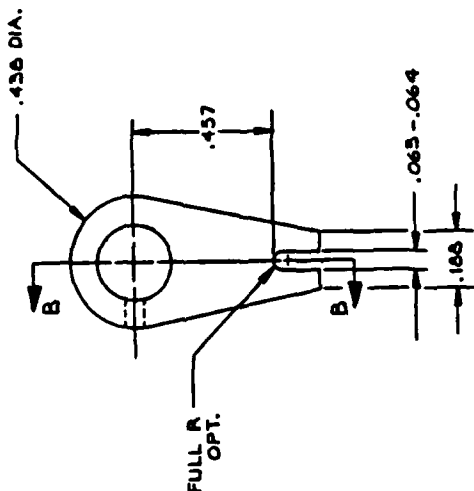
REVISIONS		DATE	APPROVAL
SYMBOL	DESCRIPTION		

FOG-RGC-13-1085 CRANK



SECTION B-B

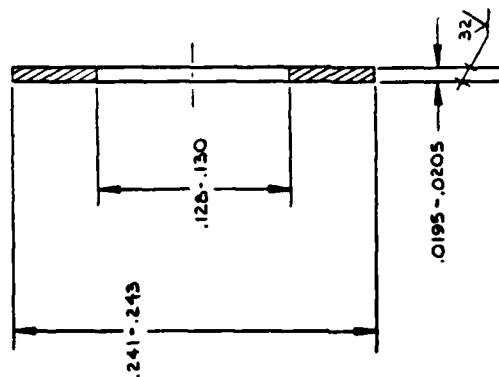
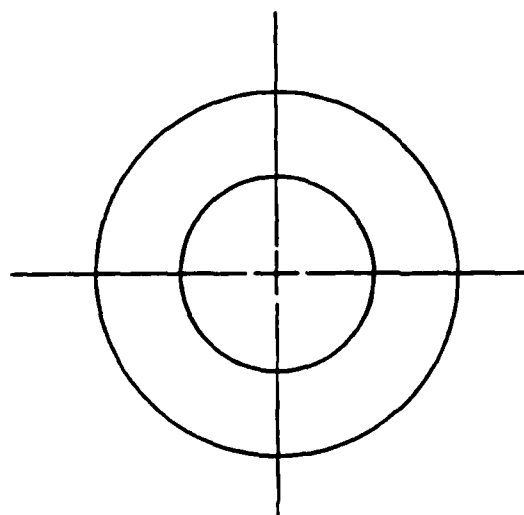
1. 125/ FINISH ALL MACHINE SURFACES
2. HEAT TREAT TO H925 PER MIL-H-6875.
3. PASSIVATE PER QQ-P-35.



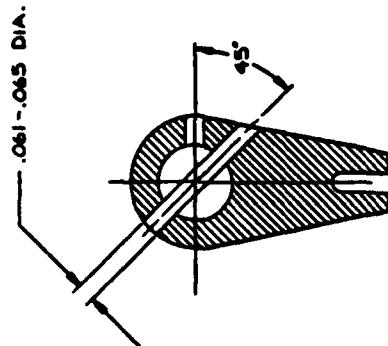
U.S. ARMY MISSILE RESEARCH & DEVELOPMENT COMMAND REDSTONE ARSENAL, ALABAMA		CRANK	
DATE 08-03-65	PREPARED BY R. B. B. / M/M/83	FIGURE NO. C 55717	DRAWING NO. FOG-RGC-13-1082
CHECKED BY	ENGINEER R. B. B. / M/M/83	SCALE 4/1	
SUBMITTED		APPROVED BY	
MATERIAL 17-4 PH CRES PER AMS 5643		SHEET 1 OF 1	
APPLICATION		USED ON	
-1088 FOG-M	MISS ARMY		
-1091 FOG-M			
-1120 FOG-M			
-1126 FOG-M			

Sheet 1 of 1 Page 4-1, 1082

REVISIONS		
SYMBOL	DESCRIPTION	DATE APPROVAL



U.S. ARMY MISSILE RESEARCH & DEVELOPMENT COMMAND REDSTONE ARSENAL, ALABAMA		WASHER-TUBE FITTING	
DATE: 02-26-65	CHECKED: [Signature]	SIZE: C 55717	DRAWING NO.: FOG-RGC-13-1111
PREPARED BY: [Signature]	ENGINEER: [Signature]	APPROVED BY: [Signature]	
MATERIAL: BRASS		SCALE: 20/1	
APPLICATION:		SHEET 1 OF 1	





B-18

Standard: 8 Weeks Oct. 1st - 7th

DISTRIBUTION

	<u>No. of Copies</u>
A. R. Barbin M.E. Department Auburn University Auburn, AL 36840	2
Bill Waldon US Naval Weapons Center China Lake, CA 93555	1
Commander US Naval Weapons Center ATTN: J. A. Knecht China Lake, CA 93555	1
Commander US Army Combined Arms Combat Development Activity Ft. Leavenworth, KS 66027	1
ITT Research Institute ATTN: GACIAC 10 W. 35th Street Chicago, IL 60616	1
Richard N. Gottron Harry Diamond Laboratories ATTN: DELHD-RT-CD 2800 Powder Mill Road Adelphi, MD 20783	1
James W. Joyce Harry Diamond Laboratories ATTN: DELHD-RT-CD 2800 Powder Mill Road Adelphi, MD 20783	1
US Army Materiel System Analysis Activity ATTN: AMXSY-MP Aberdeen Proving Ground, MD 21005	1
Albertus E. Schmidlin US Army ARRADCOM ATTN: AMDAR-LCN-C, Bldg 65 Dover, NJ 07801	1
Tor Jansen Naval Air Development Center CODE 60134 Warminster, PA 18974	1

DISTRIBUTION (Concluded)

	<u>No. of Copies</u>
David Heyser Naval Air Development Center CODE 60134 Warminster, PA 18974	1
R. L. McGiboney Naval Air Development Center CODE 60134 Warminster, PA 18974	1
Commander US Army Training and Doctrine Command Ft. Monroe, VA 23341	1
George W. Fosdick Applied Technology Laboratory ATTN: DAVOL-ATL-ASA Ft. Eustis, VA 20634	1
Defense Technical Information Center Cameron Station Alexandria, VA 22314	2
Dean Houck Naval Air Systems Command ATTN: AIR 5162C8 Washington, DC 20361	1
Headquarters Department of the Army ATTN: DAMA-WSM, MAJ Belch Washington, DC 20310	1
AMSMI-RD, Dr. McCorkle	1
Dr. Rhoades	1
-RD-GC, Dr. Yates	1
-RD-GC-T, Mr. Plunkett	20
Dr. Jacobs	1
-RD-AS-OG	1
-RE-AS-IR	1
-RD-ST-DC, J. Schaeffel	1
-RD-AS	1
-RD-RE, Dr. Hartman	1
Dr. Guenthre	1
Dr. Gamble	1
-RD-TI, Mr. E. Dobbins	1
-RD-CS-R	15
-RD-CS-T	1
-GC-IP, Mr. Bush	1

END

Dtic

5-86